TÉCNICO LISBOA

Layup influence on the cured ply thickness of a composite material manufactured by the vacuum infusion process

Luís Filipe Baptista Campos Alves

Thesis to obtain the Master of Science Degree in

Aerospace Engineering

Supervisors: Prof. Doctor. Luís Filipe Galrão dos Reis
Prof. Doctor. Aurélio Lima Araújo

Examination Committee

Chairperson: Prof. Doctor Afzal Suleman
Supervisor: Prof. Doctor Aurélio Lima Araújo
Member of the Committee: Prof. Doctor Miguel Matos Neves

December 2021

Acknowledgments

This project involved the collaboration between two significant entities, *Vestas* and *Instituto Superior Técnico* (IST). Without the common purpose shared by all parties and the willingness to strive within the project ambitions, it would not be possible to have such an enriching performance.

IST, thank you for all these years of educational background and providing an excellent environment for personal growth. Thank you also for the composites laboratory access.

Vestas, thank you for resources allocation on the project, for sharing the consolidated know-how you have in this field of expertise, and for the integration you allowed me to have within your corporate structure. Thank you for allowing me to be responsible for the project.

Professor Luís Reis and Professor Aurélio Araújo, thank you for your guidance and support throughout these months. Luís Oliveira, thank you for all the project overview, feedback, suggestions, and clarifications. José Teles, an especial thank you for being always there and significantly contributing to my professional development.

Family, thank you for your unconditional love, always believing in me, and your efforts to provide me with the best conditions. You have built the foundation for what I am today. Cátia, without your presence, nothing would be the same. Thank you for setting such high goals for both of us, for all your unconditional support, and for being the best role model one could have. Marta, thank you for your unlimited support, love, and care, for your constant presence, and all happiness we shared.

Friends from Lisbon, thank you for the fantastic moments shared and everything you taught me. Friends from *BEST*, thank you for your support and joyful moments during this project. Friends from Barcelos, thank you for believing in me, being always there, and providing the belonging feeling regardless of the time passed.

Resumo

O processo de infusão a vácuo é uma técnica de produção utilizada em diversas indústrias que conta com uma vasta gama de aplicações dos seus produtos. A falta de modelos de previsão de espessura capazes de prever com precisão a distribuição da espessura de peças curadas é um dos seus maiores desafios. As pás das turbinas eólicas da *Vestas* sofrem deste problema, e os projetos podem ser postos em risco se a conceção do processo de produção inviabilizar a entrega de peças dentro dos intervalos de segurança apropriados.

Este projeto tem como objetivo retificar esta situação e encontrar soluções alternativas às metodologias de previsão atualmente aplicadas. O seu objetivo baseia-se em desenvolver um modelo analítico capaz de prever a espessura de peças curadas com maior foco em zonas mais poblemáticas das pás.

Este projeto começa com uma revisão bibliográfica sobre esta técnica de produção e desenvolve um modelo que cumpre os seus requisitos e tem limitações aceitáveis. Seguidamente, são realizados testes experimentais com dois objetivos, o de caracterizar o comportamento de compactação do material e o de produzir peças recorrendo ao processo de infusão a vácuo. Finalmente, a precisão do modelo desenvolvido é avaliada através de comparações das previsões com as espessuras das peças curadas dos ensaios experimentais, e também recorrendo a informação disponível de espessura das pás da *Vestas*. A qualidade dos procedimentos dos testes de caracterização é avaliada, a eficácia do modelo é determinada, e etapas de continuação para futuros trabalhos são sugeridos.

Palavras-chave: Infusão a Vácuo, Pás de Turbinas Eólicas, Previsão de Espessura, Materiais Compósitos.

Abstract

The vacuum infusion process is a manufacturing technique used in several industries with a wide range of part applications. One of its main drawbacks is the lack of thickness prediction models that accurately predict the cured part thickness distribution. *Vestas*' wind turbine blades suffer from this concern, and projects can be jeopardised if the design of the production process does not deliver parts within proper safety limits.

This project aims to mitigate this problem and find alternative solutions instead of the current predictive methodologies applied. The goal is to develop an analytical model capable of predicting cured parts thickness focusing on more problematic blade areas.

This project starts with a literature review of this manufacturing technique and develops a model that meets the reality it is intended to represent and has acceptable limitations. Then, experimental tests are conducted with two purposes, to characterise the compaction behaviour of fabric and to produce parts by recurring to the vacuum infusion process. Finally, the developed model accuracy is assessed by comparing its thickness predictions against the cured part thickness of the experimental tests and resourcing to *Vestas* blades available thickness data. The quality of the characterisation tests procedure is evaluated, the model efficiency is determined, and follow up steps for future work are suggested.

Keywords: Vacuum Infusion, Wind Turbine Blades, Thickness Prediction, Composite Materials.

Contents

List of Tables

List of Figures

Nomenclature

Greek symbols

α	Scalable variable.
ϵ	Error.
μ	Viscosity.
ϕ	Porosity.
ρ	Density.

Roman symbols

h	Thickness.
K	Permeability.
k_0	Permeability empirical constant.
NF	Nesting factor.
nol	Number of layers.
nor	Number of repetitions.
P	Pressure.
R^2	R-squared factor.
V_{f_0}, B, a, b, c, d	Compaction empirical constants.
V_f	Fiber volume fraction.

Subscripts

i	Iterations index.
k	Layers index.
n	Discretisation index.

List of Acronyms

1D Unidirectional

ANOVA Analysis of Variance

B.C. Boundary Conditions

C.V. Control Volume

DIC Digital Image Correlation

DoE Design of Experiment

EOTI Equally Oriented Textile Interfaces

FDM Finite Difference Method

FE Finite Element

FEA Finite Element Analysis

FEL Flow Enhancement Layers

FEM Finite Element Method

FVF Fiber Volume Fraction

IST *Instituto Superior Técnico*

KES-F *Kawabata* Evaluation System for Fabrics

LHS Left Hand Side

LSM Least Square Method

LVDT Linear Variable Displacement Transducer

NCF Non-Crimp Fabric

NF Nesting Factor

ODE Ordinary Differential Equation

RHS Right Hand Side

RTM Resin Transfer Molding

SCRIMP Seeman Composites Resin Infusion Molding Process

SD Standard Deviation

SLS Structured Light Scanning

UTM Universal Testing Machine

VI Vacuum Infusion

VIP Vacuum Infusion Process

VOC Volatile Organic Compounds

Chapter 1

Introduction

The Vacuum Infusion Process (VIP) is a composite manufacturing process whereby resin impregnates dry fabric by a driver pressure differential. At the end of the infusion part of the process, resin and the stacking will consolidate and form a cured part possibly ready for its application. This manufacturing technique started to be investigated around the mid-twentieth century, but it was only around the 1990s with the Seeman Composites Resin Infusion Molding Process (SCRIMP) patent when it gained its due recognition and asserted itself in the market. From that point, the composites' components demand growth was accompanied by the interest of the science community to research and develop new tooling capable of predicting and improving the design of the process, revolutionising the trial and error approach used until then, [1].

VIP is a close-mould process composed of one rigid side of the mould and another flexible, figure 1.1. The preform of dry fabric is laid on the rigid part of the mould and several other components. Afterwards, the mould cavity is sealed by the application of the flexible vacuum bag. This flexible tooling will allow thickness variations during the different stages of the process that are difficult to predict accurately. Initially, the resin system is outside the mould cavity. When the vacuum is applied, the pressure gradient will serve as the driver for the fluid to enter the cavity, flowing through the fabric' porous media and changing its compaction and permeability properties along the way. Since no additional pressure is applied to the mould, only the atmospheric pressure contributes to the pressure gradient and serves as the fluid's only driver. Heating systems are typically embedded into the rigid side of the mould to fasten the solidification of the part, reducing the duration of the process, [2].

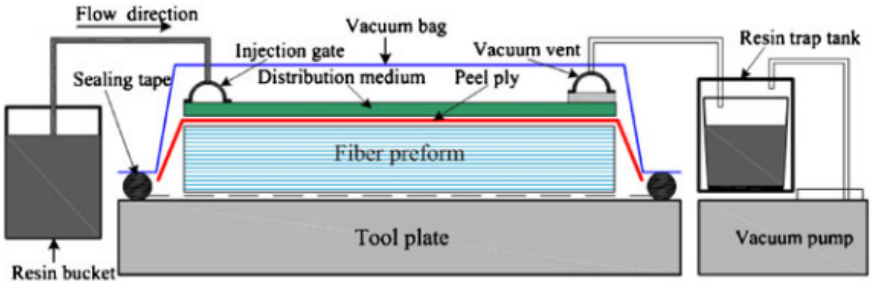

Figure 1.1: Vacuum Infusion (VI) setup components, [3].

On a positive note, the setup design and materials selection for its integration is very flexible, easing its preparation. Complex geometry parts are produced with relative comfort due to not having two sides of the mould rigid. Furthermore, the vacuum bag application improves the control over the infusion due to its transparency and takes actuation measures to overcome dry patches due to its ability to tear. The resin system only emits Volatile Organic Compounds (VOC) when being prepared before infusion. During the process, the emission is null.

The number of consumable materials wasted and the time needed for their preparation incorporate the process's disadvantages. Excellent user skills and consumable materials quality are imperative factors to achieving good part quality. The setup is always susceptible to air leaks which may compromise the whole manufacturing. Regarding the pressure levels of the VIP, the pressure gradient driving the resin is minimal, and the compaction pressure on the fabric will not be very significant. Thus, the infusion times will be raised, and the final Fiber Volume Fraction (FVF) will decrease. The non-uniformity in thickness distribution in the ply due to the flexible tooling may jeopardise the assembly or application of the final component.

It can be concluded that this process is particularly suitable for composite productions of more extensive and complex parts, such as turbine blades, boat hulls and aircraft structures. This process has applications in several industries, and its growth indicates that it will reach and cover even more areas. The marine, automotive, infrastructures, renewable energies and aerospace are the industries with more VIP applications, [2, 4]. The balance between composite materials' weight and mechanical properties is their main attribute leading to such a vast application in diverse industries. The exponential growth of composites applications in the aeronautical sector is observable in figure 1.2. Even though the slice of composite materials represented there is distributed among several production techniques, the curing on spot advantage of the VIP has conducted increments in its use in recent years. The wind energy sector has been using VIP as the election process to produce turbine blades.

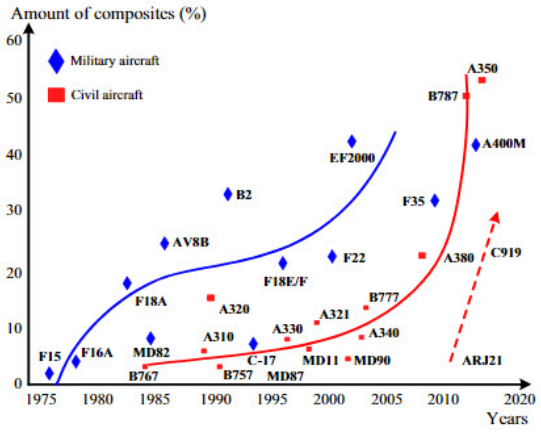

Figure 1.2: Composites applicability in the aeronautical sector, [5].

The VIP shares features of two other crucial composite manufacturing techniques. The fact that it is a close-mould process, similar to the Resin Transfer Molding (RTM), reduces the VOC emissions and the handling during the process is much cleaner and safer. The part quality and repeatability of the process

are also similar for these processes. On the other hand, the flexible side of the mould allows to scale the setup and adapt it for more extensive parts, like in the open-mould hand layup process. Since only one side of the mould is rigid, the overall cost of the process is cheaper than RTM and more expensive than hand layup.

1.1 Motivation

Vestas is a global partner on sustainable energy solutions within the wind industry. *Vestas* is responsible for the design, manufacture, installation and service of wind turbines across the world. Currently, wind turbine blades are produced by the VIP and therefore are susceptible to the process advantages and disadvantages. The final blades assembly is ultimately dependent on the thickness of each part of the blade. If predictions are not accurate, projects will suffer delays in the manufacturing stage, and their costs will rise possibly until unbearable values. Thus, *Vestas* invested in contributing to a master thesis whose goals rely on solving production problems.

On a personal level, the motivation for this thesis is based on three fundamental points. The first is related to the ambition to contribute positively to the scientific community responsible for providing all the knowledge acquired during the degree. The second point is regarding the motivation to learn in deep detail a composite manufacturing process. Mixing composite materials with the manufacturing world is a culminating point for the author's academic background. Lastly, having the opportunity to solve a problem in producing turbine blades that have a beneficial social impact on everyone's everyday life is vital for developing this work.

1.2 Objectives

Vestas' goal for this thesis relies on improving the current methodologies applied to predict the thickness of the cured turbine blades. Further objectives were agreed upon for all parts involved, having this as the common ground for the project.

The ultimate goal is to develop an analytical model capable of predicting the cured ply thickness of blades within the pre-existing admissible error interval. For that purpose, the layup influence on the ply was defined as the main target of study. Iteratively, layup factors were researched and assessed based on literature review and experimental tests to achieve the best prediction possible. For final tasks, available data from *Vestas*' blades must be compared with the predictions to understand the suitability of the developed model with the current manufacturing methodology. The developed model should account for possible minor modifications and improvements in future blades models. If fully justified and framed within these objectives, conducting experimental tests is a possibility for this project.

1.3 Thesis outline

This document structure is divided into six chapters. Chapter 1 briefly introduces the research topic and frames its motivation in the corporate environment it is inserted. The ensuing chapter 2 presents an elaborated review of the literature acknowledged for this project. Researches conducted by several authors are cited, and concepts related to the VIP are thoroughly explained to understand better the decisions made throughout this work. In chapter 3, the thickness prediction model is elected. It also counts with iterations and assumptions made during its development alongside an accurate framing of the justifications in *Vestas*' production reality. This development is followed by the experimental tests conducted, chapter 4. First, material characterisation tests are conducted, then infusion tests take place. The material characteristics are used in chapter 5 to perform the model validation against both the infusion tests and *Vestas*' blades data. Lastly, conclusions of this thesis are described in chapter 6 alongside suggestions and ideas for future follow up projects.

Chapter 2

Literature review

2.1 Vacuum infusion process

2.1.1 Process stages

The vacuum infusion process, VIP, can be divided into several stages, all in which the preform behaves under different conditions leading to a different method to predict it. Before applying vacuum, the setup preparation is a fundamental task that implies a detailed design of its components not to jeopardise the whole production. The level of setup quality is mainly dictated by the technicians' expertise and the quality of the materials. The geometry and the surface finish of the final part will determine the components applied in this stage. The mandatory ones for a simple infusion are listed below and can be seen in figure 1.1.

- **Mould**, the rigid side of the mould that must resemble the surface of the product.
- **Release Agent**, the chemical product that improves the surface finish of the product on the table side and eases the removal of the part at the demolding stage.
- **Preform**, the stacking of fabric that makes the main structure of the part.
- **Peel Ply**, a layer that allows easy separation of the part from the consumable materials.
- **Vacuum Bag**, the upper side of the mould that introduces a flexible deformation to the setup.
- **Resin Inlet and Outlet**, can be of several formats and allow the entrance and exit of air and resin.
- **Resin Hoses**, connecting different components of the setup, where air and resin flow.
- **Resin Deposit**, to prepare the resin before its infusion.
- **Resin Trap**, to save extra resin that escapes the preform, blocking it from reaching the vacuum pump.
- **Vacuum Pump**, the device that pulls air and forms vacuum conditions on the setup.

The consumable materials cannot be reused and represent the waste of production. They include the peel ply, the vacuum bag, resin inlet and outlet and the resin hoses from the above components. There are some critical details for handling each of these materials that will be detailed in chapter 4.

Having the setup prepared, the most exciting stages from a scientific point of view begin. There is the pre-filling stage when the application of vacuum compresses the preform. The vacuum pump is turned on, and air inside the mould is extracted, decreasing the setup thickness and increasing the compaction pressure and the part's FVF. Depending on the resin system preparation and size of the part, this stage can take from twenty minutes to several hours. During this stage, the preform is being compressed in its dry state. Since there is no resin inside the mould, the vacuum on the mould cavity and the time-dependent phenomena are solely supported by the fabric.

Then, the filling stage takes place, and resin makes its entrance to the mould and is distributed inside the cavity. Along with the setup preparation stage, human skills are required the most in this stage because it is possible to need real-time adjustments to the setup. If people in charge do not have that skill, the production will not be successful, and the number of wastes will increase. The pressure gradient between the setup pressure with the vacuum pump turned on and the resin system, at ambient pressure, will serve as the driver for the resin to go inside the mould cavity. The resin will enter the resin inlet and go through the whole preform until the resin outlet, assuming a well-prepared setup. It is at this stage when several thickness variation phenomena occur. These are addressed in subsection 2.1.3. In [4], the authors go through several strategies that can be applied for the resin infusion. Some of them require extra materials to the setup, being the distribution mesh the most used. This component has a very high permeability compared to the fabric in its in-plane direction. In case it is part of the setup, the resin will flow much faster in that layer, and then it will impregnate the preform by the through-thickness direction, figure 2.1, resulting in a significant reduction of the filling time, [6]. Resin films can also be embedded in the fabric layup allowing a faster flow in those layers, putting in detriment the mechanical strength of the part, [4].

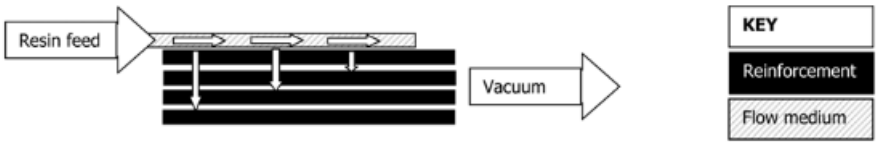

Figure 2.1: Infusion with distribution mesh, [4].

Once the resin covers the whole preform, the condition of full saturation is reached, and the post-filling stage begins. At this point, thickness changes still occur because the resin is still able to move. Therefore, it is possible to apply many strategies to manage the non-uniform pressure and resin distributions which are always present at the beginning of this stage. Since thickness changes in VIP are one factor that needs to be fully understood, several studies have targeted the post-filling stage. In [7] and [3], the introduction of a membrane in the resin outlet was analysed. Its placement implies that the vacuum pump still influences the pressure, but resin is not further allowed to be extracted. In [8], two scenarios were compared in terms of controlling actions. In case A, no control actions were ap-

plied, contrary to case B, which decreased the maximum thickness variation in this stage from 5.44% to 0.34%. [9–11] are other examples where control actions result in a significant decrease in the time necessary to uniform the pressure in the mould, resulting in lower thickness variations.

The post-filling stage reached an end, curing occurs, and some components inside the mould start to go through chemical reactions responsible for binding them into a single, rigid part. Resin systems are composed of a mixture of resin with an initiator or a hardener. The ratio of these components determines the gelation time and the curing of the part, [3, 12]. Gelation time defines the instant when the mixture stops behaving like a liquid and starts to act as a gel due to a plastic encapsulant. The mould temperature immensely influences the curing stage. If there is an integrated heating system in the setup, it is appropriate to use it to increase the temperature of the part, allowing faster curing. It is crucial to be aware of the resin characteristics because if any failure occurs, health issues will be raised, and the people conducting the process might be injured.

Demolding is the remaining and final stage of the process. The resin hoses are disconnected, the part is separated from the mould, and the consumables are stripped off. In case the part has extra fabric at some places, it will be trimmed. The final cured part will frequently go through some superficial treatments to be ready for its product application.

2.1.2 Fabric

In the composites industry, a wide variety of combinations is applied between types of fibre and resins. Nonetheless, there is a clear majority of use in products applications and research studies with mats, Flow Enhancement Layers (FEL), woven and Non-Crimp Fabric (NCF) mixed with epoxy. This tendency is most probably related to the remarkable mechanical properties of the final parts, but since it is not directly related to the goal of this thesis, it was not studied in much detail. Considering that resources are not always abundant for research projects, and laboratory conditions are imperative to achieve a certain quality level of experiments, it is common for researchers to use test fluids, as oils and corn syrup, instead of epoxy in the resin system for characterisation experiments, [13–15]. These oils application eases the handleability of components and improves tests' reproducibility, [14]. Like it was concluded in [16], resin viscosity does not have a significant influence on the overall fabric compaction behaviour.

As stated in [17], *"Non-crimp fabrics are defined as drawn parallel oriented layers of reinforcing threads or tows, which are positioned by means of an additional fixation material."*. In sum, multiple layers of unidirectional fibres are stacked with the same or different orientations between themselves and are stitched together. The compaction behaviour of the fabric will be influenced by its geometry, and there are several options for the stitching patterns, as seen in figure 2.2. This influence was studied in [9] for some stitching patterns and tensions and in [18] for the binder properties applied in the layup. The stitching patterns alignment and the superficial weight of the fabric will also influence the compaction of the preform, as measured in [19]. Several industries apply NCFs, including aerospace and wind energy, [3, 17].

(a) $0° / -45° / 90° / +45°$.

(b) $+45° / -45°$.

Figure 2.2: NCF stitching patterns, [17].

Woven fabrics are a different fabric type that includes fibre bundles in their through-thickness direction. These bundles of aligned fibres are interlaced to form a structural pattern that improves their properties in the through-thickness direction, in contrast to NCFs, figure 2.3. In [20], all levels of the structural staircase of woven fabrics were studied, and a model was presented in each one to culminate with a full geometrical model capable of predicting the properties of the whole structure. The fibres interlacement originates crimp that represents the bending and twisting of the bundles, and it will change the way that pressure between layers is distributed. Formulas were derived to assess the pressure distribution considering the contact points between layers, [21]. Warp and weft are the terminologies used to describe the essential components of woven fabrics. Warp bundles are fixed with tension in the lengthwise direction during the weaving process, while the weft bundles are placed over and under the former to achieve the desired pattern. Besides being the ones dictating the critical details of the fabric, they will significantly influence the compaction behaviour of the material. This influence was studied in [22].

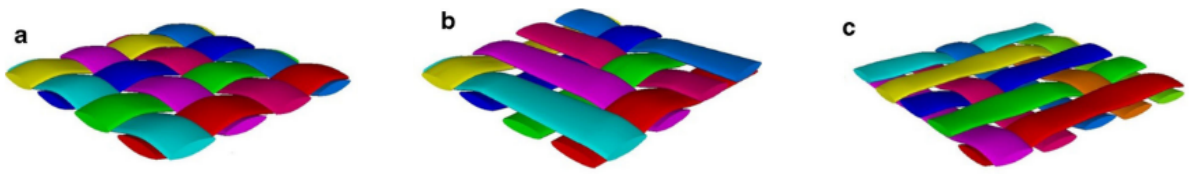

(a) Plain.

(b) 3/1 twill.

(c) 5H sateen.

Figure 2.3: Weaving patterns, [23].

Even though mats do not have as significant engineering applications as the previous fabrics in the aerospace and wind energy industry, they deserve to be mentioned due to their vast presence in researches, [11, 16, 24]. They are nonwoven fabrics composed either of chopped fibres or continuous bundles. The fibres are randomly orientated and are chemically bonded together using a binder. One reason that may explain their high presence in VIP studies, especially at the beginning of the development of this technique, may be related to the fact that their production technique is relatively more straightforward. In [24], the pressure distribution between an idealised fibre network was studied for mats and formulas were proposed to characterise it.

FEL are plies manufactured to be integrated into composite preforms to increase its overall perme-

ability and reduce the filling times during impregnation. They can be compared to resin films that are embedded in the structure, but they are composed of layers of fabric stacked in a typical sandwich-like structure, figure 2.4. Since they are included in the layup, they will be part of the final product of the process. Therefore, they will contribute to its overall properties. In terms of mechanical characteristics, Hammami [25] studied the individual compaction behaviour of FEL and its influence on the compaction behaviour of layups containing FEL and other fabrics. In [26] formulas were proposed to quantify the permeability variations with the addition of extra FEL in the layup, while in [27] the compaction behaviour of a FEL was described in terms of their fabrics' behaviour. A method for producing a sandwich panel was described in [28].

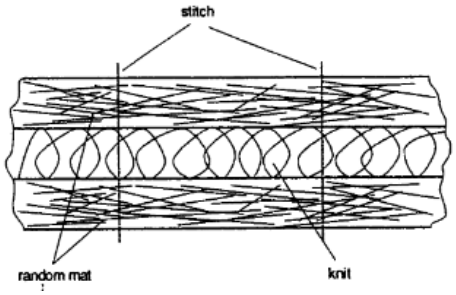

Figure 2.4: FEL composition, [27].

Simulation models of infusion processes require complete comprehension of the compaction and permeability behaviour of fabrics. Hence, the understanding of fabrics' geometries is of high importance. The diameters of bundles, their cross-section geometries, the spacing between them, and, if applied, the interlacement properties can be estimated from their manufacturing process. These characteristics can be modelled in geometry software to improve the predictions of their behaviours. Since accurate geometry modelling allows a better infusion simulation, they have been the target of several studies.

For woven fabrics, the minimum energy principle was used in [29], and the Wisetek software was used to model all structural components in [20]. NCFs porous media and stitching influence on compaction were analysed with the support of Wisetek in [30]. In [31], both NCFs and woven fabrics were analysed in the same software. Finite Elements (FEs) can also be used to represent these geometries allowing the assessment of their compaction behaviour, as studied in [32, 33] for woven fabrics. More recently, a virtual fibre modelling method that includes fiber bending stiffness as a general textile modeling framework was proposed by [34].

2.1.3 Thickness variation phenomena

Stacking layers of fabric on top of each other to form a layup makes the contact surface between consecutive layers always different due to differences between geometries and randomness itself during the process. The nesting effect is a measurable phenomenon that represents the layers' ability to slide between themselves and is related to the perfection of the layers' alignment. When the number of layers in a stack is changed, the predicted thickness cannot be considered as the sum of all layers individual

thickness but needs to be adjusted to account for the Nesting Factor (NF), [23]:

$$\text{NF} = \frac{h_T}{\sum_{k=1}^{nol} h_k} \tag{2.1}$$

where h_T is the total part thickness and h_k the individual thickness of each layer in the layup, both in the same unit of length, and nol the layup number of layers. Furthermore, when Equally Oriented Textile Interfaces (EOTI) are present, figure 2.5, the nesting effect will be more significant. In that scenario, fibre bundles will move and place themselves between two other consecutive layer bundles. Hence, each fabric will have its nesting ability depending on their geometry [23, 31], number of layers in the layup, [3, 33, 35], and number of EOTI [19]. Since increasing the nesting of a layup implicates reduction of voids in the preform while measuring permeability, it is mandatory to have full knowledge of the nesting behaviour of the fabrics. Otherwise, it will be responsible for large scatter in data, [36].

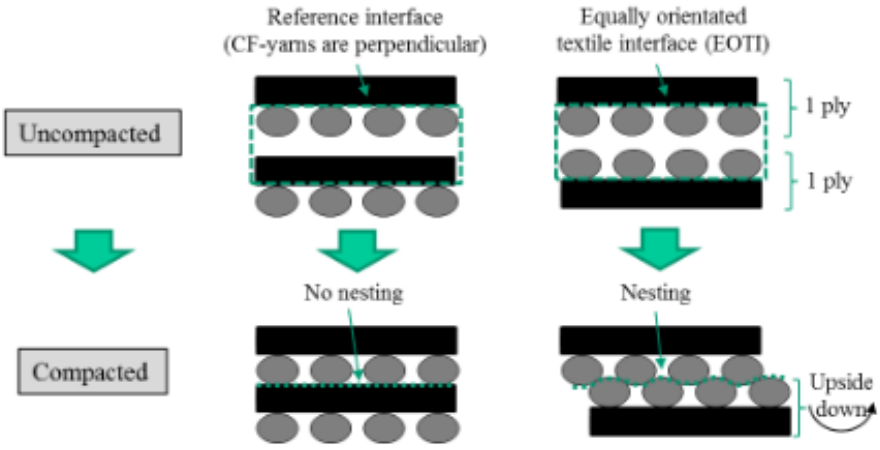

Figure 2.5: EOTI between consecutive layers, [19].

Lubrication is another measurable phenomenon that occurs in infusion processes. When Vacuum Infusion (VI) tests are being conducted without distribution meshes and with thickness measurement equipment over the preform, it is possible to measure a thickness reduction when the flow front reaches the sensor, figure 2.6. This variation results from the mixing of resin and fibres, whereas resin acts as a lubricant and allows a better accommodation of the fibres. The nesting that was already present in the preform under vacuum improves, and fibres are freer to move. This phenomenon is brief in terms of duration because the further advancement of the flow increases the local amount of resin and consequently increases the local thickness of the part. This effect was measured, and its importance was recognised in several articles [8, 37, 38]. In [37], it was concluded that the flow front velocity influences the degree of the lubrication measurements. In [39, 40], the authors measured this effect for several fabrics, noticing that its influence was more notable in random fabric, just as predicted. FEL also has a dictating influence over this effect if incorporated in the layup, as measured in [25].

When fabrics are under stress, they will deform to a new configuration. If the load is held, it can either remain with its configuration or constantly change into a different one. Materials that are considered viscoelastic will suffer changes in their geometry when facing loads for a certain period. Besides their

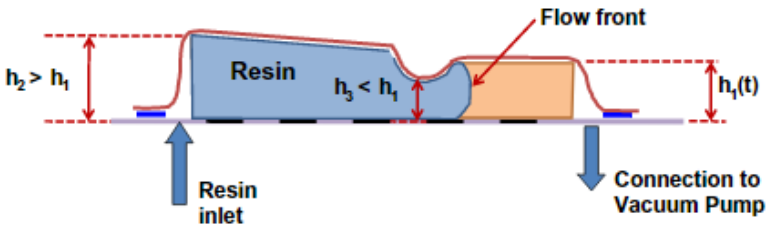

Figure 2.6: Lubrication effect demonstration in VIP, [41].

elastic behaviour, this viscoelasticity implies that these materials have time-dependent characteristics that must be acknowledged. This time phenomenon is very complex and can be attributed to a better nesting of layers during compaction and to a change of the aspect ratio of fibre bundles, [42, 43]. In VIP, there are two central moments when viscoelasticity is mainly manifested:

- **Settling**, when the fibres are compressed for the first time before infusion, in the pre-filling stage, the loads are applied for a certain amount of time, in which their thickness slowly changes with a constant load, [11, 41].
- **Relaxation**, after the preform is fully saturated and before curing starts, during post-filling, there is a period when part thickness also slowly changes, [27, 41].

The viscoelasticity is quantifiable by the relaxation factor that relates to the change in thickness during a period of steady load applied in terms of its initial value, [3, 9]. At an early stage, [27], several fabrics were studied in terms of their individual and in-stack relaxation. The relation between fabric relaxation and compaction pressure was studied in [44] and in its follow-up research, [39], it was demonstrated that there are specific locations of the preform that are severely influenced by viscoelastic effects and others where the effect can be neglected. In VIP tests on [16, 26], time lags between flow front or resin pressure and the compaction of the fabric were also attributed to the viscoelasticity of the material. This time-dependent phenomenon has real implications on the cured ply thickness of the VIP, and if the ultimate goal is to improve simulation models, this effect must be accounted and viscoelastic models should be improved and integrated into the compaction of the fabric, [11, 16, 43, 44]. Furthermore, they should also include lubrication effects in the models to fully mimic a VIP, [38].

2.1.4 Pressure and thickness plots

During the VIP the pressure and thickness varies along the length of the fabric. The vacuum level and the pressure distribution between resin and fabric inside the mould influence these moments. Typical resin pressure and associated thickness plots for filling and post-filling stages of a rectangular preform, figure 2.7(a), are visible in figures 2.7(b) and 2.7(c), respectively. At the pre-filling, before $t^* = 0\,\mathrm{s}$, the vacuum applied conducts to a steady and uniform value of pressure in the fabric. This stage corresponds to the maximum pressure supported solely by the preform and the dry regime's minimum uniform thickness. During the filling, $0 < t^* < 1\,\mathrm{s}$, resin impregnates the fabric and shares the available pressure between itself and the fabric. Hence, the resin pressure will constantly be increasing in the whole part,

proportionally increasing its thickness. When resin reaches the outlet port, $t^* = 1\,\mathrm{s}$, post-filling starts, and there is a pressure and thickness distribution plot along the length of the part. Since resin is more concentrated near the inlet than the outlet, that zone will have a higher resin pressure and thickness. The resin will be sparser in the outlet, implying a lower pressure and part thickness there. At the end of this stage for this test, $t^* = 2\,\mathrm{s}$, there is a more uniform distribution of pressure and thickness.

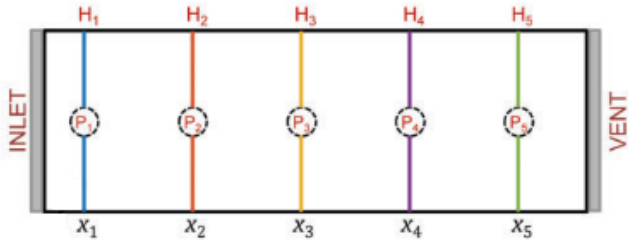

(a) Part geometry and sensors location.

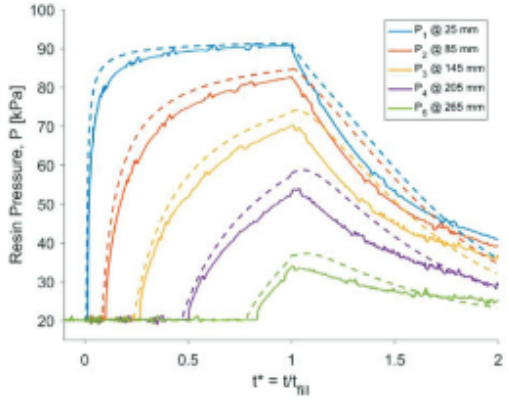

(b) Pressure Plot.

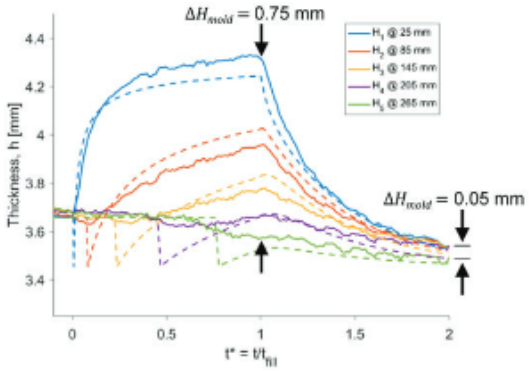

(c) Thickness Plot.

Figure 2.7: Pressure and thickness versus time measures and predictions, [11].

The pressure and thickness evolution during almost all VIP stages were reproduced for a material characterisation experiment in [39] and its pressure and thickness plots are detailed on figures 2.8(a) and 2.8(b), respectively. It is possible to calculate the thickness variations during the settling and relaxation stage using this procedure. Furthermore, the lubrication phenomenon is also measured there. The duration of all stages and the strategy used in each will influence the pressure and thickness outcomes. The viscoelasticity and pressure gradients may impose some resin movement, but they are restrained by the time available to occur. The fabric typology of each stacking is also very determinant in terms of how significant each of these thickness and pressure changes is, [16, 39, 44].

2.1.5 Simulation models

Mathematical models are tools that engineers and other professionals use to represent reality. They must be based on mathematical concepts that carry physical values. In VIP, and like in any other model, simulation models are mainly built on top of governing equations which may apply different assumptions and minor modifications to make them more accurate for specific cases. They allow the collection of simulation data that must be compared and validated with experimental data.

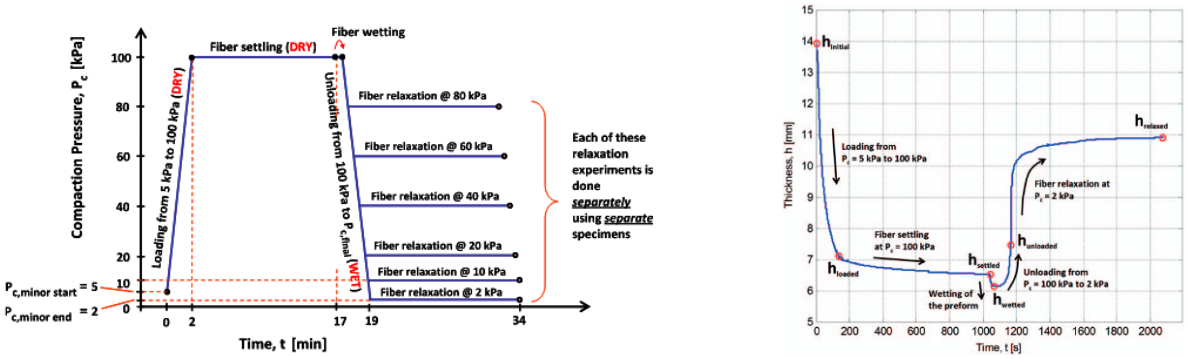

(a) Pressure Plot.

(b) Thickness Plot.

Figure 2.8: Thickness and pressure plot during a material characterisation, [44].

Governing equations

The three governing equations in VIP are the continuity equation, equation (2.2a), the momentum equation (*Darcy's Law*), equation (2.2b), and the stress equilibrium equation (*Terzaghi's Law*), equation (2.2c), [40]. The fabric's deformability is included in the model by the continuity equation, where the flow through the boundaries of a controlled volume of density ρ is related to its rates of expansion and contraction and the fluid media porosity, ϕ, [45]. The *Darcy's Law* represents the average volume velocity of a flow-through a porous media, $\vec{u}$, it was initially developed for hydrogeology, and in equation (2.2b) it is applied to a 1D flow, $\vec{u_x}$. This volume average velocity is related to the part permeability, K in $[\mathrm{m}^2]$, the resin viscosity, μ in $[\mathrm{Pa\,s}]$, and the pressure gradient, ∇P. *Terzaghi's Law* is the equation that relates the distribution of the total pressure available between the pressure supported by the fabric, P_c, and the resin, P_r, by the through-thickness direction, figure 2.9. This total available pressure equals to the atmospheric pressure, P_{atm}, that is constantly applied on the vacuum bag minus the vacuum pressure inside the mould, P_{vac}, which is mostly affected by the vacuum pump capacity and the quality of the setup.

$$\frac{\partial}{\partial t}\int_V (\rho \cdot \phi)\, dV + \oint_S (\rho \cdot u \cdot \hat{n} \rho \cdot u \cdot \hat{n})\, dS = 0 \tag{2.2a}$$

$$\vec{u} = -\frac{K}{\mu}\nabla P \rightarrow \vec{u_x} = -\frac{K}{\mu}\frac{\partial P}{\partial x} \tag{2.2b}$$

$$P_c = P_{atm} - P_{vac} - P_r \tag{2.2c}$$

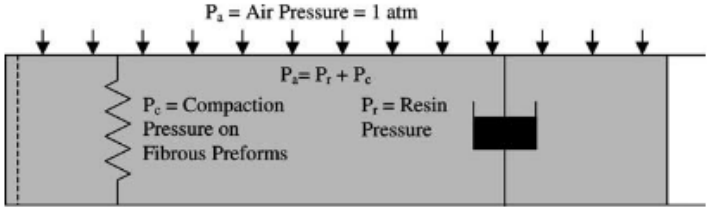

Figure 2.9: Pressure distribution inside the mould, [46].

One of the first authors developing a model integrating all these governing equations were Hammami and Gebart in [47]. The thorough study [48] followed this article, where significant VIP analytical steps were taken. With Correia et al. model, developed in [45], the pressure profile was for the first time assumed to be scalable. This model was further detailed in [45], where its assumptions and manipulations were demonstrated and justified. Correia et al. model is very well accepted in the scientific community, and several developments and validations have been conducted since then. The model was applied to predict the thickness of a part during VIP in [39, 41, 49]. [13] presents a variation of the model with an assumption that is proved to be plausible, simplifying the numerical calculations. This variation is also used in [38]. A very simplistic way to calculate the pressure profile is demonstrated in [40] and compared against the Correia et al. outcome. Besides understanding the pressure distribution in the fabric, it is imperative to fully comprehend the compaction effect on the thickness of the materials used, [39, 41], and include the typical fabric phenomena in the models. In [8], the experimentally measured lubrication was added to the Correia et al. model.

The models mentioned above are based on analytical formulas that usually are solved numerically with Finite Difference Method (FDM). Nonetheless, several software alternatives use Finite Element Method (FEM) to simulate the flow of resin through the porous media and calculate the final part thickness in VIP. In [50] the focus of the study was the inclusion of the through-thickness flow and the comparison of the results between VIP and RTM. The flow in [46] was a dual scale flow to account for the bundles' saturation, and its influence on the final part quality was assessed. The saturation model was applied in [35] and the through-thickness flow was used to separate the upper and lower mould filling times. Several engineering domains were included in a non-isothermal infusion model studied in [51]. [52] gathers outcomes from some software to have an improved characterisation of the material to include it in a multi-physics model. Other FE simulations are studied in [53, 54]. A different approach for the FE mesh is the utilisation of a level-set grid that accounts for a zone near the flow front where the fabric is neither wetted nor dried, but rather in a transition mode, [11, 55, 56].

Even though there is more content regarding the filling stage, the post-filling stage also has much scientific coverage. A model for the latter was developed in [7]. In [8], Correia et al. model was used for the filling analysis and another model was used for the post-filling. This mixing of models shows that it is possible to study both stages separately to relate them where one stage ends and the other begins. FEM is used for studying the post-filling stage in [10].

Regarding the curing stage, it is essential to highlight that this thesis does not include studies capable of predicting thickness variations in that stage. It was decided that, even though this is a very relevant stage, it is a very different field of study that requires a substantial background that is not shared with the previous two stages. This research also does not include thickness variations due to the demolding or other further part' treatments.

2.2 Experimental tests

An accurate simulation model of the VIP should include the compaction and permeability behaviour of a fabric. The constant changes in thickness during the process imply variations in its local properties. Therefore, they must be constantly updated in the model. The permeability of fabric can be summarised in its ability to allow a fluid passage through its porous media. The porosity and the channels in the geometry of the fabric will declare how difficult it is for the fluid-like resin to impregnate it. Regarding the compaction behaviour, applying a load on the fabric's surface will result in a geometrical adjustment on a mesoscale level. The fibres in each layer will convert the kinetic energy of the load into elastic and potential energy. For VIP, the compressibility is studied in the through-thickness direction since the atmospheric pressure is applied in that direction for plane setups. These behaviours can be studied and validated by experimental tests, which will be described in sub-chapters 2.2.1 and 2.2.2.

2.2.1 Compaction characterisation

The compaction behaviour of fabric is commonly described as a non-linear elastic behaviour, figure 2.10, divided into three stages, [57]. In the first section of the plot, regarding the period right after applying the load, the behaviour is linear and governed by internal adjustments of the fibre bundles that fill the pre-existing voids on the fabric. Then, a non-linear section occurs where both the voids and the fibre themselves start to be compressed. Lastly, a new linear regime is present where thickness is subjected to small deformations, and porosity almost reaches a constant value. Having acknowledged the compaction behaviour of the fabric, the next step for a complete characterisation fits the data into an empirical formula. There are several developments and approaches for this fitting, and the main idea retrieved from all possibilities is that each possible alternative of empirical formulas can be better suited for any particular type of fabric, range of pressures or layup.

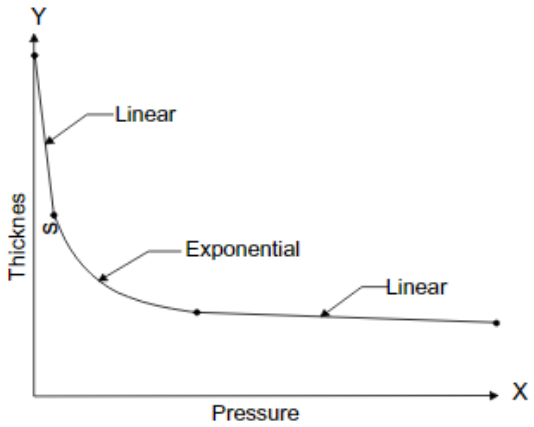

Figure 2.10: Non-linear elastic compaction behaviour, [22].

Robitaille and Gauvin in [58] gathered several data from different articles and fitted it into a two-parameter power law. The pair (V_{f_0}, B) represents the dimensionless empirical constants that describe the material, V_f the dimensionless FVF, and P_c the compaction pressure in $[\mathrm{Pa}]$. V_{f_0} is known to

represent the FVF correspondent to an application of one *Pascal* of pressure, $(P_c = 1\,\mathrm{Pa})$, and B is the compaction stiffening index, that dictates the asymptotic shape of the curve. This formula is fully adopted in the scientific community, and its application to characterise the compressibility of fabric is seen in several other articles, [11, 56, 59, 60]. In [35], a new constant was added to the previous equation to include a FVF value that represents a null compaction pressure on the fabric $(P_c = 0\,\mathrm{Pa})$. In [53], the authors split equation (2.3) in a system with two branches to account for the pressure history of the material. Variations of equation (2.3) were used in [3] for different types of compaction plots. A four-parameter power law was used in [18] to improve the fitting on a specific fabric. Other less used empirical formulas can be used to describe the material like seen in [20, 47, 61].

$$V_f = V_{f_0} \cdot P_c^B \tag{2.3}$$

Even though this is the most common approach to describing fabrics' behaviour, viscoelastic and non-elastic behaviours have also been studied. In [42], a time-dependent viscoelastic model was developed to characterise the compressibility of materials, and in [43] several similar models were analysed and compared. These models include thickness variation phenomena that are considered relevant to the simulation models of VIP, [11, 16, 38]. Nonetheless, their complex application on the existing VIP simulation models diminishes their applicability and are recurrently introduced as a follow-up step of the research. Non-elastic deformations were studied in [62], and their relevance was highlighted due to the experimental tests that show an equal level between permanent/plastic deformation and the elastic spring-back effect, figure 2.11. Furthermore, the article presented the importance of including a respectful amount of elastic, permanent and viscoelastic deformation into the compaction models to improve the thickness prediction of composites production.

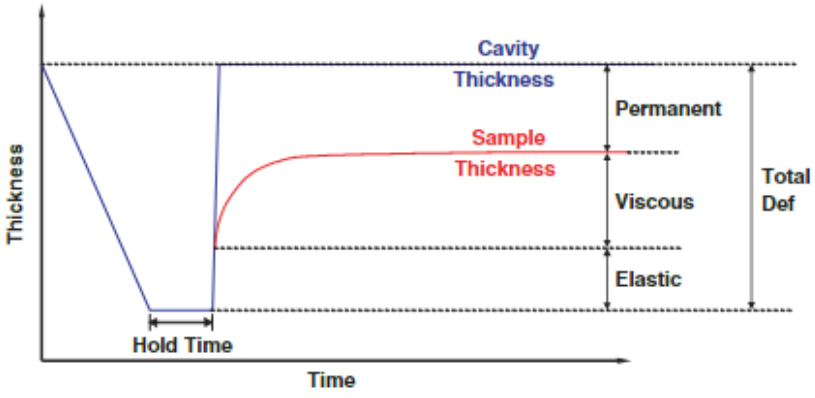

Figure 2.11: Elastic, permanent and viscous deformations, [62].

FEM approaches are also being applied to characterise the geometry and compressibility of fabric. [29] examples a mathematical model that can be used in FEM to describe the geometry of compressed woven material. In [22], energy-based numerical computations improved the predictions, and the utilisation of unit cells proved to be helpful in Finite Element Analysis (FEA). Improved models were developed in [32] with a multi-chain technique and in [33] with a hyper-elastic framework. A new constitutive model was applied in [61], but its validation was not accurate enough, and further tests are needed. More

recently, in 2021, a virtual fibre modelling technique was applied to predict the compressive response of fabric and the experimental tests support and provide promising findings for its application, [34].

The experimental tests to conduct the compaction characterisation can be done in two different setups. The traditional Universal Testing Machine (UTM) are the equipment mainly used due to its recurrent presence in universities. Its application is more forward since they are usually incorporated with the required distance and pressure sensors to retrieve the data, simplifying its preparation, [34, 41, 62]. The second option is to use a vacuum infusion setup without some resin-related components that are not necessary. Regardless of the more serious difficulty to mount the setup with proper sensor equipment, its similarity level with the one used in VIP make its use valuable, [3, 13, 63]. A complete comparison between compaction characterisation data from both alternatives is presented in [64]. Another handy piece of equipment is the *Kawabata* Evaluation System for Fabrics (KES-F) that is expensive and allows very accurate characterisation of compressibility for lower loads, [65]. This pressure range restriction can be complemented with further application of other equipment for other pressure ranges, as in [66]. Regarding the sensors equipment used in the VIP setup to measure thickness, some options are distinguishable concerning its precision and price. Further details of these devices preparation and implementation can be seen in [8, 9] for Linear Variable Displacement Transducer (LVDT), in [55, 64] for Digital Image Correlation (DIC), and in [11] for Structured Light Scanning (SLS).

During the compressibility tests, several parameters can be analysed. Some articles focus only on studying some parameters, and others look for a broader picture of the tests and, at the same time, provide a smaller analysis of them. The most recurrent parameters are:

- **Number of Layers -** The typical finding is that increasing its value will result in a best overall nesting which will reduce the thickness per layer value, reaching a higher FVF for the same compaction pressure, [12, 21, 23, 25]. In [35, 67] it was found a different trend, where the thickness per layer value increases while increasing the number of layers. In [9] and [3] a linear trend was assumed based on evidence. Since this correlation between the number of layers and FVF is mainly dependent on the nesting effect, the fabric typology and stacking procedure are believed to be the primary influencers of this trend.

- **Saturation -** The fabric can be in either one of two states, dry or wet, neglecting the transitioning state when fibres are being impregnated, and materials should be studied in each state separately, [9]. If compressing a layup in its dry state, it will reach a thickness value that will be higher than if it was in a wet state, [25, 35, 41, 68], which means that the resin present in the fabric contributes to its relative movement and allows it to better nest and achieve higher FVF values.

- **Combination of Fabrics -** Different materials can be combined in an infinite number of layups, and each one of them will have its specific behaviour worth studying, [19, 25, 68]. Regardless of that, there are similarities between individual and collective behaviour of some materials that can be standardised, allowing the assessment of a layup behaviour by its parts, [27, 60].

- **Compaction Type -** The application of a type of compaction will have a different effect than the application of different compaction, [3, 19, 68]. If the compaction pressure is applied on one

layup step by step with a holding interval in each step, the part thickness will be different from one subjected to cyclic compaction when reaching its maximum pressure. If a study is being conducted to predict a specific production process, it is important to match the analysis to that process.

- **Fabric Geometry -** The stitching type and stitching tension of a layer, the spacing between fibre bundles, the weaving pattern or any other geometric characteristic can also be the target of a study, [9, 12]. Compressing layups with different geometries may allow concluding each geometric characteristic's influence on a material's compaction.

2.2.2 Permeability characterisation

The study presented in the following chapters of this thesis is not directly related to the permeability of materials. Nonetheless, due to its high relevance in this field of studies, it is imperative to retain knowledge about this behaviour to understand the VIP fully. Similar to compressibility, there are empirical formulas capable of providing analytical estimations of the permeability values of a fabric or a layup. The most recurrent one is the *Kozeny-Carman* formula, equation (2.4), where k_0 is the empirical constant in $[\mathrm{m}^2]$ that characterises the material behaviour.

$$K = k_o \cdot \frac{(1 - V_f)^3}{V_f^2} \tag{2.4}$$

The application of equation (2.4) can be found on [8, 45, 47], some other empirical alternatives were developed and used in [13, 15, 53]. In [53], the *Kozeny-Carman* formula suffers a modification to include a new empirical constant. In [14, 15], it is possible to see different techniques which allow the calculation of the experimental permeability of fabric in its principal directions. If different layup combinations are the target of a study, some analytical formulas combine each material permeability property to calculate the overall layup permeability, [26], similar to what was mentioned for the compaction.

The permeability behaviour can be assessed by resorting to setups with both sides of the mould rigid, [38, 41], or with VI setups, [11, 26, 52, 56]. The former has some similarities to the UTM in the sense that one of the mould sides is adjustable, and its position can be defined according to the desired thickness inside the cavity. Besides the pros and cons of each setup alternative, it is believed that the main reason for the deliberation is based on the available equipment and material resources. In the rigid mould, it is vital to ensure the sealing of the cavity, which in the VI setup is ensured by its traditional experimental procedure to guarantee vacuum. Another setup alternative was developed in [36], the PIERS setup, whereby the use of electrical sensors mitigates the main drawbacks of measuring permeability due to its high bending stiffness and testing rate.

The inclusion of a distribution mesh in experiments drastically changes the resin course through the fabric. As previously mentioned, instead of occurring impregnation by the in-plane direction, the phenomenon will occur by the through-thickness direction. In [68], it is highlighted the importance of matching the permeability of the distribution mesh and the fabric to achieve a desired shape of the flow front. In case the part is a layup composed of different materials, it was discovered that the overall permeability would be very dependent on the outer layers of the layup, [60]. Another relevant parameter for

the permeability measurement is whether the preform is unsaturated or saturated, corresponding to an unsteady and steady flow, respectively. It is possible and practical first to impregnate the dry fabric and measure its unsaturated permeability, to then change the part thickness while keeping providing and collecting resin to measure saturated permeability values, [38, 41]. In [38], not only was assessed the efficiency of measuring the permeability in both unsaturated and saturated conditions, but also whether the system was under constant pressure or a constant flow rate during the infusion. The experimental tests concluded that the best combination to measure permeability is by constant pressure under unsaturated conditions.

2.2.3 Vacuum infusion

Usually, studies that contain VI tests have the main goal to validate simulation models for certain conditions. Nonetheless, some studies aim to validate setups, compaction and permeability empirical models or even study any parameter of interest. The pressure distribution profile in VIP is precious to understand because not only does it allow the calculation of thickness and FVF distributions, but it is also the first step towards the development of control actions and infusion strategies to achieve any production goal. In a wide range of particularities, it is possible to see the pressure profile of VI tests being measured by sensors, [37], and predicted by models and validated by the measurements, [11, 40, 45, 48, 55]. The pressure distribution profile is used to apply empirical compaction formulas to calculate the FVF distribution, [45]. Then, equation (2.5) can be used to calculate the thickness distribution, [37, 39, 40, 45], being h the part thickness in $[\mathrm{m}]$, ρ_{sup} the areal density in $[\mathrm{kg/m^2}]$ and ρ_{bulk} the volumetric density of the fabric in $[\mathrm{kg/m^3}]$. This equation is very well accepted in this field of studies, its application is very recurrent, and no other formula relating FVF to thickness was found. In a product or flow simulation models' development perspectives, the comprehension of the flow front progression and filling times are fundamental and therefore are the target of several studies, [13, 40, 45, 48, 49, 55].

$$h = \frac{\rho_{sup} \cdot nol}{\rho_{bulk} \cdot V_f} \tag{2.5}$$

In [37, 47], the line infusion is compared to the point infusion, presenting both benefits and drawbacks of each application. Through-thickness flow is studied in [35], where the impregnation times are compared for the upper and lower layer, and in [6] setups with and without distribution mesh, in-plane and through-thickness flows, respectively, are also compared. VIP is the sum of different stages, and the infusion can be studied in all of them, [43]. Prediction models for the post-filling stage are also a usual target of studies. Thus, there are articles in which VI experiments either focus on validating those models, [7, 8, 10], or to understand the influence and process improvements with control actions, [8, 10]. Similar to other setups, the use of the experimental equipment will define the data accuracy. Therefore, setup equipment is defined according to the goal of the study, ranging from aiming to measure the full laminate thickness, [37, 56, 63], to incorporate pressure sensors in the mould, [6, 49]. Instead of using empirical formulas to characterise the material, there is always the alternative to directly apply databases from characterisation experiments, [39, 41]. VI experiments can also be useful to validate models for

complex part geometries, [11, 52, 56], and to numerical simulation models, [53, 54].

2.2.4 Data analysis

VIP is a composite production process that is very well implemented in several industries. Thus, there are very well-structured experimental procedures to produce confidential products to be protected by the corporate world. Nonetheless, for academic research purposes, it is more beneficial to have standards in the experiments to allow authors to replicate and continue developing and validating any model or concept. Furthermore, benchmark exercises also represent a great advantage for science. These exercises aim to assess the data variability from different institutions using the same procedure for some experimental tests and define the best testing approaches in specific conditions. The mechanical behaviour of woven fabric was discussed in [69], more specifically in terms of its shear deformations in different setups, and data deviations were studied. Regarding permeability experiments, the study [15] was followed up by [14], and some improvements were made to the experimental procedure, improving the average outcomes. In terms of fabric compressibility, [70] is a benchmark that aims to standardise the way measurements are conducted. Some factors were analysed, and a vast scatter was found, leading to the recommendation and appeal for a second exercise.

Several studies follow slightly different procedures but aim to collect similar data to reach the same outcome. This data can be accessed and analysed, as it is done in experiments reviews. In [58], Robitaille and Gauvin gathered many data from similar studies and found general trends for the compaction and relaxation of different fabrics. In another study, [44], some fabrics were fully characterised, and its data developed a valuable database for other purposes. The benchmark exercises combined with a review of experiments could lead to a database created with a wide range of applications which would be helpful for any researcher in the field. The scatter on the data should be analysed well, and errors should be mitigated for the database to be effective. In [36], it is perceptible that the typical three to five repetitions per test are not enough and twenty are recommended based on statistical analysis. Some scatter reductions possibilities were well presented there. The huge scatter of the benchmarks [15, 70] and in the material characterisation in [13] support this need to increase the tests repeatability.

While defining designing of the number of tests in a study, its repeatability and conditions, it is crucial to have a holistic approach to the situation and know beforehand which factors are more important to assess and which ones can be neglected. There are several techniques for this filtration process, being the Design of Experiment (DoE) one very common. Different types of DoE must be chosen according to each situation, [71]. With this technique, it is possible to understand the individual and conjugated influence of each parameter. In [59], a DoE is fully applied. In that study, there are many input and output parameters, and the posterior data analysis resulted in analytical formulas capable of predicting the thickness of a part. [18] is another example of a DoE application, and in that particular case, the *Taguchi* model is used, and an Analysis of Variance (ANOVA) is also conducted to the parameters. In [43], a well-thought design of experiments allowed a thorough individual parameter influence, improving the conclusions of the study.

Chapter 3

Thickness prediction model

The purpose of this thesis is based on the goal to develop an analytical formula capable of predicting the cured ply thickness of a composite material. The literature review presented in chapter 2 was conducted aligned with possible solutions to this concern. However, the research direction suffered several iterations, and some alternatives were discarded during its evolution. Those iterations will be explained, and the justifications supporting all decisions will be presented in this chapter.

3.1 Model requirements

To develop the pretended model, a set of requirements were settled by all parts: the student, the professors and *Vestas*. Without these ground rules, it would be possible that the ideas from one part would not match the other, and some part of the study could be immediately discarded. Thus, alongside the literature review study, some ideas were shared, and the following terms were agreed upon:

- **Not include flow simulation -** *Vestas* was responsible for several theses in different universities, and this requirement was chosen to avoid overlapping the projects' content.
- **Use of simple software -** Again, other projects were developed to assess the utilisation of different and complex software. This model should only use simple software, such as *MATLAB*.
- **Model inputs:**
  - **Layup design -** This includes the different fabrics applied, their number of layers and the stacking sequence from top to bottom. Fibres bulk and areal density must also be included.
  - **Pressure conditions -** Referring to the available pressure on the setup.
- **Model output:**
  - **Thickness distribution -** Having the input defined for specific sections, the output should be the distribution of the blade cured ply thickness of those sections.

- **Ease of utilisation -** In case the model is validated, it should be integrated into the current methodologies applied by *Vestas* for the production of blades. Therefore, its use should be easy to understand and shared by employees.
- **Ease of material database update -** The model will be developed with its limitations, addressed in section 3.3, which include the materials characteristics. Since the materials used may change from project to project, and the industry evolution will bring more material alternatives, it is crucial to develop the model so that these updates can be easily integrated.
- **Admissible error percentage -** The model validation was designed to be within the range of possible values, calculated with a predetermined admissible error percentage, chapter 5. This error is calculated to solve the current concern at the product production.

3.2 Model development

Step 1 | **Models benchmark**

As previously mentioned in section 2.1.5, Correia et al. model is well accepted within the scientific community due to its validations by experimental tests. Since its application suited the model requirements and it was possible to find all the empirical data needed to run it in literature, it was decided to use it as a first approach for the prediction model. Furthermore, Akif Yalcinkaya and Sozer model, demonstrated in [13], is a simplification of the former model, which was also corroborated by experimental tests. Thus, Correia et al. model will be demonstrated, and then the simplification will be explained. For an initial phase for the model development, these were the elected ones for study.

The conditions to apply these models include the use of a VI setup without distribution mesh, to have an in-plane impregnation, using simple geometry to assume to be standing before a unidirectional flow. The model uses the governing equations of VIP to predict the resin pressure distribution in the preform by successful iterations, allowing to use *Terzaghi's Law*, equation (2.2c), to calculate the compaction pressure distribution. Later, the pressure is used to calculate and update thickness in each iteration, consecutively using equations (2.3) and (2.5) for that purpose.

It is important to distinguish the resin pressure field from a resin transfer moulding process, RTM, and another from VIP. Since both sides of the mould in RTM are rigid, it is possible to impose a constant cavity thickness during the whole process, figure 3.1, which is impossible in VIP. This restriction implicates that during all RTM process stages, the compaction and permeability properties are constant. Therefore, the resin pressure field in RTM will be represented by a linear field from the inlet, $P = P_{in}$, until the outlet, $P = P_{out}$.

The governing equations (2.2) must be manipulated and interconnected to develop the prediction models. Initially, the continuity equation (2.2a) must be simplified to an unidirectional flow embracing the whole thickness of the part. The manipulations are detailed in appendix A.1 and the final outcome is presented in equation (3.1):

$$\frac{\partial h}{\partial t} = -\frac{\partial}{\partial x}\left(\vec{u}h\right) \tag{3.1}$$

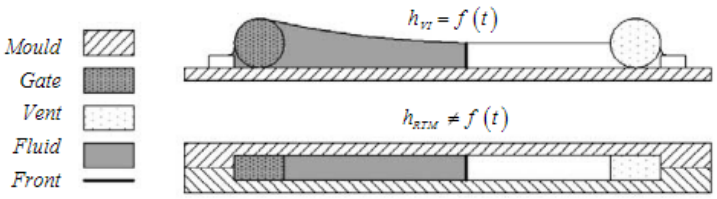

Figure 3.1: VIP versus RTM thickness progression, [45].

Then, the average fluid velocity represented by *Darcy's Law*, equation (2.2b), can be integrated in the continuity equation. The mathematical manipulations from equation (3.2a) to equation (3.2b) are detailed on appendix A.2.

$$\frac{\partial h}{\partial t} = -\frac{\partial\left(-\frac{h \cdot K}{\mu} \cdot \frac{\partial P}{\partial x}\right)}{\partial x} \tag{3.2a}$$

$$\Leftrightarrow \quad \frac{\partial^2 P}{\partial \alpha^2} = \left(\frac{h^* \cdot \alpha - 1}{h} \cdot \frac{\partial h}{\partial P} - \frac{1}{K} \cdot \frac{\partial K}{\partial P}\right) \cdot \left(\frac{\partial P}{\partial \alpha}\right)^2 \tag{3.2b}$$

The dimensionless variable α represents the scalability, $\alpha = 0$ corresponds to the setup inlet and $\alpha = 1$ to the flow front, regardless of time. The variable h^* represents the dimensionless thickness of the preform at the flow front, and P represents the fluid pressure inside the cavity. Equation (3.2b) is an Ordinary Differential Equation (ODE), and by its definition, it is an equation that contains one or more functions of one independent variable and its derivatives. In this particular case, the independent variable is the resin pressure, and there are present two functions, the thickness and the permeability of the stacking. One essential characteristic of this ODE is that it is not time-dependent. During the manipulations, it was assumed that the resin pressure field was scalable. This scalability means that independently of the flow front position on the fabric, the pressure field of the resin from the inlet until the flow front is known. If the preform is fully saturated, it means that this pressure field goes from the inlet to the outlet port of the setup, figure 3.2.

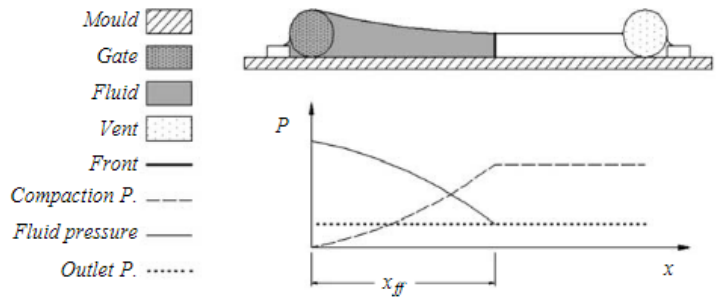

Figure 3.2: Scalability of the flow front, [45].

Having reached the ODE, it is clear that a material characterisation regarding its compaction and permeability behaviour is mandatory. As mentioned in chapter 2, there are two ways to include the material characterisation, fitting the experimental data into empirical formulas or using databases and applying

FDM for the derivatives. In literature, there is a higher abundance of empirical data than databases. Therefore, empirical formulas will be used. It was decided to apply the main empirical formulas for each behaviour in order to increase the data available, being them equation (2.3) for the compaction and equation (2.4) for the permeability. Their derivatives are presented in equation (3.3a) and equation (3.3b), respectively. Their demonstrations are available in appendix A.3.

$$\frac{\partial h}{\partial P} = \frac{\rho_{sup} \cdot nol}{\rho_{bulk}} \cdot \frac{B}{V_{f_0} \cdot P_c^{B+1}} \tag{3.3a}$$

$$\frac{\partial K}{\partial P} = k_o B \cdot \frac{\left(-3P_c^{-B-1} \cdot V_{f_0} + P_c^{B-1} \cdot V_{f_0}^3 + 2P_c^{-2B-1}\right)}{V_{f_0}^2} \tag{3.3b}$$

Finally, the ODE must be solved numerically. For that purpose, some discrete central differences are applied, and a numerical solution is achieved, equation (3.4), with n being the index of the discretisation and i the iteration number. Full demonstration of these expansions are detailed in appendix A.4.1.

$$(P_{n-1} - 2P_n + P_{n+1})|_i = \left[\left(\frac{h_n^* \alpha_n - 1}{h_n} \cdot \left(\frac{\partial h}{\partial P}\right)_n - \frac{1}{K_n} \cdot \left(\frac{\partial K}{\partial P}\right)_n\right) \cdot \left(\frac{P_{n+1} - P_{n-1}}{2}\right)^2\right]\Bigg|_{i-1} \tag{3.4}$$

Regarding the Boundary Conditions (B.C.), the pressure on the inlet and on the outlet must serve an input for the model. The first and the last unit of discretisation will have fixed pressures, $P_1 = P_{in}$ and $P_n = P_{out}$. where P_{in} equals to the ambient pressure minus the pressure losses between the resin deposit and the setup due to gravity, $P_{in} = P_{atm} - \rho_r g h$, and P_{out} equals to the vacuum pressure, $P_{out} = P_{vac}$. The variable ρ_r represents the resin density in $\left[\mathrm{kg/m^3}\right]$ and g the gravitational acceleration in $\left[\mathrm{m/s^2}\right]$ The inlet pressure does not include pressure loses by friction in the formula but an accurate calculation should assess this concern.

Akif Yalcinkaya and Sozer model assumes that thickness variation is independent of time and approximates the Left Hand Side (LHS) of equation (3.2a) to zero, leading to equation (3.5). Although this seems to approximate thickness constant in time, the authors' highlight that resin pressure will be solved in a quasi-steady approach and thickness will be updated in each iteration. At the results section of [13], the order of magnitude of each term of the equation that led to equation (3.5) prove that the assumption is valid. The numerical solution of this model is detailed in appendix A.4.2.

$$\frac{\partial}{\partial x}\left(Kh \cdot \frac{\partial P}{\partial x}\right) = 0 \tag{3.5}$$

Step 2 | **Models application**

MATLAB software was used to implement both numerical solutions. The variables presented in table 3.1 serve as input parameters for the model. All fabric properties were collected from [45], and at this stage, it is important to highlight the saturation conditions used for the material characterisation. Ideally, this characterisation is conducted for both saturation conditions. Knowing the fabric behaviour for both its dry and wet state would be useful for running these models. At the pre-filling, the fabric is compressed

in its dry state. Then, the compaction pressure decreases with the resin entrance during the filling stage, and the fabric will unload in the wet state. At the post-filling, the resin pressure will mainly decrease in the fabric to find a better equilibrium, decreasing more at the inlet and increasing in a minimal amount at the outlet, provoking a wet state loading of the preform at the inlet and small unloading at the inlet. Even though Correia et al. acknowledge this lack of efficiency, they only use dry state data for running the model. The pressure conditions in table 3.1 were defined to represent a typical VIP.

Table 3.1: Input data for *MATLAB*.

Fabric Properties	$\rho_{sup}\ [\mathrm{g/m^2}]$	1000	V_{f_0}	0.11	$k_0\ [\mathrm{m^2}]$	71.8×10^{-12}
	$\rho_{bulk}\ [\mathrm{kg/m^3}]$	2540	B	0.126	nol	6
Pressure Conditions	$P_{atm}\ [\mathrm{mbar}]$	1013	$P_{in}\ [\mathrm{mbar}]$	900	$P_{out}\ [\mathrm{mbar}]$	30

While running the model, the resin pressure field is initiated as if it was a RTM process, being represented by a linear distribution from P_{in} to P_{out}. In each *MATLAB* iteration, the field will curve in the upward direction, representing a typical VIP resin pressure field. In figure 3.3(a) it is possible to observe the outcome of Correia et al. model in terms of its resin and compaction pressure, being the initial RTM pressure also represented for comparison, and both the thickness and FVF distributions of the part, 3.3(b). As predicted, the concentration of resin at the inlet, $\alpha = 0$, leads to a lower compaction pressure, higher thickness and lower FVF. At the outlet, $\alpha = 1$, the inverse is observed.

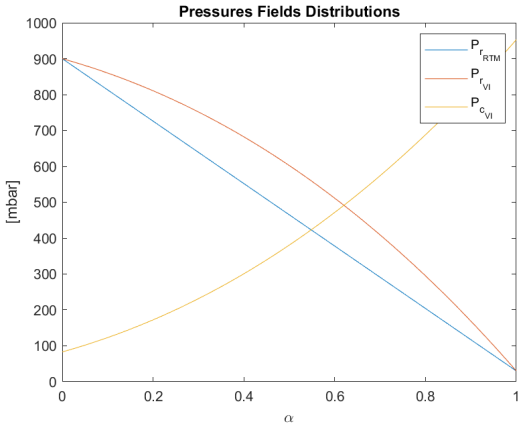

(a) Predicted Pressure Field.

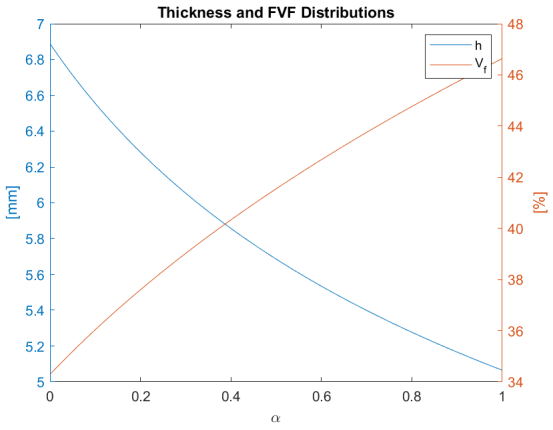

(b) Predicted Thickness Field.

Figure 3.3: Pressures, thickness and FVF predicted distributions.

Step 3 | Models comparison

The comparison between both models for the previous stacking showed that their differences could be considered insignificant and neglected. The number of layers of the stacking is irrelevant because the thickness prediction is directly proportional to this variable, implying that the relative error will be the same for a thinner or a thicker layup. Changing the number of layers would only imply a difference if new empirical constants were introduced to characterise the layup.

The maximum relative deviation between Correia et al. and Akif Yalcinkaya and Sozer models thick-

ness predictions is calculated by equation (3.6). Correia et al. predicted thickness is used in the denominator because thickness values throughout the preform length are always smaller for this model, except for the inlet and outlet where the thickness is the same.

$$\epsilon_{r_n} = \frac{|h_{Correia_n} - h_{Yalcinkaya_n}|}{h_{Correia_n}} \cdot 100 \quad \Rightarrow \quad \epsilon_{r_{max}} = 0.5456\,\% \tag{3.6}$$

with $h_{Correia_n}$ being the predicted thickness of a discrete unit by the Correia et al. model and $h_{Yalcinkaya_n}$ the one from the Akif Yalcinkaya and Sozer model, both in the same unit of length, and ϵ_{r_n} the relative error in $[\%]$ for that same discrete unit. The variable $\epsilon_{r_{max}}$ represents the maximum error value within all discrete units.

Since the difference between the outcome of the models can be neglected, Akif Yalcinkaya and Sozer model is considered to be the best approach since its code is slightly faster to run.

Step 4 | Inclusion of layups from different materials

To achieve the goal of developing a model capable of predicting the cured ply thickness of a layup with varied fabric, it is necessary to have some equations relating the different materials. As mentioned in subsections 2.2.1 and 2.2.2, some formulas characterise an overall layup by the individual behaviours of its components. The approach followed for the model development is based on integrating those formulas in the prediction model to achieve the goal of having as an input variable the layup structure.

Regarding the compressibility of the preform, equation (3.7) presented in [60] is considered to include the layup effects and will be applied. In a scenario where fabric is characterised for a certain number of layers (i.e. $nol = 5$) but in the layup, its number of layers is higher (i.e. $nol = 10$), it is essential to include the nesting effect has a thickness variability factor. Therefore, equation (2.1) is also included in the model for this specific situation. Furthermore, the nesting factor of the fabric must be measured or approximated for the transition from the characterised to the layup layers (i.e. $nol = 5 \rightarrow 10$).

$$V_f = \frac{\sum_{k=1}^{nol} \rho_{sup_k} \cdot nol_k}{\sum_{k=1}^{nol} \frac{\rho_{sup_k} \cdot nol_k}{V_{f_k}}} \tag{3.7}$$

For the stacking permeability, a weighted average approach was applied, as in [26]. The use of equation (3.8) is not very representative for thicker layups because for that cases the flow front can be very distinctive from layer to layer.

$$K = \frac{\sum_{k=1}^{nol} K_k h_k}{h_T} \tag{3.8}$$

These formulas will be applied in each iteration of the model. The individual compaction and permeability are calculated for each fabric using the pressure field. These formulas are applied to calculate the total compaction and permeability of the layup, and finally, a new iteration can be followed using the overall layup properties.

3.3 Model limitations

Mathematical models are developed to be as accurate and possible. To achieve this accuracy, the developers should account for all phenomena included, be careful with assumptions and manipulations, and assess the model limitations to mitigate them as further as possible, [72]. The model developed in the previous section also has its limitations, and it is essential to acknowledge them before defining its range of applicability.

The first mathematical manipulations assume that the model is applied to a unidirectional flow for a part with simple geometry. Hence, it does not include drape deformations present in moulds with complex geometries. Even though the model is pretended to predict the cured ply thickness of composite material, it only accounts for the pre-filling and filling stage. The reason to not include the post-filling stage is related to the VIP applied at *Vestas*, where the gelation time of the resin system is elected to more or less correspond to the instant when resin reaches the outlet. The goal is to shorten the blades' production duration since the market is very competitive, and this characteristic may be decisive for the project to thrive. It was already stated that the curing and demolding stages would not be assessed in this thesis due to a mismatch of educational backgrounds. The interference of the consumable materials was also not included in the model because the industry considers it does not have any relevant impact.

Even though different authors validate both models from literature, the sample is still tiny and systematic errors can occur. Furthermore, they do not include either possible lack of repeatability in VIP or possible loading history of fabric. The materials suppliers for the production also have a significant role in the models' accuracy related to the quality of their deliveries. The models will not include deviation on materials properties such as densities, viscosity, and fabric geometries that are not expected to be significant.

The material characterisation tests have an extreme impact on the prediction models. If these tests are conducted without special attention, their outcomes may be corrupted and jeopardise the prediction. These characterisations also imply a limitation of the model because they can only be applied to previously characterised materials. Furthermore, even if associated with a small error, empirical formulas will always input errors to the prediction. The empirical formulas used to describe the compaction behaviour only have non-linear elastic behaviour. Viscoelastic and permanent deformations are not included and, depending on the VIP procedure, may have a very significant impact on the final thickness. The nesting phenomenon is very well understood in the science community, but its effects in interfaces between different fabrics and the influence of EOTI has not been the target of enough studies and still has a lot to be studied. Thus, these two points will also serve as limitations to the developed model.

3.4 Model applicability at *Vestas*

The developed model and its outcomes were presented to *Vestas*' employees to understand how the available data in the company could be used to validate and improve the model. Several discussions noticed that this model would not match most composite productions, including blades, even if wholly

validated. Therefore it would not be applicable for *Vestas*. This section will present the incompatibility between the model and the process alongside a solution and a structured plan for accomplishing the thesis objectives.

3.4.1 Blades design

The major adversities that do not allow to apply this model to the production of the blades are presented in bullet points:

- **Distribution mesh -** Almost all composite materials produced by the VIP use distribution meshes in their setup in order to reduce the infusion times. Particularly to the turbine blades, their relative thickness would make it unfeasible to match product deliveries deadlines.
- **Layup variability -** In a typical blade, the layup in the root only has only a few similarities with the one on the tip. Since the structural efforts in both zones are different, the layup will vary according to its needs.
- **Permeability and compaction data -** *Vestas* has many data regarding previous blade models and has already conducted some studies to acknowledge these properties for the fabric used in the layups. Nonetheless, these studies were not similar to the ones necessary to run the prediction model. There is a lack of data regarding these two properties of the fabric applied in the current layups.
- **VI stages duration -** Each blade model has its defined procedure that must be followed during the process. Nevertheless, infusions of such considerable-sized parts have several obstacles that may affect the duration of all stages, especially during the pre-filling stage. If any air leak is present, it is required to analyse the whole blade, which could take a significant time.
- **Setup complexity -** The setup to produce a blade is not similar to the ones presented in any of the articles in the chapter 2. The resin inlets and outlets are not as linear as usual, and a very complex system combining different inlets and outlets is applied in the production of a blade. Furthermore, the fluid does not flow in a plane mould since blades have a curvature associated.

All of these production characteristics violate the principles that support the developed model. At this point, it was decided that even if validated, the model would not be appropriate to predict the thickness of a blade and would not be helpful for *Vestas*. The option of validating the model was still at reach, but it was decided to look for other options to predict the cured ply thickness of a blade that would have more meaning for *Vestas*.

3.4.2 Main carbon path

Vestas' blades are mainly produced with glass fibre combined with other materials, and there are only two sections where carbon fibres are also included. These sections are denominated as main carbon

path and trailing edge carbon path. This thesis will not address the reasons to have these carbon-rich zones nor the justifications for their positioning.

Focusing on the main carbon path, the section has some characteristics which make it more suitable for this study:

- **Setup geometry -** Despite being a rough approximation, in this section, the setup can be considered plane. The blade curvature is estimated to start at both ends of the main carbon path in the chordwise direction.

- **Number of layers -** As previously mentioned, the layup varies significantly throughout the spanwise direction. Nonetheless, all radius sections can be addressed separately. Besides the thick zones, thinner layups are also better to assess for a first model validation due to the lack of error propagation by layers increment.

- **Fabric variability -** Blades are produced with several fabrics in different parts according to the structural needs. At the main carbon path, the variability of fabric is not complex, and only a few materials are combined, relatively to other blade sections. Besides reducing the complexity of the prediction model, the material characterisation does not need to include several fabrics.

A great advantage of applying a prediction model to this section is related to its importance. The final blade incorporates a web in the spanwise direction assembled on top of the main carbon path. Having a predicted thickness inside the admissible error interval will allow its assembly into the final part. Therefore, it is imperative to predict the thickness in this section accurately.

The primary difficulty in assessing the main carbon path is due to the presence of carbon fibre. Since the carbon used is pultruded, its thickness will not change during VIP. Nonetheless, its weight impacts the layup pressure in the layup below. The carbon block is inserted between two blocks of glass fibre. Hence, the pressure in the upper block will differ from the lower block, and this pressure gradient should be assessed. Besides these points, carbon is neither present at the root nor the blade's tip, leaving some sections in the main carbon path, including glass fibre in the layup and some other less relevant components.

3.4.3 Model simplification

The primary outcome of the previous model was based on calculating the pressure distribution after the filling stage, and with that assess the thickness and FVF distribution. The model can be severely simplified by removing pressure as a variable. Instead of needing to understand the pressure field evolution, to predict the thickness along the main carbon path, it is only necessary to apply an empirical formula to calculate FVF, and thus thickness, from the local compaction pressure, like equation (2.3). The distribution of pressure is still present in the blade from inlet to outlet, but each section will be considered individually with a specific pressure condition. This pressure condition is further explained in chapter 5.1.

To apply this alternative simplified model, permeability data would not be needed. The model input would be the layup sections through the main carbon path, including the number of layers of each fabric and stacking sequence, and the empirical formulas would be applied to predict each different layup thickness. This method allows to development of a thickness prediction for the whole path.

The goal would be to find the best empirical formula capable of predicting the cured ply thickness more accurately at this point. A benchmark was conducted to find other options for empirical formulas. Equations (3.9a) and (3.9b) were found to be good alternatives for empirical formulas due to their validation in [3] and [18], respectively. Each formula has a set of empirical constants associated, being them (a, b, c) and (a, b, c, d).

$$V_f = a \cdot P_c^b + c \tag{3.9a}$$

$$V_f = \left(a \cdot P_c^b + c\right) e^{d \cdot P_c} \tag{3.9b}$$

The most recurrent formula, equation (2.3), is found to be the best approach due to its high applicability in the field and avoids the measurement of the constant c. This empirical constant corresponds to the FVF for a zero applied load, $(P_c = 0\,\mathrm{Pa})$, which is difficult to measure accurately. The goal is to use the main empirical formula and then compare the predictions using the other formulas if needed.

Even though this drastic simplification of the model to just an application of a set of formulas, it will be continued to be treated as a model and a *MATLAB* code will be developed to integrate the whole main carbon path layups and deliver a thickness prediction for the whole section of the blade.

3.4.4 Experimental tests plan

Having presented to *Vestas*' employees this alternative and have agreed on its advantages, a structured plan for the experimental tests and model validation was defined. This plan includes steps that will not be addressed in this thesis due to resource restrictions but will be included in future steps. The stages for this plan are:

1. **Material characterisation experiments -** Since there is no compaction data from the fabrics used in the blades layups, it was decided to conduct characterisation experiments as a first step, described in section 4.1. These tests exclude the need to use literature values of similar fabrics.

2. **Infusion tests for thinner composites -** To reduce error in the thickness prediction due to setup complexity and use of a higher number of layers, infusions of thinner plies will take place, described in section 4.2.

3. **Validation with cutup data -** *Vestas* cutup data will be used to validate the model predictions for determined blades, described in section 5.2.

4. **Pressure gradient analysis -** As mentioned, producing thicker laminates implies a pressure gradient in the through-thickness direction that may be assessed with the use of unique setups, which

include pressure sensors embedded in the mould, figure 3.4. The pultruded carbon should also be part of the design of experiment for these tests in order to assess its weight impact on the layup and pressure gradient.

5. **Pressure loss analysis -** The resin in the VIP of blades has to flow by the resin channel, and this will imply some pressure losses that will have some impact on the prediction model. Experimental tests can be conducted to assess this loss.

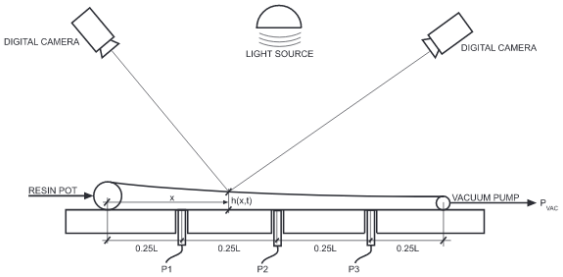

Figure 3.4: Setup with embedded pressure sensors, [55].

The last two points of the list will not be addressed in this work. Validation with the cutup data should be indicative enough to understand if the pressure gradient in the through-thickness direction and the pressure losses in the inlet are a priority, and other experimental tests should be conducted from there.

Chapter 4

Experimental tests

Aligned with the tests plan developed in subsection 3.4.4, two types of tests will be conducted, the material characterisation and the infusion tests. This thesis will not assess the permeability because it is not imperative to describe this behaviour in the current model.

The main reason to conduct the material characterisation experiments is based on the lack of available data of the individual compaction behaviour of the fabric applied on blades. Even though in literature similar materials were characterised, they do not have the same geometry nor properties. The infusion tests will be conducted to validate the model in a more controlled environment, involving a simple setup without complex geometries, avoiding stackings with non characterised fabrics and using the same number of layers as the ones characterised.

The first tests, described in section 4.1, can be easily distinguished from the second tests by the exclusion of the resin system. For the characterisation tests, the only fluid used is air. The resin system will only be applied for the infusions in the second type of test, section 4.2.

All tests were conducted by the author of this thesis in the composites laboratory in IST.

4.1 Material characterisation tests

The goal of these tests is to assess the compaction behaviour of fabric during two of the VIP stages, the settling and the unloading. The former is of particular interest for *Vestas* and not for the material characterisation itself. Blades production may have different settling duration per production, resulting in variability in the cured ply thickness that can be assessed in these tests. The unloading part of the tests will serve to calculate the empirical constants that describe the material's compaction behaviour. The thickness measurements during this stage will serve to calculate the FVF and later the empirical constants.

The saturation of the fabric is an important variable to define for these tests. The unloading stage can be either made with the fabric in the dry or wet regime. Ideally, as mentioned in the literature review, the characterisation is conducted for both regimes separately. Nevertheless, dry regime values are also well accepted in the community and validated by infusion experiments. An essential benefit of using

the fabric in its dry regime is that resin application concerns are avoided, the experimental procedure is simplified, and health risks are removed from the tests.

It is crucial to mention that regardless of the abundance of similar material characterisation tests to the ones conducted here, standard procedures to conduct these types of tests were not found. Usually, for several types of tests, there are norms to follow. For this particular case, the procedure was developed based on the literature review and *Vestas*' expertise in the VIP. Since this procedure was only experienced here, some adjustments were made throughout the tests, described in subsection 4.1.6.

4.1.1 Design of experiments

The DoE consists of the structured plan for the tests, namely to define the variables that will be assessed, the factors, and the range of each of them, the levels. This plan was developed aligned with the desired outcomes of the tests and its utility for *Vestas*. The three agreed factors to address in the tests were the number of fabrics, the number of layers and the number of repetitions for each test. Another variable that was considered as a possible factor was the number of EOTI. Its inclusion would culminate in a much higher degree of complexity.

The introduction of error due to lack of human experience in conducting the tests was predicted while designing them. Therefore, the strategy chosen was first to conduct the characterisation of one fabric only and improve the methodology used by the previous experience. Then, a second material could be characterised. The fabric chosen for the first tests was the glass fabric that is more present in the main carbon path, the unidirectional glass fabric with twelve hundred grams per square meter, UD $1200\ gsm$. Due to third parties imposing time restrictions, delays in the tests made it impossible to characterise more than one fabric.

Regarding the number of layers, the main carbon path goes from the root, thick plies, to the tip, thin plies, which is difficult to the idealisation of the DoE. Thus, thin to thicker layups were assessed, and only numbers of layers of power two were chosen to ease data interpretation between tests, $nol = \{2, 4, 8, 16, 32\}$. However, a first approach characterising $nol = \{4, 8, 16\}$ would be followed and after that data analysis, a decision would be made to characterise or not the rest of the number of layers, $nol = \{2, 32\}$.

The number of repetitions, nor, for each test was chosen according to what is more typical in the science community and adjusted to the time restrictions present. Each test was set to be repeated three times, $nor = \{3\}$.

It is recommended to randomise the order of tests to remove possible bias. Therefore, a randomiser algorithm was used and the final order is presented on table 4.1.

Table 4.1: DoE tests order for material characterisation tests.

Run	R1	R2	R3	R4	R5	R6	R7	R8	R9
nol	8	4	16	8	4	16	8	16	4

4.1.2 Setup design

The most expensive equipment for VIP is present in the IST laboratory, being them the vacuum pump and the resin trap, figures 4.1(a) and 4.1(b), respectively. The vacuum pump imposes a pressure differential in the setup, which acts as the fluid driver. The resin trap is a piece of essential equipment to use when conducting the VIP. Once resin surpluses are extracted from the preform, they will flow in the resin hoses until the resin trap, where a specific deposit is present to gather this excess and avoid the risk of resin reaching and damaging the vacuum pump. The lab equipment was cleaned, and further measures to ensure proper sealing were taken. Both devices were tested to ensure their good performance, and the vacuum levels reached were successful, $P_{vac} \approx 5\,\mathrm{mbar}$.

(a) Vacuum pump.

(b) Resin Trap.

Figure 4.1: Laboratory equipment.

Three variables were recorded with the assistance of sensors, the room temperature, the absolute pressure inside the cavity of the setup and the thickness of the fabric. For this concern, a manometer and two micrometres were used. The manometer displayed not only the absolute pressure but also the room temperature, figure 4.2(a). Its pressure resolution was of $0.01\,\mathrm{mbar}$. The usage of the digital, 4.2(b), and the analogical micrometer, 4.2(c), was quite different. Besides being easier to read values in the digital device, its tip arm length was appropriate for the thickness of all the preforms tested. The tip arm length of the analogical device was not long enough to measure the thickness of the thicker layups. Furthermore, the resolution of the digital device was of $0.001\,\mathrm{mm}$ against the resolution of $0.01\,\mathrm{mm}$ for the analogical device. Thus, it was decided only to use the digital device to have a more coherent thickness measurement.

It is important to ensure that the tip of the micrometre is not causing any indentation on the fabric. For that purpose, a metal presser foot is placed below the micrometre tip, figure 4.3. This part also has the advantage of measuring an averaged value of thickness below itself instead of a very punctual measure.

The majority of the materials was shipped from *Vestas* facilities, including the fabric and part of the consumable materials, such as the vacuum bag, release agent, peel ply, distribution mesh, the tapes

(a) Manometer.

(b) Digital micrometer.

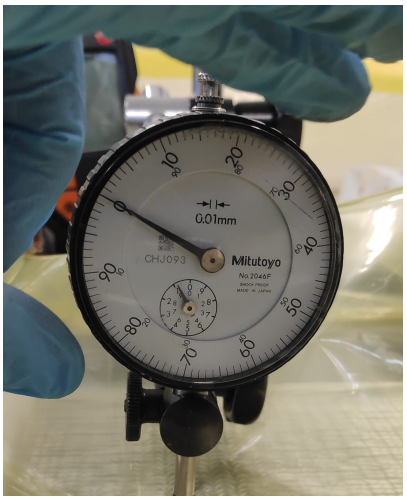

(c) Analogical micrometer.

Figure 4.2: Measuring equipment.

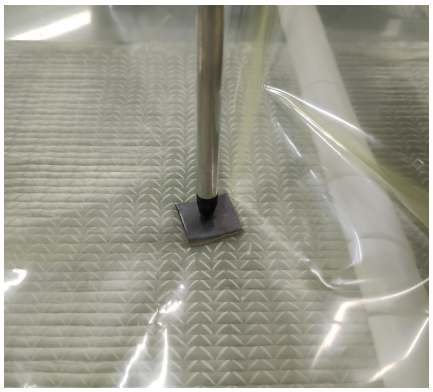

Figure 4.3: Presser foot application.

and the materials for the resin system. Some other consumable materials were bought in a local store, always resembling the ones used at *Vestas* productions. Not all of these materials were used for the material characterisation tests, as described below.

For both the material characterisation and the infusion tests, a disposable acrylic was used as the rigid side of the mould. The fabric dimensions were $200 \times 450 \quad \mathrm{mm}^2$ and the boundaries of the cavity, defined by the tacky tape, were around $350 \times 550 \quad \mathrm{mm}^2$. The setup preparation is described in the following steps:

1. **Preparing the materials -** Cutting the fabric and the consumable materials. For this task, tools from the IST workshop were used.

2. **Placing the tacky tape -** Defining the limits of the setup, figure 4.4(a).

3. **Placing the fabric -** Centralised with the tacky tape, figure 4.4(a).

4. **Fixing resin inlet and outlet -** Including resin hoses and resin spirals. Universal tape was used to fix these components, figure 4.4(b).

5. **Placing the vacuum bag -** Most challenging task because absolute sealing must be ensured. In strategic parts of the vacuum bag it was needed to build pleats to avoid to rip the vacuum bag after vacuum application, figure 4.4(c).

6. **Placing the sensors framework -** Using a metallic structure capable of fixing the equipment using its magnetic properties, figure 4.4(d).

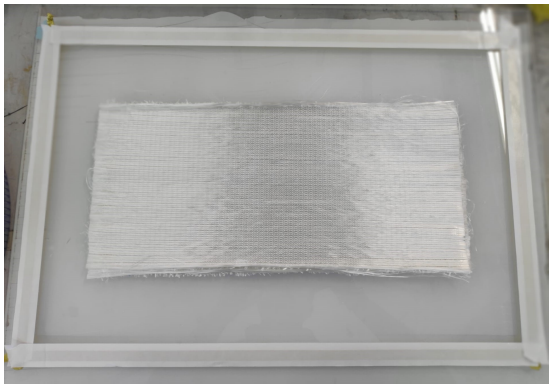

(a) Steps 2 and 3: Tacky tape and fabric.

(b) Step 4: Resin inlet and outlet.

(c) Step 5: Vacuum bag.

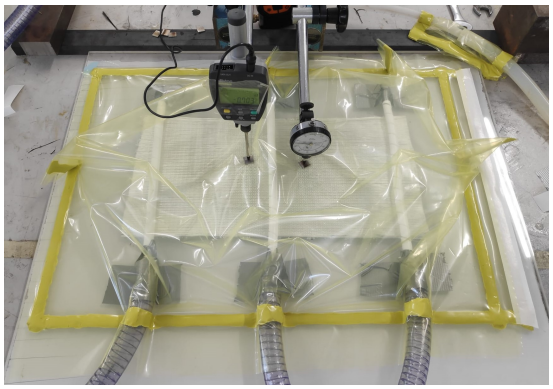

(d) Step 6: Micrometers.

Figure 4.4: Setup preparation steps for material characterisation tests.

Figure 4.4(d) still has both micrometres because the photo was taken during the first test. The values read in the analogical micrometre were discarded, and for the remaining tests, only the digital micrometre was used.

Regarding the resin inlet and outlet, figure 4.4(b), it is possible to see three exits from the setup. Typically, in VIP, two resin channels are placed, one at each end of the preform. Since these characterisation tests do not include resin, a different approach was considered. Both the left and the right spirals were used to extract air and were connected to the resin trap and vacuum pump by the utilisation of a tee connector, figure 4.5(a), to ensure a more homogeneous distribution of the vacuum pressure on the setup. The central spiral serves to connect the setup to the manometer, figure 4.5(b). With this approach, the micrometre can be placed close to the central spiral, at the centre of the preform. Thus, its thickness measurements will be associated with a high degree of accuracy to the pressure read on the manometer.

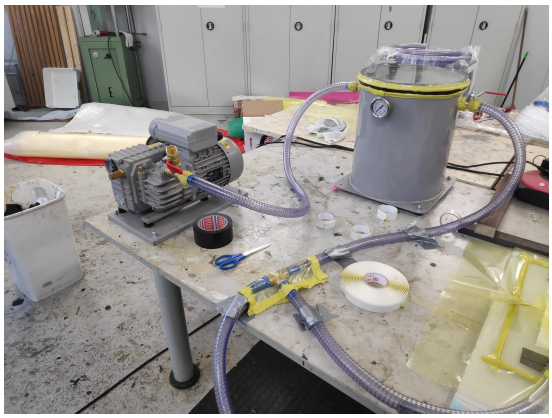

(a) Hoses from setup to vacuum pump.

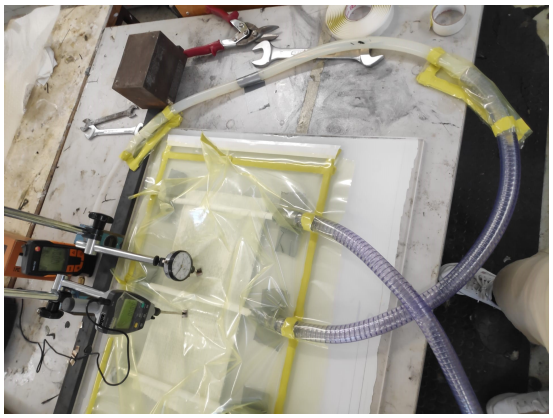

(b) Hose from setup to manometer.

Figure 4.5: Hoses from setup to vacuum pump.

The ball valve connected to the vacuum pump is helpful to control the airflow inside the vacuum pump, figure 4.6. When it is closed, the vacuum pump works at its maximum capacity. When the valve is opened, the pump performance will decrease, and full vacuum will not be reached on the setup. The air extraction will be balanced with the new entrance of airflow.

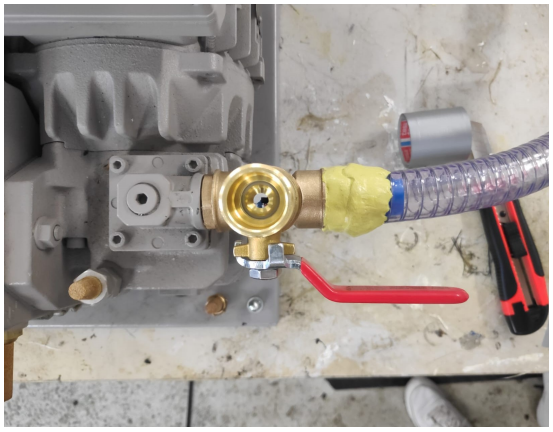

Figure 4.6: Vacuum pump ball valve.

Another great advantage of characterising the fabric in its dry state is that the resin hoses do not need to be replaced from test to test. Air is the only fluid flowing inside the hoses, and it does not compromise them for further applications, reducing the consumables of the tests and the time required for their preparation.

4.1.3 Experimental procedure

Before beginning to place the consumables in the setup, the fabric was measured in three areas represented in figure 4.7. An average of these values was calculated and was considered to be the initial thickness of the fabric, $h_{initial}$. Afterwards, the fabric was weighted, and the setup was prepared. At the final stage of the setup preparation, the micrometre was placed and was set to zero. Thus, its measures represent the thickness variations. During the tests, the thickness was calculated by equation

(4.1), with h_{sensor} being the thickness variation measured by the micrometre.

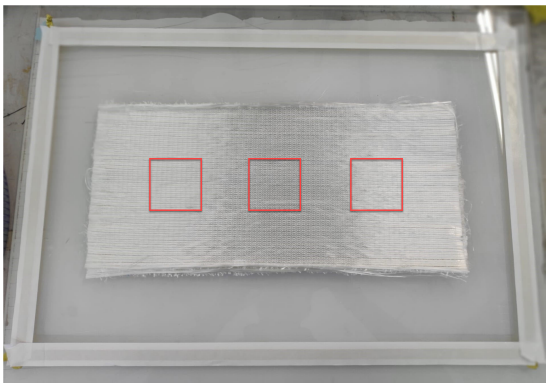

Figure 4.7: Areas for thickness measurements of fabric.

$$h = h_{initial} - \Delta h_{sensor} \tag{4.1}$$

Having the setup fully prepared for the test, the pressure plot visible in figure 4.8(a) is applied to the preform. In figure 4.8(b) a correspondent thickness plot is presented for a test with eight layers.

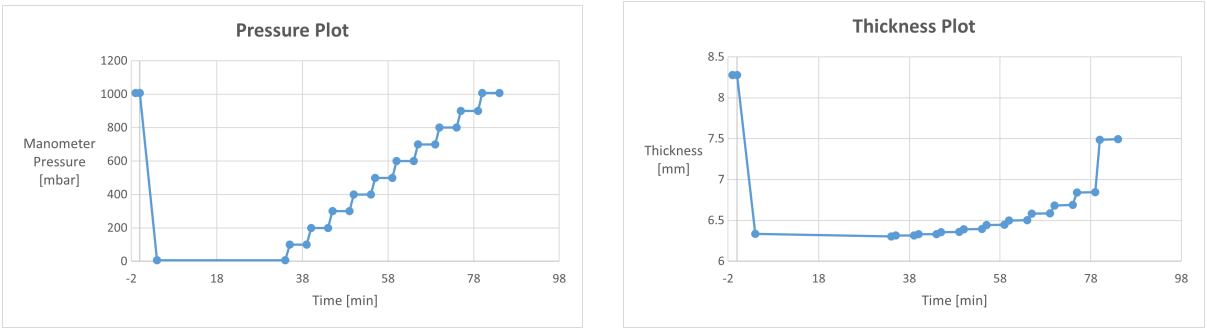

(a) Pressure plot.

(b) Thickness plot for $nol = 8$ test.

Figure 4.8: Pressure and thickness plots for material characterisation tests.

The pressure plot is divided into three stages:

- **Loading -** When The vacuum pump extracts the air from the setup and the pressure measured by the manometer goes from the atmospheric pressure until the vacuum pressure, $P_{vac} \approx 7\,\mathrm{mbar}$. Since infusion will not occur in these tests, the part will not be cured, and therefore there is no need to turn off the vacuum pump. This detail allows reaching low and constant pressure values in the setup without checking for potential leaks.

- **Settling -** The pressure is constant for thirty minutes, and thickness is measured in intervals of five minutes. During this stage, thickness is constantly decreasing at a slow rate.

- **Unloading & Relaxation -** Instead of splitting the unloading and the relaxation stages, the strategy adopted allowed to combine both. The ball valve was adjusted ten times in each test, representing increments of the pressure of around one hundred millibars, $\Delta P_{manometer} = 100\,\mathrm{mbar}$. The setup was unchanged for four minutes to account for the relaxation effects after opening the ball valve

and stabilising pressure at a new value. Thickness was measured in two moments in each iteration, at the instant when pressure stabilised and after the four minutes.

It was decided to neglect the values during the loading stage due to literature recommendations. During the filling and post-filling stages in the VIP, the thickness variations mainly occur due to unloading of the compaction pressure. Therefore, it is widely accepted that retrieving values for the material characterisation during this stage instead of the loading stage improve any thickness prediction model. Thus, the loading values in all tests were neglected, and the empirical calculations occurred for the last stage of the experimental procedure. The goal of mixing the unloading and the relaxation stages was to account for viscoelastic effects in the characterisation.

All characterisation tests were conducted to follow this experimental procedure in the most homogeneous manner possible to avoid human error in any quantity.

4.1.4 Data analysis - 1

This analysis is divided into two stages, the settling and the combination of unloading and relaxation.

Settling

The analysis conducted for this stage is based on the thickness variation from the instant when settling starts and when it ends. The formula applied to calculate the thickness variation in percentage, Δh_{set}, is presented in (4.2), where $h_{set_{initial}}$ and $h_{set_{final}}$ represent the thickness when settling starts and ends, respectively.

$$\Delta h_{set} = \frac{h_{set_{initial}} - h_{set_{final}}}{h_{set_{initial}}} \cdot 100 \tag{4.2}$$

The application of this formula for all tests led to the development of table 4.2. From this table, it is possible to understand that the ninth run represents settling values very disruptive while compared with the rest of the runs. Nothing unusual was reported during the test, but its values will be neglected and not considered for the rest of the analysis. The settling stage analysis can also be clustered by the number of layers, as presented in table 4.3.

Table 4.2: Thickness variation during settling.

Run	R1	R2	R3	R4	R5	R6	R7	R8	R9
nol	8	4	16	8	4	16	8	16	4
$\Delta h_{set}\,[\%]$	0.254	0.522	0.147	0.358	0.424	0.148	0.498	0.227	3.423

Table 4.3: Thickness variation during settling clustered by number of layers.

Number of Layers		4	8	16
$\Delta h_{set}\,[\%]$	Average	0.473	0.370	0.174
	Standard Deviation (SD)	0.049	0.100	0.038

Even though the Standard Deviation (SD) does not follow any trend related to the number of layers, the variation in the percentage of thickness variation during the settling stage has a clear trend with the number of layers. The average per cent thickness variation during the settling stage decreases with the number of layers. This trend supports the conclusion that the viscoelastic effect in time is less effective for a higher number of layers. The alignment of the fabric during stacking could be better performed for thinner layups, improving its nesting ability during settling than for thicker layups.

Unloading & Relaxation

The main principle for the analysis of this combined stage is based on applying linear regression to the data to calculate the pair of empirical constants that describe the compaction behaviour of the material, (V_{f_0}, B).

Linear regression relates two variables into a linear equation. In this scenario, the two variables are the FVF and the compaction pressure. Through the empirical formula (2.3) it is not possible to find a linear relationship between the variables. The logarithmic scale has to be applied for that purpose, equation (4.3).

$$V_f = V_{f_0} \cdot P_c^B \quad \Leftrightarrow \quad \log(V_f) = B \cdot \log(P_c) + \log(V_{f_0}) \tag{4.3}$$

Applying a linear regression to equation (4.3) is instantaneous, the relation between the linear regression and the empirical constants is demonstrated in the system of equations (4.4). In this equation, m and b represent the slope and the intercept, respectively. The Least Square Method (LSM) is used to apply the linear regression. The set of formulas to apply this method is presented on equation (4.5a) and (4.5b), with n being the length of the vectors x and y, or in this case, the number of points retrieved during the unloading and relaxation stage. While applying the LSM it is important to calculate the error associated with the fitting of the data. For that purpose, the R-squared factor is used, calculated according to equation 4.6.

$$\begin{cases} V_f = V_{f_0} \cdot P_c^B \\ \\ y = m \cdot x + b \end{cases} \quad \Rightarrow \quad \begin{cases} B = m \\ \\ V_{f_0} = e^b \end{cases} \tag{4.4}$$

$$m = \frac{n \cdot \sum(xy) - \sum(x)\sum(y)}{n \cdot \sum(x^2) - \left(\sum(x)\right)^2} \tag{4.5a}$$

$$b = \frac{\sum(y) - m \cdot \sum(x)}{n} \tag{4.5b}$$

$$R^2 = \frac{\left(\sum(xy) - \dfrac{\sum(x) \cdot \sum(y)}{n}\right)^2}{\left(\sum(x^2) - \dfrac{\left(\sum x\right)^2}{n}\right) \cdot \left(\sum(y^2) - \dfrac{\left(\sum y\right)^2}{n}\right)} \tag{4.6}$$

To ease the calculation of the empirical constants of all tests, a *MATLAB* code and a *Microsoft Excel* sheet were used. The thickness data was converted to FVF by the aid of equation (2.5), and then

the LSM was applied. The atmospheric pressure, the superficial weight and the initial thickness were measured for all tests using the manometer, a balance and the micrometre, respectively. These values are presented at table 4.4. Even though the unloading and relaxation were combined into one stage, the empirical constants were calculated for both distinctively. The thickness measurements from the moment when pressure stabilised in each pressure increment were used for the unloading calculations, and the ones measured after the four minutes waiting were used for the relaxation calculations. All empirical constants and the error associated with the LSM are presented in table 4.5.

Table 4.4: Conditions of the material characterisation tests.

Run	R1	R2	R3	R4	R5	R6	R7	R8	R9
nol	8	4	16	8	4	16	8	16	4
$\rho_{sup}\,[\mathrm{kg/m^2}]$	1.218	1.228	1.303	1.085	1.233	1.303	1.246	1.240	1.233
$P_{atm}\,[\mathrm{mbar}]$	1008.4	1006.9	1005.0	1008.1	1006.7	1007.8	1006.8	1010.5	1010.1
$h_{initial}\,[\mathrm{mm}]$	8.895	4.538	19.333	8.685	4.468	18.676	8.279	18.142	4.218

Table 4.5: Empirical constants calculated with LSM.

Run		R1	R2	R3	R4	R5	R6	R7	R8	R9
nol		8	4	16	8	4	16	8	16	4
Unloading	V_{f_0}	0.3842	0.4101	0.3856	0.4262	0.3924	0.3675	0.4072	0.3853	0.4257
	B	0.0337	0.0201	0.0276	0.0242	0.0329	0.0325	0.0324	0.0349	0.0280
	R^2	0.9996	0.9233	0.9954	0.9806	0.9702	0.9965	0.9924	0.9950	0.9562
Relaxation	V_{f_0}	0.3806	0.4102	0.3851	0.4197	0.3902	0.3654	0.4044	0.3822	0.4232
	B	0.0345	0.0201	0.0276	0.0256	0.0334	0.0330	0.0330	0.0357	0.0285
	R^2	0.9997	0.9232	0.9949	0.9834	0.9704	0.9966	0.9926	0.9948	0.9571

The R-squared factor values represent a successful fitting of the data into the chosen empirical formula. Therefore, for the first validation of the model, it was decided only to use this formula.

The empirical data for all tests were plotted in clusters of the number of layers to analyse their values separately. The average values of each cluster were also plotted for comparison. These plots are presented in figure 4.9, and their analysis enables it to understand that the SD does not represent any trend with the increment of the number of layers. The SD increases while passing from four to eight layers but severely decreases when passing from eight to sixteen layers. This variation can support the recognition of these tests as non-conclusive. When increasing the number of layers, the randomness of the results should be reduced by having more layers involved. Thus, the standard deviation should always decrease while increasing the number of layers.

If the results of these tests would be considered conclusive, it would be possible to assume that increasing the number of layers results in the best ability for the layers to nest and therefore increase its FVF, figure 4.9(d). Nevertheless, the amount of SD in the clusters analysis of unloading and relaxation makes it impossible to support this as a relevant conclusion. Furthermore, it goes against the conclusion made in the settling stage analysis.

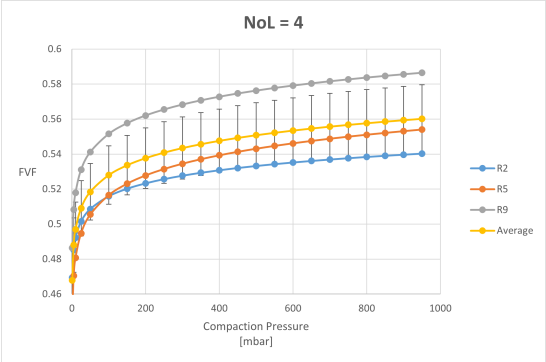

(a) Cluster of four number of layers.

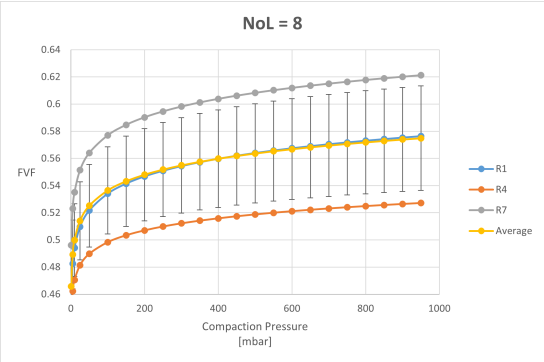

(b) Cluster of eight number of layers.

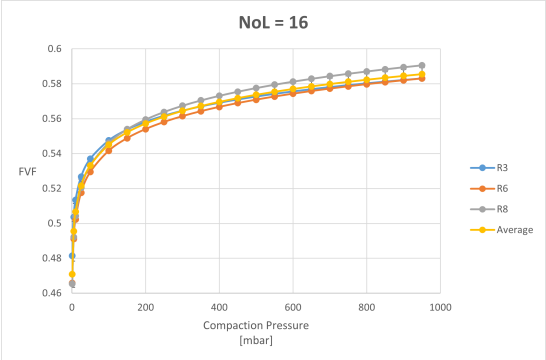

(c) Cluster of sixteen number of layers.

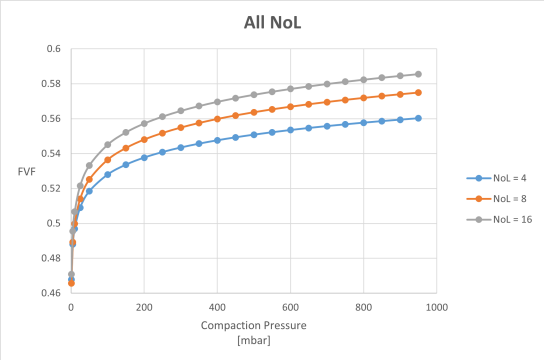

(d) Cluster of sixteen number of layers.

Figure 4.9: Empirical plots for all tests clustered by number of layers and average curves.

4.1.5 Error analysis - 1

A further analysis of the experimental setup and procedure was conducted to assess whether the SD could be a reflection of using this specific fabric or if the tests could be improved. The following points were found to be possible factors of error origin:

1. **Micrometer alignment -** In case the micrometre was not placed vertically, its measurements would not correspond to the actual thickness variation.

2. **Presser foot deformation -** The presser foot was formed by cutting a metal sheet with a workshop tool without sanding the part afterwards, resulting in some deformations on its edges.

3. **Vacuum bag compaction -** If the vacuum bag for some reason was compacted during the vacuum application, its thickness variation was not being subtracted from the measurements.

4. **Central spiral indentation -** The presser foot were placed close to the central spiral. If the spiral provoked a significant indentation during the compaction, that would influence the micrometre measurements.

5. **Vacuum control -** Air was constantly flowing inside the fabric because the vacuum pump was always on, which could impose any thickness variations.

6. **Thickness measurement methodology -** The initial thickness measurement methodology could

also be an error origin factor, mainly due to the displacement of the fabric from the setup after the measurements for the setup preparation.

7. **Number of data points -** Ten pressure increments were imposed in all tests, resulting in ten unloading and ten relaxation points. Increasing this number of increments could also improve the results.

8. **Cyclic compaction -** Imposing a pressure increment of one hundred millibars by manipulating the ball valve is challenging, and rectifications to the openness of the ball valve were required.

9. **Table tilting -** The vacuum pump was placed on the same table as the resin trap and the setup. Its performance could be shaking the table, inducing some fluctuations in the measurements.

10. **Equipment calibration -** Both the micrometre and the manometer could be providing wrong values if not accurately calibrated.

11. **Areal density calculation -** The areal density value was calculated for all tests but could have been used as the standard value of the fabric.

The vacuum bag was confirmed to not have any interference in the compaction measurements by *Vestas* employees. The vacuum control concern regarding the continuous fluid passing between the fabric could be mitigated by conducting a drop test in each pressure increment. The drop test is a technique applied to ensure proper vacuum in the setup, and if accurate, no air stream would be present in the preform. Its introduction in all increments would drastically increase the time required per test, which was not feasible. Nevertheless, after each pressure increment, no sudden changes in thickness were recorded during the four minutes waiting, leading to the acceptance of the vacuum control as a non-significant factor. The calibration of the sensors would require special techniques that the user did not feature. The equipment providers did not mention any previous calibration but recommended assuming that they were calibrated.

The number of data points was also considered a non-significant factor because the empirical curves had continuous profiles and the ten points were good enough for the linear regression. Similarly, the cyclic compaction for some pressure increments never represented pressure variations higher than fifty millibars. Nothing in literature was found to prove that such a slight pressure variation would impose any compaction variability. This very low-pressure variation was neglected, and the factor was considered non-significant. The central spiral indentation was not experimentally measured, but during a trial compaction test, several photos were taken to the central spiral, and none of them supports its influence in the measurements made, figure 4.10.

Regarding the micrometre alignment, one error propagation was calculated for a simulated inclination of the micrometre of four degrees, which can be considered an exaggerated inclination because this would be easily noticed and corrected. The error propagation allowed it to conclude that this was not an essential factor. Nonetheless, a right angle rule was used from then on to ensure its vertical alignment, figure 4.11.

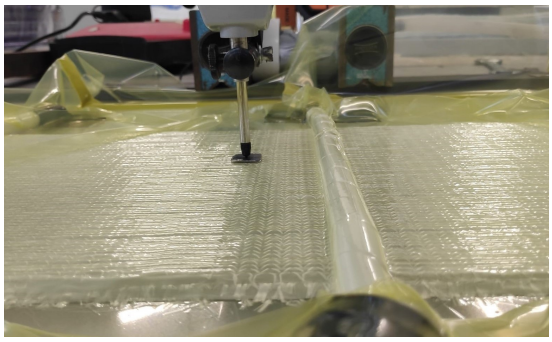

(a) Front view.

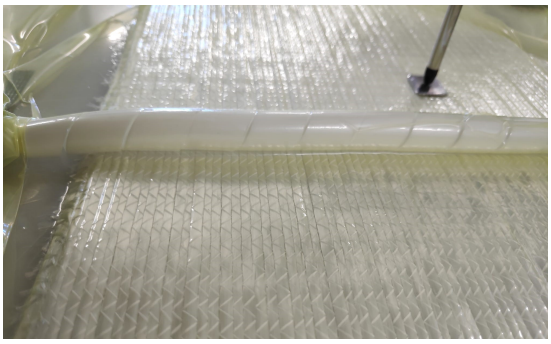

(b) Side View.

Figure 4.10: Central spiral indentation for a layup with eight layers.

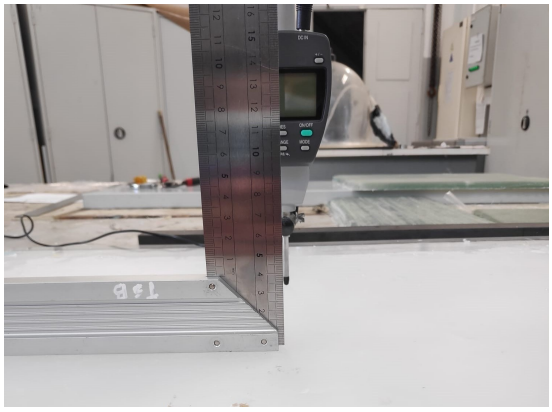

(a) Front View.

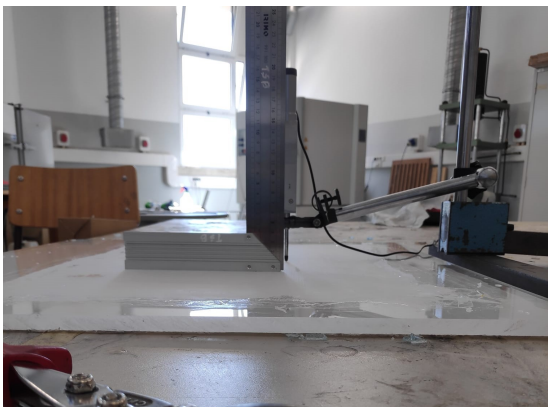

(b) Side view.

Figure 4.11: Use of right angle rule for micrometer alignment.

The remaining factors are the ones with more relevance for the error. While preparing the setup for the first time, the vacuum pump was thought to have some suspension not to propagate the vibration to its base. It was noticed that this was not accurate, and the table was constantly shaking due to the pump actuation. The vacuum pump was transposed to another table to mitigate this concern, and with this, the recorded thickness values stopped fluctuating around the actual value and started to display a continuous thickness measurement. The presser foot thickness variation from corner to corner was measured, and its influence on the results was proven to be significant, figure 4.12(b). Even though it would be complicated for the presser foot to deviate the whole length between corners during a test, any minor deviation would impose relevant thickness measurements variations. The part was sanded to mitigate this error, and only an insignificant deformation was remaining in the component, figure 4.12(c)

The areal density calculated for all tests was considered not to be representative of the fabric. The fabric column below the presser foot was approximately homogeneous and therefore could be characterised by the fabric standard properties. Density variations between tests result from the cutting procedure on its edges. These edges are considered to be considerably far from the measurement area. As previously mentioned, the thickness was measured in three different areas, and an average value was calculated for the initial thickness. After these measurements, the fabric would be transported to the balance and then back to the setup. This procedure introduces two different errors in the data. The first is related to the average thickness value, which is a flawed approach since the thickness

variation is measured on the central position of the fabric and not on the whole fabric. The second is transportation, which will automatically impose thickness variations in the stacking due to layers sliding movement. These two error factors could be easily rectified in the *MATLAB* code by using the standard areal density and using the central thickness measurement instead of the average value. New data was calculated under these conditions and is presented in figure 4.13. The individual plots for all revised tests are presented in appendix B.1.1.

(a) Resetting the micrometer. (b) Deformation before sanding. (c) Deformation after sanding.

Figure 4.12: Presser foot deformation from corner to corner.

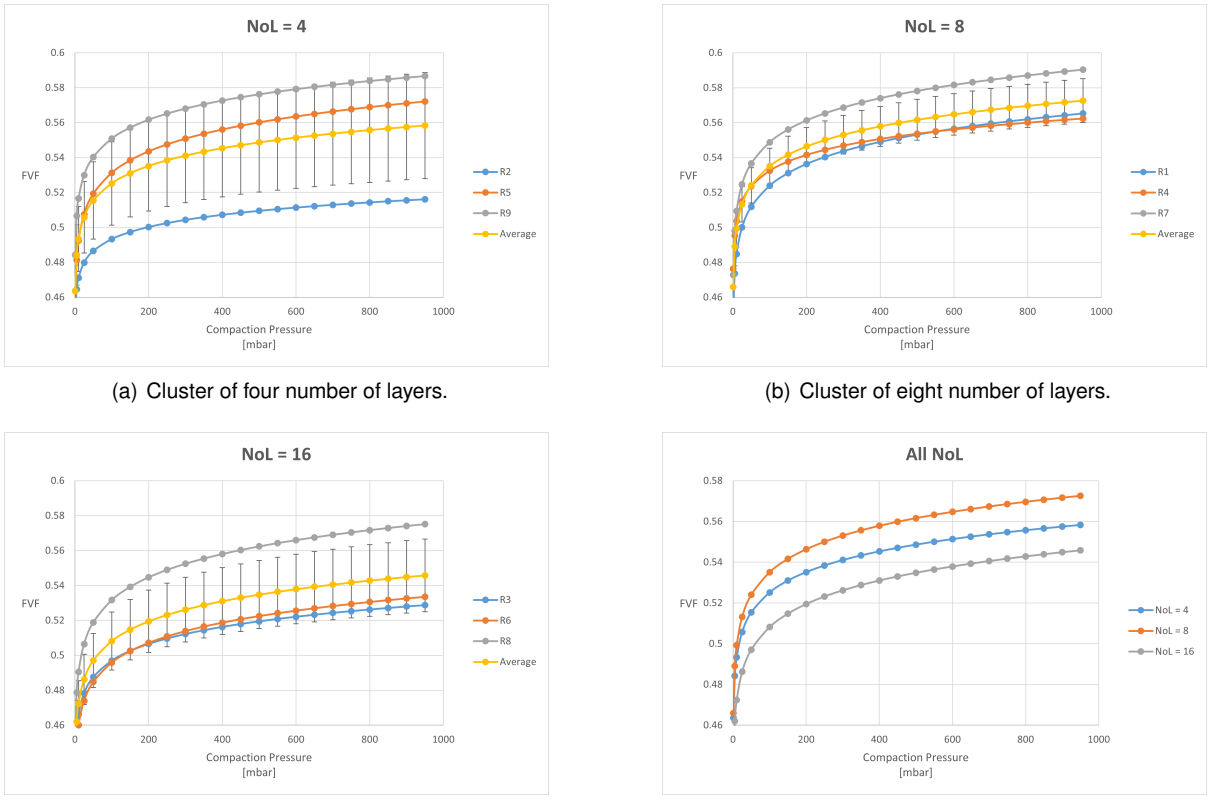

(a) Cluster of four number of layers. (b) Cluster of eight number of layers.

(c) Cluster of sixteen number of layers. (d) Average values per cluster.

Figure 4.13: Revised empirical plots for all tests clustered by number of layers and average curves.

The SD for eight number of layers improved significantly, but the evolution of the standard error with the increasing number of layers is still not following what was expected. The average values for each cluster of the number of layers are presented in figure 4.13(d). The evolution of the empirical curve from four to eight layers shows a better nesting ability, and from eight to sixteen number of layers shows a very contradictory trend. Nevertheless, it is possible to conclude that the accuracy of the areal density and the initial thickness is imperative for a suitable material characterisation due to its influence on the outcome plots.

4.1.6 Methodology improvement

Even though the data improved rectifying the areal density and the initial thickness measurement, it is still not conclusive enough. A new methodology will be developed, and tests will be repeated. Delays for the infusion tests supported a methodology improvement and the tests repetition due to more available time. Without confidence in the characterisation tests, the model validations would not be assertive and meaningful. The list of factors introducing errors in the data was taken into account, and some other improvement points were considered in this subsection.

As seen in appendix B.1.1, for all individual tests, the curves of unloading and relaxation were on top of one another. The thickness variations during the four minutes of relaxation were not as significant as previously thought. Contrarily, during the settling stage, the deformation curve for the thirty minutes duration had a good slope and the values never stabilised. Even though these deformations were relatively low in percentage, analysing the curve behaviour was one goal of the tests. Therefore, the four minutes waiting in all tests was removed from the procedure, and the settling stage was extended to one hour. The updated pressure plot, figure 4.14(a), has unloading as the third stage alone, without relaxation. The corresponding thickness plot is presented in figure 4.14(b). This new procedure means that after opening the ball valve and the compaction pressure stabilised, the micrometre data was measured, and another increment would uninterruptedly occur. Since less time is required for this stage, data points were increased to fifteen as a precaution.

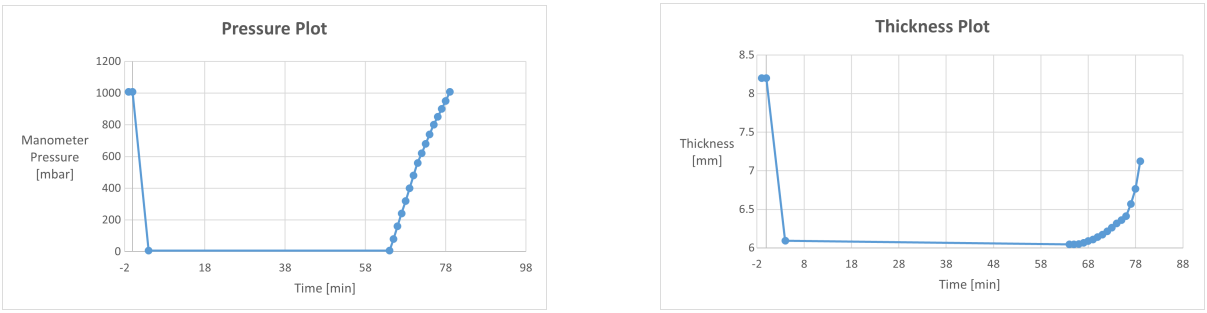

(a) Revised pressure plot.

(b) Thickness plot for $nol = 8$ test.

Figure 4.14: Pressure and thickness plots for new experimental procedure.

The methodology to measure the initial thickness of the part was also improved. The new method counted with stacking the fabric on the mould table. This way, no further transportation was needed. The thickness would be recorded only after having the setup fully prepared. When the sensors were

placed, the table and the fundamental components for the test were moved to align the micrometre tip with an area where only the vacuum bag was present, figure 4.15(a). At that place, the micrometre was resettled, and then the mould was again moved to its position, figure 4.15(b). This method of measuring thickness was proved to be accurate, and no relevant variations were measured on the trials. Another improvement on this method is related to the air inside the mould for the initial measurement. Instead of having much air trapped in the cavity, the vacuum pump would be turned on with the ball valve completely open, corresponding to an insignificant compaction pressure on the preform, $P_c \approx 10\,\mathrm{mbar}$, but to an advantageous reduction of the air between the vacuum bag and the fabric, easing the micrometre tip placement on the presser feet.

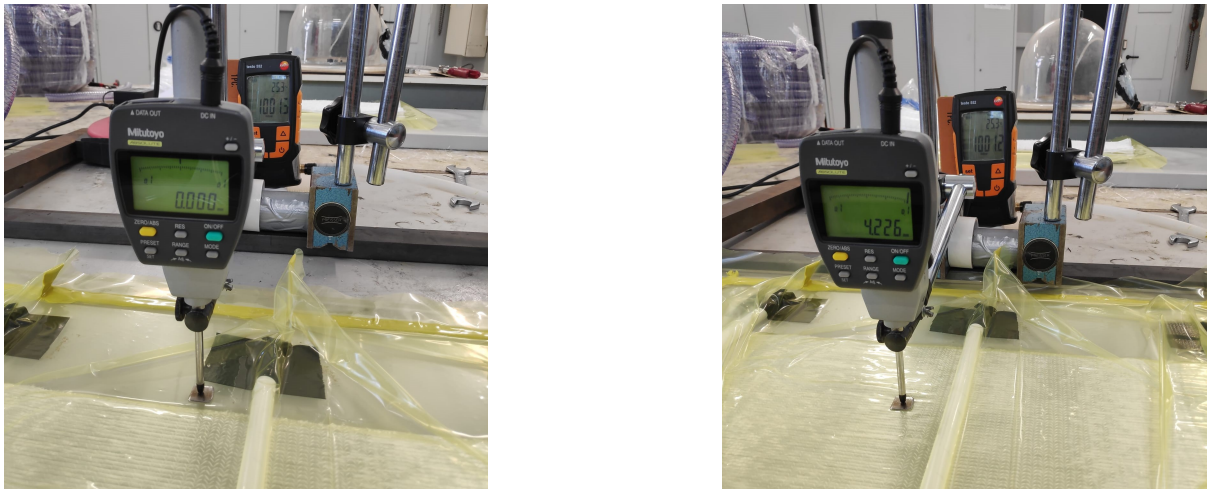

(a) Ressetling the micrometer.

(b) Initial thickness measurement.

Figure 4.15: Initial thickness measurement for new experimental procedure.

4.1.7 Data analysis - 2

Having decided to repeat all tests for the material characterisation, the randomness of the tests was applied and the DoE is presented in table 4.6, alongside the atmospheric and the initial thickness measurements. The weight of the layups were measured but the areal densities were not calculated. This time, relaxation was discarded, and no stage of the pressure plot includes this phenomenon, as justified in subsection 4.1.6. For this second analysis, the unloading stage will be assessed first.

Table 4.6: DoE tests order and conditions of all tests.

Run	R10	R11	R12	R13	R14	R15	R16	R17	R18
nol	4	8	4	16	4	8	16	16	8
$P_{atm}\,[\mathrm{mbar}]$	1008.9	1008.4	1004.9	1005.2	1004.3	1005.7	1006.5	1006.1	1004.1
$h_{initial}\,[\mathrm{mm}]$	4.488	8.199	4.226	17.659	4.311	8.594	16.431	17.169	8.453

Unloading

The same *MATLAB* code and *Microsoft Excel* spreadsheet were used to calculate the empirical constants since the procedure for these calculations had not changed. The empirical constants results are presented in table 4.7. The R-squared factor values continue to represent a successful fitting of the data. The individual empirical plots are presented in appendix B.2.1 for all tests. The empirical curves clustered by the number of layers are presented in figure 4.16. For the repeated tests, the trend between standard deviation and number of layers was visible and measured, the deviations between identical runs were reduced while increasing the number of layers. This trend was not present for the tests previous to the methodology improvement.

Table 4.7: Empirical constants calculated with LSM.

Run		R10	R11	R12	R13	R14	R15	R16	R17	R18
nol		4	8	4	16	4	8	16	16	8
Unloading	V_{f_0}	0.4098	0.4334	0.4447	0.3975	0.4281	0.4217	0.4295	0.4126	0.4347
	B	0.0283	0.0318	0.0319	0.0323	0.0303	0.0285	0.0282	0.0307	0.0285
	R^2	0.9557	0.9828	0.9298	0.9959	0.9371	0.9776	0.9965	0.9973	0.9736

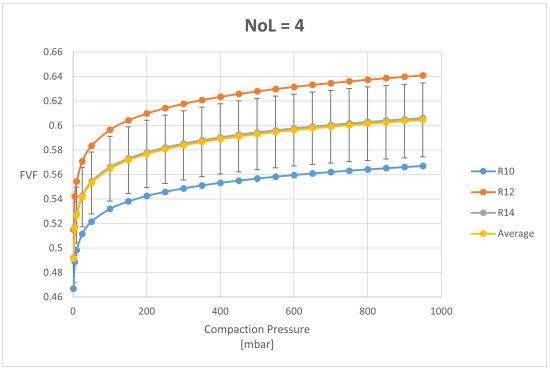

(a) Cluster of four number of layers.

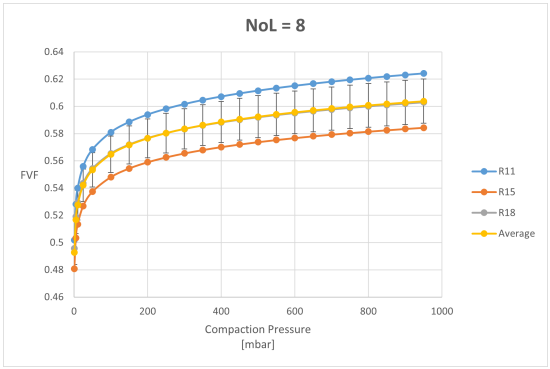

(b) Cluster of eight number of layers.

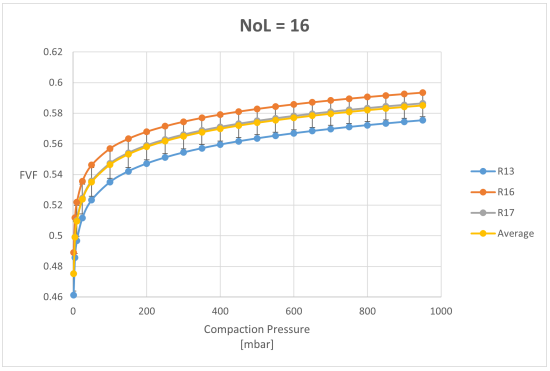

(c) Cluster of sixteen number of layers.

Figure 4.16: Empirical plots for all repeated tests clustered by number of layers.

At this point, the decision to assess a higher or a lower number of layers was made. The two options were to use the number of layers equal to two or thirty-two, $nol = 2, 32$. It was decided to study $nol = 32$ for two reasons:

- ***Vestas* applicability -** Wind turbine blades have a more considerable percentage of thick layups when compared to thin layups. Having the characterisation for a higher number of layers available would be more useful.

- **Standard deviation -** For a higher number of layers, the characterisation is more reliable than for a lower number due to a significant lower SD. Thus, studying $nol = 32$ may correspond to exact data whilst $nol = 2$ may not be conclusive.

The three tests for this new level of the number of layers was conducted consecutively. Their conditions and empirical outcomes are presented in table 4.8 and figure 4.17. For the point of highest compaction plotted, $P_c = 950\,\mathrm{mbar}$, the SD was reduced by 46.19% by passing from four to eight layers, 54.24% by passing from eight to sixteen layers and 85.95% by passing from sixteen to thirty-two layers. This trend supports the statement that standard deviation should follow a decreasing trend with incrementing the number of layers.

Table 4.8: Empirical constants calculated with LSM.

Run	R19	R20	R21
nol	32	32	32
$P_{atm}\,[\mathrm{mbar}]$	1007.3	1006.3	1006
$h_{initial}\,[\mathrm{mm}]$	37.073	35.962	35.87
V_{f_0}	0.3959	0.3997	0.3990
B	0.0324	0.0311	0.0315
R^2	0.9910	0.9906	0.9896

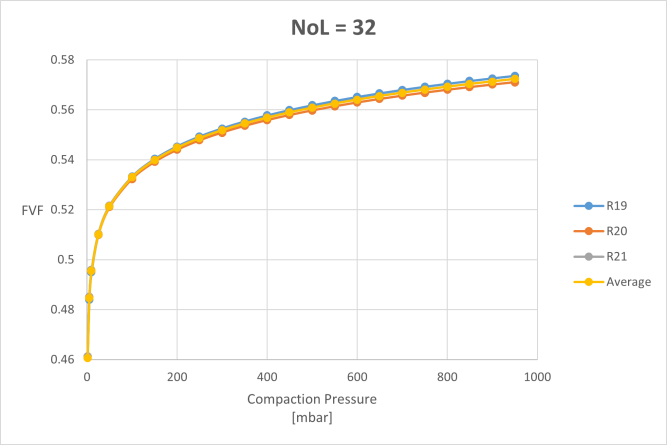

Figure 4.17: Cluster of thirty two number of layers.

The plot with all the average values per cluster is presented in figure 4.18, and their respective empirical constants are presented in table 4.9. The evolution of the empirical curves with the increasing number of layers supports that thicker layups have their nesting ability reduced. Thus, the FVF will be lower for thicker than for thinner layups for the same compaction pressure. The following points are presented to validate this data:

- **Literature review -** In subsection 2.2.1, some articles were cited which defended that nesting would improve, not be influenced and would decrease with the increment of the number of layers. Therefore, any possible trend was expected for this analysis.
- **Nesting definition -** Nesting is directly related to the alignment perfection of all layers in the layup. This alignment is more difficult to achieve for a higher number of layers. Thus, it is expected to have a worse nesting ability for thicker layups. If measures were taken to ensure a proper alignment, it would be expected to improve nesting by incrementing the number of layers.
- ***Vestas* production -** In the wind industry blades production, very thick layups are not stacked by roving and all layers are not fully aligned. Due to the complex geometry of the blade and the concentration of layers present, it is not easy to ensure a proper alignment of the layers and tolerances are applied. Therefore, this mismanaged alignment during the stacking is similar to the one at *Vestas* and, consequently, can be considered representative.

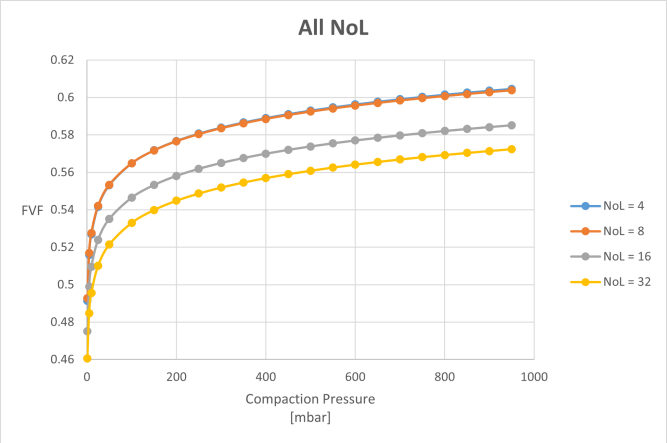

Figure 4.18: Empirical plots for average values per cluster of repeated tests.

Table 4.9: Empirical constants per number of layers.

nol	4	8	16	32
V_{f_0}	0.4275	0.4299	0.4131	0.3982
B	0.0302	0.0296	0.0304	0.0317

Another visible fact on figure 4.18 is that the empirical curves for four and eight layers are overlapping, which was not expected but can be accepted due to their deviations. These curves' high standard deviation values imply that their characterisation is inaccurate, and the natural curves are comprehended inside an interval.

Settling

Equation (4.2) was applied to all tests to calculate the thickness variation during this stage. Since this stage duration was doubled, the thickness variation was calculated for thirty minutes, $\Delta h_{set}|_{30}$, and

sixty minutes duration, $\Delta h_{set}|_{60}$, table 4.10. The settling plots for all nine tests are presented in appendix B.2.2. The clustering of the settling data by the number of layers is presented in table 4.11.

Table 4.10: Thickness variation during settling.

Run	R10	R11	R12	R13	R14	R15
nol	4	8	4	16	4	8
$\Delta h_{set}\|_{30}$ [%]	0.685	0.394	0.475	0.272	0.891	0.462
$\Delta h_{set}\|_{60}$ [%]	1.043	0.575	0.611	0.423	1.527	0.771
Run	R16	R17	R18	R19	R20	R21
nol	16	16	8	32	32	32
$\Delta h_{set}\|_{30}$ [%]	0.265	0.270	0.334	0.162	0.187	0.165
$\Delta h_{set}\|_{60}$ [%]	0.367	0.385	0.398	0.214	0.277	0.225

Table 4.11: Thickness variation during settling clustered by number of layers.

nol		4	8	16	32
$\Delta h_{set}\|_{30}$ [%]	Average	0.684	0.397	0.269	0.171
	SD	0.170	0.052	0.003	0.011
$\Delta h_{set}\|_{60}$ [%]	Average	1.060	0.581	0.392	0.239
	SD	0.374	0.152	0.023	0.027

This percentage variation can be plotted versus the number of layers, figure 4.19. Both plots have a power function plotted which represent the relation between both variables. With those curves equations, it is possible to calculate an approximation of what should be the percentage thickness variation for a thirty and sixty minutes settling duration, equation (4.7a) and (4.7b), respectively.

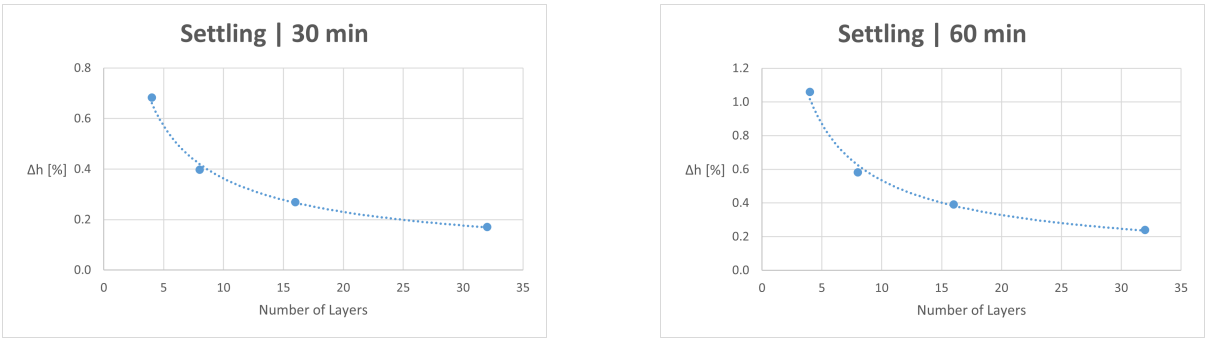

(a) Settling during thirty minutes.

(b) Settling during sixty minutes.

Figure 4.19: Thickness variation during settling stage.

$$\Delta h_{set}|_{30} = 1.6384 \cdot nol^{0.655} \tag{4.7a}$$

$$\Delta h_{set}|_{60} = 2.6896 \cdot nol^{0.702} \tag{4.7b}$$

4.1.8 Error analysis - 2

Having the second round of tests finalised, a new error analysis was conducted to assess what could still be improved. This analysis did not intend to be followed up by new characterisation tests but only to build a more considerable foundation of experimental design and procedure for possible further study over this topic. Here is the list of factors introducing error in the tests:

1. **Presser feet and micrometer tip pressure -** The system of the presser feet and micrometre tip imposes pressure on the preform and therefore alters the thickness results. Even though this variation was not considered significant, it may have a more relevant impact for thinner layups.
2. **Number of micrometers -** The design of the setup counted with two devices, but only one was used. Nonetheless, only using two micrometres will not provide an average thickness measurement of the preform. A more robust sensors framework has to count with more devices.
3. **Fabric storage -** The fabric in the laboratory was stored in a shape that implied foldings at several parts. This option resulted in non-homogeneous layers whose deformations interfered with the results.
4. **Metal sheet table -** The acrylic table used is more prone to deformations than a metal sheet table.
5. **Stacking procedure -** Discrepancies between the initial thickness of tests with the same layup conditions are mainly affected by handling during the stacking. Ensuring proper alignment only by the human eye brings many variations between tests.

The first two points of the list could be improved with one change on the setup. Instead of using micrometres and having local measures of thickness influenced by the additional pressure, other equipment systems could be used. As mentioned in subsection 2.2.1 of the literature review, DIC and SLS are other alternatives for measuring thickness in VIP. None of them implies additional pressure on the preform due to their resource of visual images. Furthermore, both alternatives allow the full thickness measurement of the preform and are not limited by local measurements.

To improve the fabric store, it is recommended to have it stored in a rolled format. Besides removing the folding deformations, this alternative would also ease the cutting of the fabric. After all tests, the acrylic deformation was not verified, and therefore its influence is not assessed here. Nevertheless, using a less deformable mould should be one improvement point for conducting these tests. One possible option for reducing the variation of initial thicknesses between tests with identical layups can be an application of cyclic compaction at the beginning of each test. After one cycle, it is believed that the thickness discrepancies would not be as significant, but since this was not tested, there is data supporting the statement.

4.2 Infusion tests

While defining the structure of this thesis, it was decided to validate the model under more uncomplicated conditions than the ones present in blades production. For that purpose, infusion tests were

integrated into the plan to produce cured parts with simple setups and non-complex layups. A goal of these tests is the reduction of the discrepancies of conditions between the material characterisation tests and the model validation. This chapter explains how these tests were conducted and presents the infusion results.

Similarly to the previous tests, infusion tests also do not have stipulated guidelines for their procedure. Nonetheless, they are more recurrent, and there is a solid common practice within the science community and corporate application. The experimental procedure used for these tests is based on the common practice framed in *Vestas* production reality. Furthermore, several health precautions were taken to avoid health hazards related to the use of the resin system, which comprises a significant health risk for its user.

4.2.1 Design of experiments

The DoE for the infusion tests was conditioned by the material characterisation because the goal is to mimic the conditions of the previous tests, not to add new variables to the tests. The fabric in the analysis was the UD $1200\ gsm$, and the remaining two factors were the number of layers and number of repetitions. It was decided to keep constant the number of repetitions for a coherence matter, $nor = 3$. Having this settled, time restrictions in using the laboratory made it mandatory only to use two levels of the number of layers in the analysis. Thus, $nol = 4, 16$ were chosen to be part of this analysis to have a thinner and a thicker layup analysed.

After having conducted the material characterisation tests with a different DoE, the DoE for the infusion tests was also rectified. One outcome of subsection 4.1.7 was that the standard deviation is higher for tests with thinner layups. Thus, it was decided to change the DoE to study $nol = 8, 16$ instead of the previous levels presented. This option would ease the validation of the model by removing variability due to thinner layups. Nevertheless, the infusion tests were delayed due to third parties influence, and not all tests in the DoE were conducted. Only four infusions occurred, and their conditions are presented in table 4.12.

Table 4.12: DoE tests order for infusion tests.

Infusion	I1	I2	I3	I4
nol	8	16	16	16

The first test with eight layers was initially considered a trial test to improve the user experience in conducting infusion tests. Since the test followed the same procedure as the remaining tests and was considered a successful test, the cured ply data was also used for the model validation. This decision implies that for thinner plies, only one repetition occurred, decreasing its significance. Since the remaining tests had the same layup conditions, it was not necessary to randomise their order.

4.2.2 Setup design

All equipment used for the characterisation tests were also used for the infusions. It is relevant to mention that the resin trap has a significant role here because it is the device responsible for avoiding damages on the vacuum pump by resin. Regarding the sensors, the manometer still had a crucial application for the drop test, and the micrometre had a less relevant application. Even though thickness was measured during the infusion, the actual goal is to measure the cured ply thickness of the part. Therefore, the thickness variations during the test are not relevant.

The release agent, peel ply and distribution mesh are only used for this set of tests. Their objective is to ease the demolding of the part, ease the removal of the consumable materials from the part and allow a faster infusion of the fluid, respectively. Furthermore, the resin system was also only used for these tests. This system is composed of epoxy resin and a hardener. As referred to in the literature review, subsection 2.1.1, the ratio between resin and hardener defines the gelation and the curing times of the part. Since this field of studies was not thoroughly acknowledged, predefined ratios used by *Vestas* were used for the tests, described in subsection 4.2.3.

Steps for setup preparation:

1. **Preparing the materials -** Including cutting the fabric and the consumable materials. For this task, tools from the IST workshop were used.
2. **Placing the tacky tape -** Defining the limits of the setup, figure 4.20(a).
3. **Applying the release agent -** Over the area where the fabric will be placed.
4. **Placing the fabric -** More or less centralised between the tacky tape, figure 4.20(a).
5. **Placing the peel ply -** Covering the whole fabric, figure 4.20(b). It was fixed with universal tape.
6. **Placing the distribution mesh -** Covering the inlet of the setup and with safe margins to the outlet and the horizontal sides of the preform, figure 4.20(c). It was fixed with universal tape.
7. **Fixing resin inlet and outlet -** Which include resin hoses and resin spirals, figure 4.20(d). Fixed with universal tape.
8. **Placing the vacuum bag -** Most challenging task, absolute sealing must be ensured. In strategic parts of the vacuum bag, it was needed to build pleats to avoid the break up of the vacuum bag after the vacuum is applied, figure 4.20(e).
9. **Placing the sensors -** Setting the micrometre to zero above the presser feet, figure 4.20(f).
10. **Start the experimental procedure -** Described in subsection 4.2.3.

The release agent must be applied after the tacky tape placement because their properties have contradictory purposes. The tacky tape serves as an excellent adherent to the mould to block air from entering beneath it, whether the release agent serves to avoid full adherence between the mould and the components above its application area. Tacky tape on top of the release agent would not fully glue

to the mould, and the vacuum would not be achieved. The release agent was applied with the aid of a brush, figure 4.21.

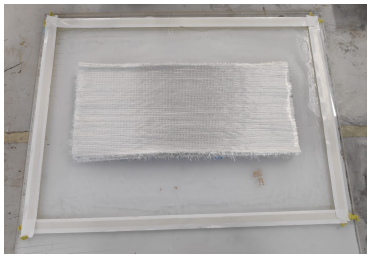

(a) Steps 2, 3 and 4: Tacky tape, release agent and fabric.

(b) Step 5: Peel ply.

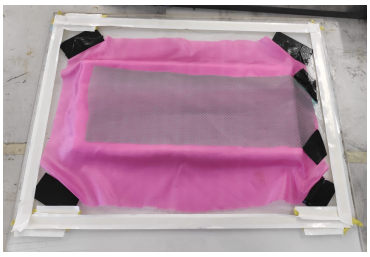

(c) Step 6: Distribution mesh.

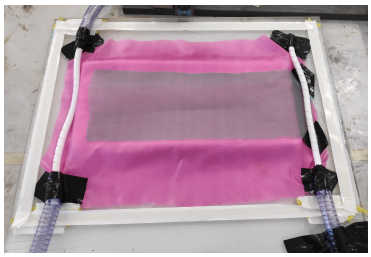

(d) Step 7: Resin inlet and outlet.

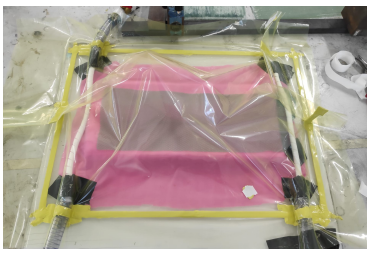

(e) Step 8: Vacuum bag.

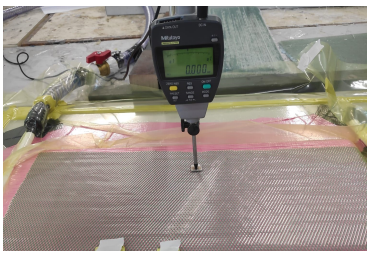

(f) Step 9: Micrometer.

Figure 4.20: Setup preparation steps for infusion tests.

Figure 4.21: Brush to apply release agent.

The distribution mesh serves as a fastener for the infusion due to its significantly high permeability values. If it were directly connected to the resin outlet, it would create a channel for the resin to flow from the inlet to the outlet almost without impregnating the fabric. Furthermore, the race tracking phenomenon could also occur, and some areas of the fabric could be left unsaturated. Thus, safety margins are applied to the distances between the distribution mesh and the resin outlet and the preform horizontal sides. A good example proving the excellent practice of this safety measure is presented in figure 4.22.

One difference in this setup is related to the number of inlets and outlets. Here, one channel is used for the resin to enter the setup, on the right of figure 4.20(d) and the other channel, on the left of the figure, has two different purposes. One is to extract air and later resin, and the other is for pressure measurements. The resin hoses are connected to the setup in three different zones, and all of them are associated with a determined ball valve. The inlet ball valve integrates the resin inlet hose, figure 4.23(a), then there is the sensor ball valve in the sensor hose, figure 4.23(b), and the outlet ball valve on the outlet hose, figure 4.23(c), which connects to the resin trap and then the vacuum pump. These ball valves are helpful for the experimental procedure described in subsection 4.2.3. The outlet and sensor

hoses share the same resin spiral to reduce the number of consumable materials per test.

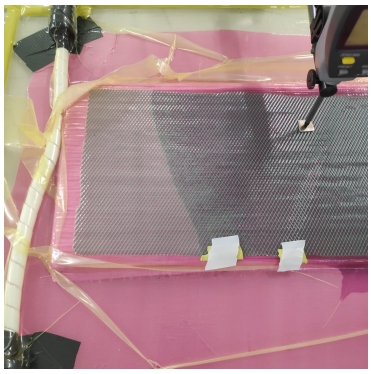

(a) At the midle of the fabric.

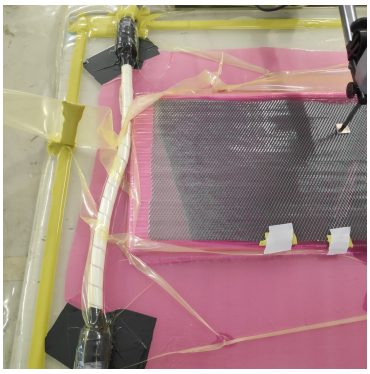

(b) Close to the end of the fabric.

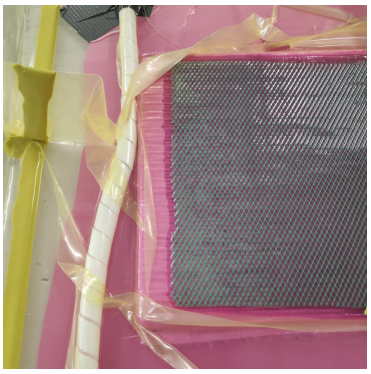

(c) After the distribution mesh.

Figure 4.22: Racetracking phenomenon during infusion.

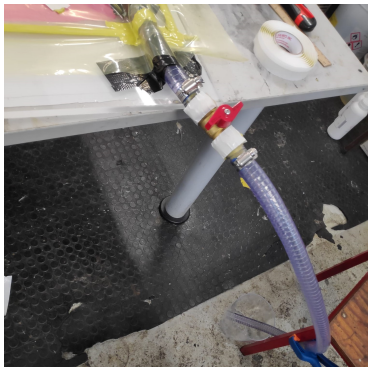

(a) Inlet ball valve.

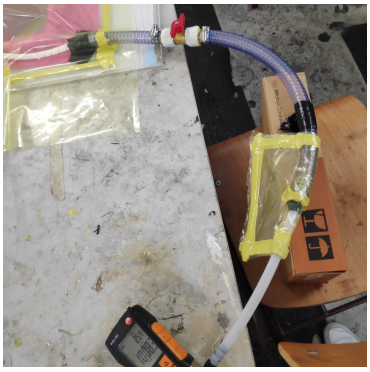

(b) Sensor ball valve.

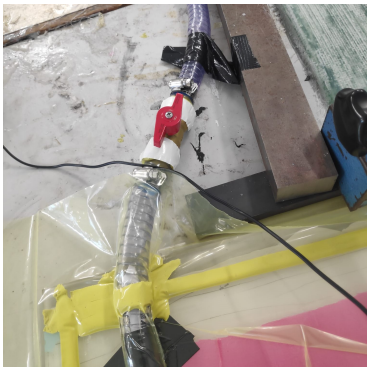

(c) Outlet ball valve.

Figure 4.23: Ball valves on the setup.

Due to the higher health risks associated with the resin system application, improved measures to prevent health hazards was taken during the assembly of the connections between ball valves and their respective hoses. In figure 4.24 it is possible to observe how these connections were handled. The tacky tape serves to block air entrance in the connection. The hoses' clamps input extra pressure on the hoses to not be separated during the infusions. Since resin will flow inside the hoses with significant pressure, in case connections were not clamped enough, it would be possible that any connection could be dropped, and the laboratory would be contaminated.

Figure 4.24: Setup improved connections.

The hoses need to be replaced for all tests because the resin will flow inside them. Thus, before mounting the setup on the mould, it is mandatory to remove the previous hoses and place new ones. All connections in the ball valves should be placed carefully due to health reasons and ensure a proper vacuum in the setup.

4.2.3 Experimental procedure

Contrarily to what occurred for the characterisation tests, recording thickness measurements during the tests was not necessary for the infusions, and no specific stage was the target of the analysis. Thus, the ultimate goal during the experimental procedure was to achieve a good vacuum inside the cavity. Every setup preparation stage was performed with attention to avoid wasting material and shorten the available time for the tests.

The pressure plot applied only consists in applying the vacuum in the setup. The manometer pressure will go from the atmospheric pressure to the vacuum pressure when the air exits the setup. Ideally, the pressure would remain constant until the fluid entrance into the cavity. Thickness values were not measured during the whole infusion process due to its long duration.

The experimental procedure steps are the following ones:

1. After having the setup fully prepared, the vacuum pump is turned on, and the air is pulled from the preform. During this extraction, only the inlet ball valve is closed.

2. A few minutes later, depending on the thickness of the preform, the pressure read by the manometer will correspond to vacuum pressure, $P_{vac} \approx 6\,\mathrm{mbar}$, and the setup will be isolated. All ball valves are closed, and the pump is turned off at this moment.

3. The drop test takes place to ensure proper vacuum. After around five minutes of closing the ball valves, the sensor ball valve is opened, and the manometer reads the pressure inside the cavity. Then, there are two possible scenarios:

    - If $P_{vac} \leq 30\,\mathrm{mbar}$, the setup is ready for the infusion and the procedure continues to the next step.
    - If $P_{vac} > 30\,\mathrm{mbar}$, there is a leak and air is entering the setup. This leak must be found, and tacky tape should be pressed in those and other potentially leaking areas. The procedure must be repeated from the beginning until the drop test is a success.

4. All ball valves are closed, and the resin system is prepared and placed.

5. The vacuum pump is turned on, and the outlet and inlet ball valves are opened consecutively with a small interval between openings.

6. Whenever the resin reaches the outlet spiral and passes to the resin outlet hose in direction to the resin trap, a few moments are waited, $(\approx 1\,\mathrm{min})$, and the outlet ball valve is closed. A few moments later, $(\approx 1\,\mathrm{min})$, the inlet ball valve is also closed.

7. The resin inlet hose is cut of and displaced to a safe area due to its resin content, figure 4.25.

8. Twenty four hours later, the demolding stage takes place, and the part is retrieved fully cured.

9. The acrylic table is cleaned to prevent interference in further infusions.

Figure 4.25: Resin inlet hose cut after the filling stage.

Step 4 of the procedure is complex and must be explained in more detail. The resin system is prepared with *Vestas* standard ratios and duration. First, the weight of the preform will be equalised by the weight of the resin system. Then, the ratio between resin epoxy and hardener is established as $76\,\%$ of resin for $24\,\%$ of hardener. For each infusion, the weights of each component are presented in table 4.13. To prepare the resin system, the resin deposit is placed on the balance, and the equipment is zeroed. Then, the resin is placed on the deposit until its mark, figure 4.26(a), and the balance is zeroed again to place the hardener until its mark, figure 4.26(b). After mixing both components, 4.26(c), it is crucial to leave the deposit for around fifteen minutes for the degassing process. Air bubbles trapped in the deposit will be extracted, and only then the resin system be fully prepared to be connected to the resin inlet hose. A spatula is used to mix both components, figure 4.27(a). It is important to ensure that the resin inlet hose does not disconnect from the deposit. For that purpose, a clamp is placed in the resin deposit blocking the hose movement, figure 4.27(b).

The lubrication phenomenon mentioned in subsection 2.1.3 was pondered to be a target of study during the infusion tests. Nonetheless, the use of distribution mesh in the setup made it impossible to measure this effect accurately. Without distribution mesh, lubrication would start at the instant when resin reached the tip of the micrometre placed above the preform. After the flow front passed that point, a sudden decrease in thickness measurement would be attributed to this effect. With the application of distribution mesh, the instant when resin reaches the tip of the micrometre does not represent a total saturation of the fabric below but only the saturation of the high permeability layer. Along the through-thickness direction of the fabric, some parts would be possibly saturated, and the lubrication phenomenon would be occurring, whereas layers on the bottom would still dry. Thus, it is impossible to quantify this effect only with the instruments used here.

Table 4.13: Components weights for the resin system.

Infusion	I1	I2	I3	I4
nol	8	16	16	16
Fabric [g]	857	1747	1692	1732
Resin [g]	651	1327	1286	1316
Hardener [g]	206	420	406	416

(a) Placing the resin in the deposit.

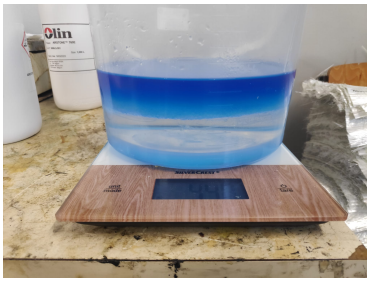

(b) Placing the hardener in the deposit.

(c) Resin system mixture.

Figure 4.26: Resin system mixing.

(a) Use of spatula to mix the resin system.

(b) Use of clamp to fix the inlet hose.

Figure 4.27: Resin system preparation and positioning equipment.

4.2.4 Data analysis

The cured parts are presented in figure 4.28. It is easily noticed that the second infusion, with sixteen layers, does not have the same quality as its counterparts, figure 4.28(b). This defect was the result of an air leak in the setup that was not noticed. During the procedure of the second infusion, I2, the sensor hose also leaked, making it impossible to use the device for the drop test. The resin trap pressure sensor was used to measure the pressure inside the setup, replacing the manometer. During the drop test, the resin trap sensor did not change its value, and the setup was wrongly assumed to be ready for the infusion. Since the resin trap has a much higher volume than the setup, it is believed that the pressure variation in the setup was diluted in the resin trap and the sensor only presented a negligible variation. After the post-filling stage started, it was possible to notice air entering the cavity and compromising the part. After this test, the sensor was duly strengthened, and the vacuum was ensured.

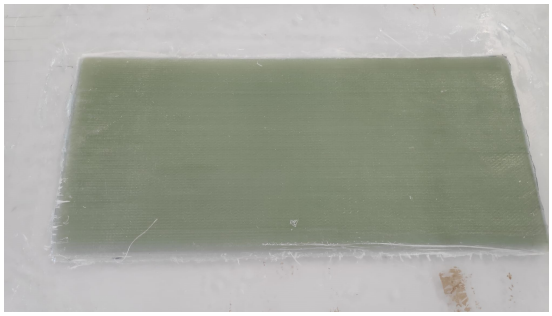

(a) First infusion.

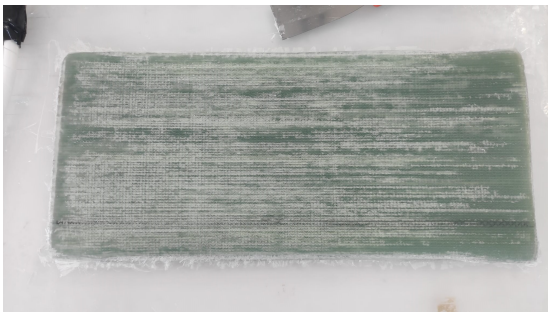

(b) Second infusion.

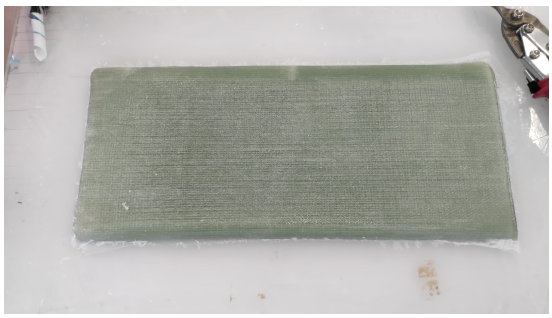

(c) Third infusion.

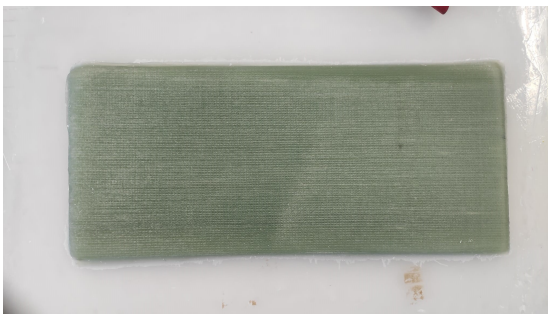

(d) Fourth infusion.

Figure 4.28: All cured parts.

Additionally, another preventive measure was taken regarding vacuum insurance. Instead of the traditional stripe of tacky tape around the hoses on the setup, two other stripes were placed outside and inside the cavity to ensure that the vacuum bag around the hoses was protected and the air was not allowed to enter, figures 4.29(a) and 4.29(b). This measure was taken because tacky tape entered the mould cavity below the hoses throughout the infusion tests, figure 4.29(c). The air suction implied a deformation in the weakest areas of the setup, which are around the hoses. The remaining two infusions were conducted without any measurable leaks.

(a) Three stripes placement.

(b) Vacuum bag placement.

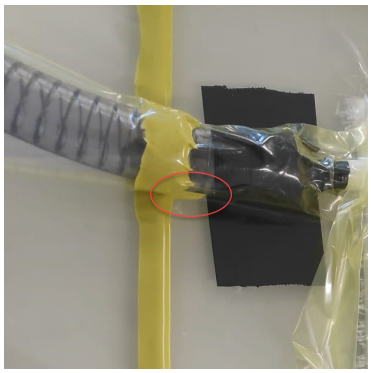

(c) Tacky tape suction effect.

Figure 4.29: Resin system preparation and positioning equipment.

Having the fully cured parts removed from the mould, it is possible to measure their thickness. For this task, nine measures were taken to all parts. The areas of the measures were the same for all parts and are visible in figure 4.30. The measurements are presented in table 4.14. Looking at the thickness values of both the third and fourth infusions, I3 and I4, it is possible to understand that their values

are within a small range of discrepancies. Comparing those infusion measurements with the second infusion, I2, it is immediate to understand the air's impact on the curing process.

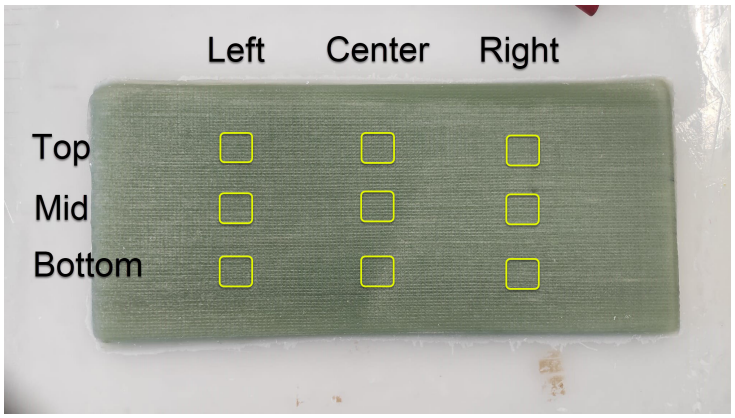

Figure 4.30: Areas for cured ply thickness measurements.

Table 4.14: Cured ply thickness measuremnts.

Infusion	I1			I2		
	Left	Center	Right	Left	Center	Right
Top	7.358	7.261	7.144	16.475	16.514	16.397
Mid	7.209	7.150	7.069	16.569	16.515	16.480
Bottom	7.235	7.050	7.008	16.668	16.614	16.529
Infusion	I3			I4		
	Left	Center	Right	Left	Center	Right
Top	14.011	13.875	14.124	14.113	13.873	14.175
Mid	14.336	14.333	14.177	14.108	13.983	14.131
Bottom	14.474	14.268	14.147	14.472	14.448	14.208

It is crucial to highlight that these thickness measurements have an associated error to their methodology. It was noticed that moving the heavy cured parts on the table resulted in variations in the thickness measurements of the micrometre. These variations were of a small order of magnitude but will impact the validation of the model. Ideally, the cured parts would be cut recurring to specific tools, and then a calliper rule would be used for measuring the thickness. Since proper tooling for the trimming was not available, the micrometre measurements were used.

Chapter 5

Model validation

The validation of the model developed in this thesis will be divided into two phases. Firstly, the infusion tests conducted in the laboratory will be used, and only then *Vestas* blades thickness data will be used to validate the model.

The goal is first to assess the prediction error in a more straightforward setup, identical to the one used for the material characterisation tests. Afterwards, under complex conditions of the blade infusion, the main carbon path thickness data will be assessed against the predictions.

5.1 Infusion tests

The setup for the infusion test was defined to resemble the setup for the material characterisation. The ultimate goal of characterising a fabric is to understand how it behaves under determined conditions, resembling the setup for the infusion tests results in a reduction of external variables interfering in the prediction.

Since the second infusion was compromised and its thickness values are not representative of an accurate infusion, they will not be used for validation. Only the remaining tests will be validated in this section.

5.1.1 Pressure range

Having the layup sequence acknowledged, the compaction pressure is the remaining variable to run the model. In the VIP, after the filling stage, the fluid pressure tends to equalise in the preform. The longer the duration of the post-filling stage, the more even will be the pressure field. The inclusion of distribution mesh also contributes to a faster equilibrium of pressure since it serves as a channel for the fluid to move more freely and balance pressure. A higher number of layers also has a similar effect but on a significantly lower scale. Figure 5.1 presents two different fluid pressure plots. In both cases, the fluid pressure tends to the vacuum pressure value applied at the setup before infusion. Thus, the setup corresponding to figure 5.1(a) had a lower vacuum pressure than in figure 5.1(b), $P_{vac} \approx 50\,\mathrm{mbar}$ and $P_{vac} = 400\,\mathrm{mbar}$, respectively.

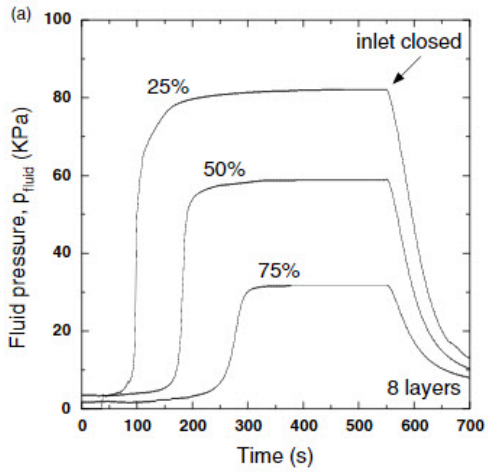

(a) Pressure plot with $P_{vac} \approx 50\,\text{mbar}$, [6].

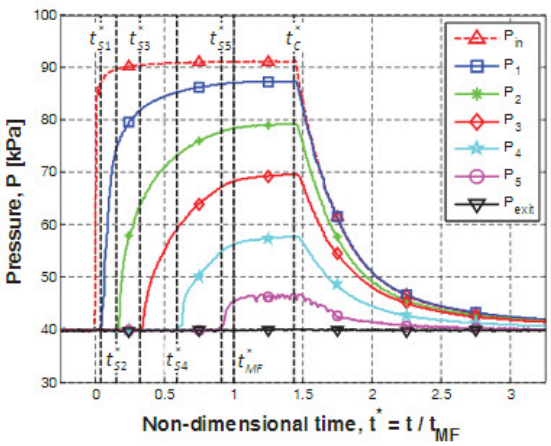

(b) Pressure plot with $P_{vac} = 400\,\text{mbar}$, [8].

Figure 5.1: Examples of pressure plots during the VIP.

It is crucial to highlight that resin enters its solidification stage after the post-filling. The atmospheric pressure applied to the vacuum bag has to be balanced inside the setup cavity. The vacuum pressure, the air still left on the setup, and the part already composed of fabric and resin will support this pressure. Full compaction pressure will be used to run the model for the predictions of each test, which means that it will be compared full compaction pressure applied on dry fabric against full compaction pressure applied on saturated fabric. One of the primary outcomes of this model validation will be discovering the compaction pressure that needs to be applied to the dry fabric to equal the cured ply thickness of the same fabric.

The available pressure inside the cavity of the setup relates to the atmospheric and the vacuum pressure achieved in each test. It is calculated according to (5.1) and the pressure conditions per test are presented in table 5.1.

$$P_{available} = P_{atm} - P_{vac} \tag{5.1}$$

Table 5.1: Pressure conditions in all infusion tests.

Infusion	I1	I3	I4
nol	8	16	16
P_{atm} [mbar]	1007.9	1006.7	1008.2
P_{vac} [mbar]	25.23	19.01	16.32
$P_{available}$ [mbar]	982.7	987.7	991.9

5.1.2 Thickness prediction

Since the layups of the infusion tests are only composed of one fabric, the formulas that relate and stack several fabrics together were not included in the model. Furthermore, to run the model for each infusion, it is only necessary to use the respective number of layers empirical constants presented on

table 4.9. Nevertheless, since the empirical data for thirty-two layers had the lowest deviations, those empirical constants were used to predict all infusion tests. The goal is to analyse the hypothesis to use the best fitted empirical data instead of the respective number of layers characterisation data. In table 5.2, both the predictions with the respective number of layers empirical constants, $h_{model_{8,16}}$, and the predictions with the empirical constants of thirty-two number of layers, $h_{model_{32}}$ are presented.

Table 5.2: Thickness predictions for all infusion tests.

Infusion	I1	I3	I4
nol	8	16	16
$h_{model_{8,16}}\,[\mathrm{mm}]$	6.256	12.900	12.898
$h_{model_{32}}\,[\mathrm{mm}]$	6.593	13.184	13.182

5.1.3 Model accuracy

The infusion tests setup was designed to resin impregnate the preform in its length direction, allowing to assume to be standing before an Unidirectional (1D) flow. In this scenario, thickness measurements in the same width cross-section can be more easily related than measurements from different ones. Even though a homogeneous compaction pressure is assumed in the setup cavity for the model prediction, the pressure history in different zones of the fabric is not the same, whilst for a width cross-section, it can be approximated to be the same. Thus, clustering the measurements data per width cross sections is analysed. The three cross-sections clusters are represented in figure 4.30 and correspond to the ”Left”, ”Center” and ”Right” sections, their average values per test are presented in table 5.3.

Table 5.3: Averaged thickness values clustered by width wise cross sections.

Infusion	I1	I3	I4
nol	8	16	16
$Left$	7.267	14.274	14.231
$Center$	7.155	14.159	14.101
$Right$	7.074	14.149	14.171

From this data, it is observable that the fluid tends to agglomerate in the outlet channel, cross-section denominated ”Left”. Therefore, the thickness here will be higher than the rest of the part, corresponding to a lower compaction pressure. The remaining cross-sections, center and right, have very identical measurements for $nol = 16$ and slightly different for $nol = 8$. A justification for this fact can be the facilitated resin distribution for more layers due to more channels in the layers interface. Since the closest section to the outlet is influenced by a variable not included in the model, its influence will be neglected, and only the remaining sections will be assessed. The averages of both ”Center” and ”Right” sections will be used from now on, $h_{average}$. Even though this modification does not change the measurements significantly, it improves the conditions for the model prediction.

The percentage relative error for each model validation, ϵ_{model}, was calculated according to equation (5.2). The thickness average values, the prediction values with different sets of empirical constants

and the error of each prediction are presented in table 5.4. It is clear that using the empirical data for thirty-two layers significantly improves the prediction. Furthermore, the prediction error for thinner plies is higher than for thicker plies. This error can be related and associated with the standard deviations calculated in the material characterisation data. Thinner layups imply more variability in the handling and may result in a broader range of cured thickness. The assessment of only one infused part with eight layers limits this analysis severely and does not support this conclusion, regardless of being aligned with previous evidence from other tests.

$$\epsilon_{model} = \frac{|h_{model} - h_{average}|}{h_{average}} \cdot 100 \tag{5.2}$$

Table 5.4: Predictions error.

Infusion	I1	I3	I4
nol	8	16	16
$h_{average}$ [mm]	7.115	14.154	14.136
$h_{model_{8,16}}$ [mm]	6.256	12.900	12.898
$\epsilon_{model_{8,16}}$ [%]	12.07	8.86	8.76
$h_{model_{32}}$ [mm]	6.593	13.184	13.182
$\epsilon_{model_{32}}$ [%]	7.33	6.86	6.75

5.1.4 Ideal pressure

To calculate the ideal compaction pressure corresponding to a zero error, the formulas integrated into the model must be applied backwards. The outcomes are presented in table 5.5. From this table, it is concluded that the compaction pressure applied to the dry fabric corresponding to the layup's cured ply thickness is shallow. This pressure is dependent on the number of layers and the empirical data used. This compaction pressure relation between dry fabric and cured ply thickness will be further studied for the cutup data validation in the following section.

Table 5.5: Ideal compaction pressure for thickness predictions.

Infusion	I1	I3	I4
nol	8	16	16
$P_{c,ideal_{8,16}}$ [mbar]	12.75	46.65	48.61
$P_{c,ideal_{32}}$ [mbar]	88.98	105.12	109.34

5.2 Cutup data

The cutup data consists of the thickness data collection of mock-ups produced with the same conditions as the turbine blades. These parts are cut at specific points, and thickness is measured at different

zones of the section. Even though *Vestas* has several cutup data, only a few were used for this model validation.

5.2.1 Layup conditions

Since blades have complex setups, procedures and layups associated with their production, only a specific part of the blade was selected for this study. For structural reasons, the root of blades is typically thicker than their tips. Besides this thicker area, the layup on the root also includes more fabric variability, leading to a more complex interaction between consecutive layers. Closer to the tip, thinner and less complex layups are part of the setup making this a more suitable area to validate the model. Reducing the number of interfering variables is always an objective for this study to reduce the discrepancies to the experimental tests conducted.

Furthermore, some blade models share the same layup for some blade radius. This fact provides the alternative to directly compare and validate the model with cutup data of different models. The layup scheme is not illustrated. One important point to underline is that several fabrics are part of this layup, and only one of them was studied in compaction behaviour. Thus, the empirical characterisation of the remaining fabrics will be researched and used from the literature, introducing a new error factor in the prediction model. The thickness of the three materials on the bottom of the stacking (SPL, Surface Veil and Gel Coat) will be considered in the model according to *Vestas* predictions because their empirical constants were not found in the literature. The remaining two materials (Biax and Triax) have their constants presented in table 5.6. The characterisation of the Biax and the Triax materials were conducted in [38] and [3], respectively. The Biax data was fitted into equation (2.3) while the Triax data was fitted into equation (3.9a).

Table 5.6: Empirical constants data of Biax and Triax.

Biax		**Triax**		
V_{f_0}	B	a	b	c
0.3621	0.0317	32.88	0.267	42.13

5.2.2 Thickness prediction

The available vacuum pressure for all blades productions is estimated to be around $P_{available} = 950\,\mathrm{mbar}$. Similar to what occurred for the infusion tests, the empirical data calculated in the experimental tests will be used for the respective and the remaining number of layers clusters. The layup has eight layers of the characterised material, but the pair of empirical constants of sixteen and thirty-two layers will also be used. Thickness predictions are presented in table 5.7.

Table 5.7: Layup thickness predictions.

h_{model_8} [mm]	10.56
$h_{model_{16}}$ [mm]	10.75
$h_{model_{32}}$ [mm]	10.90

5.2.3 Model accuracy

The previous predictions will be compared to two different blades models. In both models, four sections match the layup presented, and their thickness measurements are available. The models will be denominated A and B for simplification, and the sections will be enumerated from one to eight. The cutup thickness values are presented in table 5.8. The calliper used for the model B measurements is less accurate, and therefore their values are not very precise. Equation (5.2) was used to calculate the error between each section and the thickness predictions. The errors of each prediction are presented in table 5.9. Since all model B data has the same value, it will be assessed as only one section.

The error analysis in terms of the empirical constants number of layers cluster is very conclusive and indicates that using the pair of constants with the higher number of layers, the one with the lowest standard deviation, is more accurate than using the respective pair of constants of the number of layers present in the layup. This conclusion was also drawn from the infusion tests where only one fabric was present. The rest of this analysis will only use the predictions with the characterisation of thirty-two layers.

Table 5.8: Cutup data thickness measurements.

Model A		**Model B**	
h_1 [mm]	11.33	h_5 [mm]	11.00
h_2 [mm]	11.68	h_6 [mm]	11.00
h_3 [mm]	11.13	h_7 [mm]	11.00
h_4 [mm]	10.82	h_8 [mm]	11.00

Table 5.9: Thickness predictions deviations to cutup data.

$nol = 8$				$nol = 16$				$nol = 32$			
Model A		**Model B**		**Model A**		**Model B**		**Model A**		**Model B**	
ϵ_1 [%]	6.80	ϵ_B [%]	4.00	ϵ_1 [%]	5.12	ϵ_B [%]	2.27	ϵ_1 [%]	3.80	ϵ_B [%]	0.91
ϵ_2 [%]	9.56			ϵ_2 [%]	7.94			ϵ_2 [%]	6.65		
ϵ_3 [%]	5.15			ϵ_3 [%]	3.44			ϵ_3 [%]	2.10		
ϵ_4 [%]	2.43			ϵ_4 [%]	0.68			ϵ_4 [%]	0.71		

Regardless of the indication provided by this error analysis, it is furthermore needed to analyse the thickness variation between predictions and actual values, table 5.10. While assembling the turbine blade, the thickness has to be included in an interval defined in millimetres and not a percentage. These differences between actual and predicted thickness are very well inserted between the desired limits. Nevertheless, since this section can be considered thinner, it is relatively easier to be within the admis-

sible interval. Further validations for other parts of the blade should be conducted in further work. To understand if this model can represent a possible improvement to *Vestas* current prediction methodologies, the thickness prediction from the company was used in the analysis presented in table 5.11.

While compared to the predictions error calculated for the thirty-two layers cluster, some of *Vestas*' predictions were improved, and some of them got worse than this thesis' predictions. Nonetheless, *Vestas* used models for all particular fabrics in the layup while in this thesis, only one of the three main fabrics were assessed, the rest has their behaviour characterised by similar materials found in the literature. This analysis does not defend that using this model would result in an improvement for *Vestas* because there are still some variables that must be mitigated.

Table 5.10: Variation between real and predicted thickness.

Model A		**Model B**	
$\Delta h_1\,[\mathrm{mm}]$	0.43	$\Delta h_B\,[\mathrm{mm}]$	0.10
$\Delta h_2\,[\mathrm{mm}]$	0.78		
$\Delta h_3\,[\mathrm{mm}]$	0.23		
$\Delta h_4\,[\mathrm{mm}]$	0.08		

Table 5.11: *Vestas*' thickness predictions deviation to cutup data.

Model A		**Model B**	
$\epsilon_1\,[\%]$	0.70	$\epsilon_B\,[\%]$	3.59
$\epsilon_2\,[\%]$	2.34		
$\epsilon_3\,[\%]$	2.42		
$\epsilon_4\,[\%]$	5.14		

To understand the improvement from using the empirical data gathered in the experimental tests for the glass fabric, empirical data found on literature for similar fabrics was used to run the model. In [3], an unidirectional glass fiber with identical areal density was characterised, using its empirical constants results in a thickness prediction of $h_{model} = 10.60\,\mathrm{mm}$. This thickness prediction was compared to the cutup sections evaluated in this thesis, and a maximum and minimum associated error of $\epsilon_{max} = 9.22\,\%$ and $\epsilon_{min} = 2.06\,\%$ were calculated, respectively. This analysis alone does not conclude that the characterisation of the fabric in the experimental tests resulted in a more accurate prediction but sustains a considerable motivation to pursue the characterisation of the remaining fabrics.

5.2.4 Ideal pressure

Similarly to what was conducted to the infusion tests, the ideal pressure will be calculated to understand the pressure that leads to a zero error prediction. The ideal pressure values are presented in table 5.12.

Since the layup in the analysis is relatively thin, a thickness variation of $0.85\,\mathrm{mm}$ corresponds to a variation of the ideal pressure of $1041\,\mathrm{mbar}$. This variation proves that this ideal pressure analysis is not very accurate for such thin plies. The ideal pressure for section four is higher than the atmospheric

pressure. This comparison can result from a lousy fibre placement during the blade stacking, resulting in fewer layers than expected in the section. Nevertheless, the ideal pressure analysis for the infusion setups presented shallow values, whilst there are very high values of ideal pressures for the cutup data. This discrepancy is believed to be justified by the blades production procedure. Usually, the resin inlets and outlets are closed before the resin arrives at the outlet to shorten the process duration. This procedure will result in a lower amount of resin relative to the one in the infusion tests. In the infusion tests, the channels were closed a while after resin arrived at the outlet hose. This lower amount of resin will result in thinner plies, associated with higher ideal pressures.

Table 5.12: Ideal compaction pressure for thickness predictions.

Model A		**Model B**	
$P_{c_{ideal,1}}$ [mbar]	301		
$P_{c_{ideal,2}}$ [mbar]	117	$P_{c_{ideal,B}}$ [mbar]	722
$P_{c_{ideal,3}}$ [mbar]	512		
$P_{c_{ideal,4}}$ [mbar]	1158		

Chapter 6

Conclusions

6.1 Main findings

Regardless of the immense research found about the VIP, the industry still lacks the utilisation of norms and general standards for the experimental tests related to the process. The community would gain many benefits if some guidelines were developed and used by the majority, but only a few efforts were made in that direction.

There is a lot of available data regarding the compaction behaviour of several fabrics, but since blades projects use state of the art materials, it is not common to find recent materials characterisation data.

The degree of complexity of a blades geometry and the usage of distribution mesh are determinant factors to complicate the validation of the most recurrent models to predict the pressure distribution field. It is recommended to use a more simple approach based on academic models coupled with an intense validation against experimental results to develop a thickness prediction model for the infusion of turbine blades.

The methodology applied for the characterisation tests was analysed in terms of error introducing factors and was improved based on the analysis. Nevertheless, some improvement points were still noticed, and their mitigation is recommended to any research looking to conduct similar tests.

The settling stage duration was proved to impact the thickness due to the time-dependent phenomenon. A power law was fitted into the settling data to represent the thickness variation by the number of layers present in the layup.

The material characterisation for dry state fabrics was proved to be accurate, but it was acknowledged the importance of combining these tests with the others with the fabric in the wet state to describe the fabric compaction behaviour completely.

In the material characterisation tests, increasing the number of layers reduced the standard deviation, improving the tests' repeatability. Furthermore, this increment also results in a higher thickness per layer in the layup, lowering the final FVF value for thicker laminates. This trend is believed to result from a worst layers alignment in the stacking procedure, culminating in a worse nesting ability of the overall

layup.

While infusing any composite layup, it is crucial to ensure a proper vacuum in the cavity to avoid tests miscarriages and wasting resources. Improved placement of tacky tape and improvements in the resin hoses connectors were believed to avoid air leaks better.

The lubrication phenomenon is more difficult to quantify while using distribution mesh in the setup due to a lack of homogeneity in the through-thickness direction in terms of saturation conditions of the layup.

The thickness predictions using the simplified model for the infusion tests presented considerably high errors. The thickness measurement methodology for the cured parts can be significantly improved if using trimming equipment and callipers. The methodology used for the measurements was believed to contribute negatively to the accuracy of the measurements. The ideal pressure values to achieve a zero error in the prediction were similar to the vacuum pressure.

Data from the characterisation with thirty-two layers showed better predictions than using the respective number of layers empirical data. This information states that characterisation with lower standard deviations, therefore more exact, can more accurately describe the compaction behaviour of a fabric. It also supports decisions not to characterise thinner layups and only focus on the characterisation of fabrics with a high number of layers on the DoE.

The model validation against specific cutup data from *Vestas* was very accurate, and considerably low error values were found. The layup that was assessed integrated different fabrics that were either characterised by literature empirical data or by *Vestas* previous data, which introduced a new degree of uncertainty to the results. Again, the empirical data for the thirty-two layers was more accurate and associated with a lower error degree.

The thickness differences between the predictions and the cutup data was inside the admissible thickness interval that avoided clashes in the blade assembly. When compared to *Vestas* methodologies, some sections were better predicted by *Vestas* and others by this thesis model, leading to an inconclusive state that needed further validations on different main carbon path sections.

Using the empirical data gathered from the experimental tests resulted in an improvement for the prediction. Empirical data found in the literature for a very similar fabric was used in the model, and the predictions error increased. This verification supports the need to characterise the rest of the fabrics used in this layup to understand their accuracy in the model validations.

The ideal pressure for the cutup data were very discrepant mainly due to the low thickness of the layup. The difference between conditions on the setup used in the experimental tests and the one used for producing blades is also believed to impact these ideal pressure discrepancies significantly.

6.2 Future work

The work conducted in this thesis has improved *Vestas* knowledge regarding the compaction behaviour of one of the most used fabrics in the production of the blades. Furthermore, it has provided a model with a vast academic background capable of predicting the thickness of some main carbon

path sections with a high degree of accuracy. Nevertheless, substantial future work must be conducted to prove the actual value of this work and to possibly include it in the current predictive methodologies used by *Vestas*. For that purpose, some suggestions will be stated here to raise awareness over lacking phenomena in the model, improvement points on the experimental tests and continuation of the model validation using *Vestas* data.

The viscoelasticity of the fabric is proved in literature to impact the permanent deformation of the material significantly. There are already some models characterising this behaviour that could be incorporated into the model. The lubrication phenomenon could also be assessed by using a setup without a distribution mesh. Their values can also be inserted into the thickness prediction model. Regarding the nesting effect, different alignments can be prepared in the stacking procedure of the characterisation tests in order to evaluate the relation between perfectness of alignment and nesting ability during compaction, thus understanding the empirical curves evolution while increasing the number of layers.

The first recommendation related to the experimental tests is about the number of repetitions per test. Three is believed to be a low value for this variable, and it is suggested to adjust this value to reach a statistically relevant analysis. Only under these conditions, it would be appropriate to characterise a lower number of layers. To fully characterise a fabric, it is more meaningful to test it in its dry and wet state to understand its behaviour better and approximate it to actual infusion conditions in the predictive model.

The utilisation of a mould with embedded pressure transducers to assess the pressure distribution in the through-thickness direction. An analysis of this pressure would allow adjusting the compaction pressure condition of thicker layups, including pultruded carbon in its core.

The number of characterised fabric is also another vital variable to expand its range. Having a characterisation of more than one fabric would significantly improve the possibilities for the model validation against infusion tests and cutup data. Furthermore, the interaction between the interface of their layers could also be a factor for the characterisation tests. This analysis would ease conclusions about similar layups on the model validation and could even improve predictions.

Regarding the model validations, only a particular section of the blade was used to compare its cutup data with the predictions. It is mandatory to validate it for almost all blade sections to assess this model value accurately. This validation includes thicker laminates close to the root and layups, including pultruded carbon. *Vestas* current methodologies must also be fully acknowledged, and if possible, part of this method can be incorporated in the new methodology, using their extensive knowledge on the field to reach an improved predictive method.

Bibliography

[1] R. Pemberton, J. Summerscales, and J. Graham-Jones. *Marine Composites : Design and Performance*. Cambridge: Woodhead Publishing, 2019. ISBN 9780081022641.

[2] S. G. Advani and K. T. Hsiao. *Manufacturing techniques for polymer matrix composites (PMCs)*. Cambridge: Woodhead Publishing, 2012. ISBN 9780857090676. doi: 10.1533/9780857096258.

[3] J. Yang, J. Xiao, J. Zeng, D. Jiang, and C. Peng. Compaction behavior and part thickness variation in vacuum infusion molding process. *Applied Composite Materials*, 19(3-4):443–458, 2012. ISSN 0929189X. doi: 10.1007/s10443-011-9217-8.

[4] J. Summerscales and T. J. Searle. Low-pressure (vacuum infusion) techniques for moulding large composite structures. *Proceedings of the Institution of Mechanical Engineers, Part L: Journal of Materials: Design and Applications*, 219(1):45–58, 2005. ISSN 14644207. doi: 10.1243/146442005X10238.

[5] L. Zhang, X. Wang, J. Pei, and Y. Zhou. Review of automated fibre placement and its prospects for advanced composites. *Journal of Materials Science*, 55(17):7121–7155, 2020. ISSN 15734803. doi: 10.1007/s10853-019-04090-7. URL `https://doi.org/10.1007/s10853-019-04090-7`.

[6] J. Vilà, C. González, and J. Llorca. Fabric compaction and infiltration during vacuum-assisted resin infusion with and without distribution medium. *Journal of Composite Materials*, 51(5):687–703, 2017. ISSN 1530793X. doi: 10.1177/0021998316649783.

[7] P. Šimáček, D. Heider, J. W. Gillespie, and S. Advani. Post-filling flow in vacuum assisted resin transfer molding processes: Theoretical analysis. *Composites Part A: Applied Science and Manufacturing*, 40(6-7):913–924, 2009. ISSN 1359835X. doi: 10.1016/j.compositesa.2009.04.018. URL `http://dx.doi.org/10.1016/j.compositesa.2009.04.018`.

[8] B. Yenilmez, T. Akyol, B. Caglar, and E. M. Sozer. Minimizing thickness variation in the vacuum infusion (VI) process. *Advanced Composites Letters*, 20(6):157–168, 2011. ISSN 2633366X. doi: 10.1177/096369351102000603.

[9] N. M. Barkoula, B. Alcock, N. O. Cabrera, and T. Peijs. Flame-Retardancy Properties of Intumescent Ammonium Poly(Phosphate) and Mineral Filler Magnesium Hydroxide in Combination with Graphene. *Polymers and Polymer Composites*, 16(2):101–113, 2008. ISSN 09673911. doi: 10.1002/pc.

[10] B. Caglar, B. Yenilmez, and E. M. Sozer. Modeling of post-filling stage in vacuum infusion using compaction characterization. *Journal of Composite Materials*, 49(16):1947–1960, 2015. ISSN 1530793X. doi: 10.1177/0021998314541305.

[11] B. Caglar, M. Hancioglu, and E. M. Sozer. Monitoring and modeling of part thickness evolution in vacuum infusion process. *Journal of Composite Materials*, 2020. ISSN 1530793X. doi: 10.1177/0021998320963173.

[12] R. A. Saunders, C. Lekakou, and M. G. Bader. Compression in the processing of polymer composites 1. A mechanical and microstructural study for different glass fabrics and resins. *Composites Science and Technology*, 59(7):983–993, 1999. ISSN 02663538. doi: 10.1016/S0266-3538(98)00137-7.

[13] M. Akif Yalcinkaya and E. M. Sozer. Effect of part thickness variation on the mold filling time in vacuum infusion process. *Journal of Reinforced Plastics and Composites*, 33(23):2136–2150, 2014. ISSN 15307964. doi: 10.1177/0731684414554938.

[14] N. Vernet, E. Ruiz, S. Advani, J. B. Alms, M. Aubert, M. Barburski, B. Barari, J. M. Beraud, D. C. Berg, N. Correia, M. Danzi, T. Delavière, M. Dickert, C. Di Fratta, A. Endruweit, P. Ermanni, G. Francucci, J. A. Garcia, A. George, C. Hahn, F. Klunker, S. V. Lomov, A. Long, B. Louis, J. Maldonado, R. Meier, V. Michaud, H. Perrin, K. Pillai, E. Rodriguez, F. Trochu, S. Verheyden, M. Weitgrefe, W. Xiong, S. Zaremba, and G. Ziegmann. Experimental determination of the permeability of engineering textiles: Benchmark II. *Composites Part A: Applied Science and Manufacturing*, 61:172–184, 2014. ISSN 1359835X. doi: 10.1016/j.compositesa.2014.02.010. URL `http://dx.doi.org/10.1016/j.compositesa.2014.02.010`.

[15] R. Arbter, J. M. Beraud, C. Binetruy, L. Bizet, J. Bréard, S. Comas-Cardona, C. Demaria, A. Endruweit, P. Ermanni, F. Gommer, S. Hasanovic, P. Henrat, F. Klunker, B. Laine, S. Lavanchy, S. V. Lomov, A. Long, V. Michaud, G. Morren, E. Ruiz, H. Sol, F. Trochu, B. Verleye, M. Wietgrefe, W. Wu, and G. Ziegmann. Experimental determination of the permeability of textiles: A benchmark exercise. *Composites Part A: Applied Science and Manufacturing*, 42(9):1157–1168, 2011. ISSN 1359835X. doi: 10.1016/j.compositesa.2011.04.021.

[16] C. I. Zénone, P. Le Grognec, and C. H. Park. Characterization and modeling of composite Vacuum Infusion process: Influence of fabric type, resin viscosity and strain rate. *IOP Conference Series: Materials Science and Engineering*, 406(1), 2018. ISSN 1757899X. doi: 10.1088/1757-899X/406/1/012062.

[17] S. V. Lomov. *Non-crimp fabric composites: manufacturing, properties and applications*. Cambridge: Woodhead Publishing, 2011. ISBN 9781845696566.

[18] W. Wu, B. Jiang, L. Xie, F. Klunker, S. Aranda, and G. Ziegmann. Effect of compaction and preforming parameters on the compaction behavior of bindered textile preforms for automated com-

posite manufacturing. *Applied Composite Materials*, 20(5):907–926, 2013. ISSN 0929189X. doi: 10.1007/s10443-012-9308-1.

[19] T. Grieser and P. Mitschang. Influence of compaction behavior of carbon NCF on preform mechanics for continuous profile preforming. *ICCM International Conferences on Composite Materials*, 2015-July(July):19–24, 2015.

[20] S. V. Lomov, G. Huysmans, Y. Luo, R. S. Parnas, A. Prodromou, I. Verpoest, and F. R. Phelan. Textile composites: Modelling strategies. *Composites - Part A: Applied Science and Manufacturing*, 32(10):1379–1394, 2001. ISSN 1359835X. doi: 10.1016/S1359-835X(01)00038-0.

[21] B. Chen, E. J. Lang, and T. W. Chou. Experimental and theoretical studies of fabric compaction behavior in resin transfer molding. *Materials Science and Engineering A*, 317(1-2):188–196, 2001. ISSN 09215093. doi: 10.1016/S0921-5093(01)01175-3.

[22] P. Potluri and T. V. Sagar. Compaction modelling of textile preforms for composite structures. *Composite Structures*, 86(1-3):177–185, 2008. ISSN 02638223. doi: 10.1016/j.compstruct.2008.03.019.

[23] Z. Yousaf, P. Potluri, and P. J. Withers. Influence of Tow Architecture on Compaction and Nesting in Textile Preforms. *Applied Composite Materials*, 24(2):337–350, 2017. ISSN 15734897. doi: 10.1007/s10443-016-9554-8.

[24] S. Toll and J. A. Manson. Elastic compression of a fiber network. *Journal of Applied Mechanics, Transactions ASME*, 62(1):223–226, 1995. ISSN 15289036. doi: 10.1115/1.2895906.

[25] A. Hammami. Effect of reinforcement structure on compaction behavior in the vacuum infusion process. *Polymer Composites*, 22(3):337–348, 2001. ISSN 02728397. doi: 10.1002/pc.10542.

[26] H. M. Andersson, T. S. Lundström, B. R. Gebart, and R. Långström. Flow-enhancing layers in the vacuum infusion process. *Polymer Composites*, 23(5):895–901, 2002. ISSN 02728397. doi: 10.1002/pc.10486.

[27] Y. Luo and I. Verpoest. Compressibility and relaxation of a new sandwich textile preform for liquid composite molding. *Polymer Composites*, 20(2):179–191, 1999. ISSN 15480569. doi: 10.1002/pc.10345.

[28] A. J. Malcom, M. T. Aronson, V. S. Deshpande, and H. N. Wadley. Compressive response of glass fiber composite sandwich structures. *Composites Part A: Applied Science and Manufacturing*, 54:88–97, 2013. ISSN 1359835X. doi: 10.1016/j.compositesa.2013.07.007. URL `http://dx.doi.org/10.1016/j.compositesa.2013.07.007`.

[29] S. V. Lomov and I. Verpoest. Compression of woven reinforcements: A mathematical model. *Journal of Reinforced Plastics and Composites*, 19(16):1329–1350, 2000. ISSN 07316844. doi: 10.1106/50RF-DQJ7-9RN3-6CPX.

[30] S. V. Lomov, E. B. Belov, T. Bischoff, S. B. Ghosh, T. Truong Chi, and I. Verpoest. Carbon composites based on multiaxial multiply stitched preforms. Part 1. Geometry of the preform. *Composites Part A: Applied Science and Manufacturing*, 33(9):1171–1183, 2002. ISSN 1359835X. doi: 10.1016/S1359-835X(02)00090-8.

[31] S. V. Lomov, I. Verpoest, T. Peeters, D. Roose, and M. Zako. Nesting in textile laminates: Geometrical modelling of the laminate. *Composites Science and Technology*, 63(7):993–1007, 2003. ISSN 02663538. doi: 10.1016/S0266-3538(02)00318-4.

[32] S. D. Green, A. C. Long, B. S. El Said, and S. R. Hallett. Numerical modelling of 3D woven preform deformations. *Composite Structures*, 108(1):747–756, 2014. ISSN 02638223. doi: 10.1016/j.compstruct.2013.10.015. URL http://dx.doi.org/10.1016/j.compstruct.2013.10.015.

[33] A. J. Thompson, B. El Said, D. Ivanov, J. P. Belnoue, and S. R. Hallett. High fidelity modelling of the compression behaviour of 2D woven fabrics. *International Journal of Solids and Structures*, 154: 104–113, 2018. ISSN 00207683. doi: 10.1016/j.ijsolstr.2017.06.027. URL https://doi.org/10.1016/j.ijsolstr.2017.06.027.

[34] L. Daelemans, B. Tomme, B. Caglar, V. Michaud, J. Van Stappen, V. Cnudde, M. Boone, and W. Van Paepegem. Kinematic and mechanical response of dry woven fabrics in through-thickness compression: Virtual fiber modeling with mesh overlay technique and experimental validation. *Composites Science and Technology*, 207(January):108706, 2021. ISSN 02663538. doi: 10.1016/j.compscitech.2021.108706.

[35] F. Klunker, S. Aranda, G. Ziegmann, P. Fideu, P. Baisch, and A. Herrmann. Permeability and compaction models for NCFs to preform 3D filling simulation of vacuum assisted resin infusion. *The 9th International Conference on Flow Processes in Composite Materials*, 9(July), 2008. URL https://www.fose1.plymouth.ac.uk/sme/fpcm/fpcm09/pdf/PC1/4.pdf.

[36] K. Hoes, D. Dinescu, H. Sol, R. S. Parnas, and S. Lomov. Study of nesting induced scatter of permeability values in layered reinforcement fabrics. *Composites Part A: Applied Science and Manufacturing*, 35(12):1407–1418, 2004. ISSN 1359835X. doi: 10.1016/j.compositesa.2004.05.004.

[37] K. D. Tackitt and S. M. Walsh. Experimental study of thickness gradient formation in the vartm process. *Materials and Manufacturing Processes*, 20(4):607–627, 2005. ISSN 10426914. doi: 10.1081/AMP-200041896.

[38] M. A. Yalcinkaya, B. Caglar, and E. M. Sozer. Effect of permeability characterization at different boundary and flow conditions on vacuum infusion process modeling. *Journal of Reinforced Plastics and Composites*, 36(7):491–504, 2017. ISSN 15307964. doi: 10.1177/0731684416684211.

[39] B. Yenilmez and E. M. Sozer. Compaction of e-glass fabric preforms in the vacuum infusion process: (A) use of characterization database in a model and (b) experiments. *Journal of Composite Materials*, 47(16):1959–1975, 2013. ISSN 00219983. doi: 10.1177/0021998312453075.

[40] G. Goncharova, B. Cosson, and M. Deléglise Lagardère. Analytical modeling of composite manufacturing by vacuum assisted infusion with minimal experimental characterization of random fabrics. *Journal of Materials Processing Technology*, 219:173–180, 2015. ISSN 09240136. doi: 10.1016/j.jmatprotec.2014.12.010. URL http://dx.doi.org/10.1016/j.jmatprotec.2014.12.010.

[41] B. Yenilmez, M. Senan, and E. Murat Sozer. Variation of part thickness and compaction pressure in vacuum infusion process. *Composites Science and Technology*, 69(11-12):1710–1719, 2009. ISSN 02663538. doi: 10.1016/j.compscitech.2008.05.009. URL http://dx.doi.org/10.1016/j.compscitech.2008.05.009.

[42] P. A. Kelly, R. Umer, and S. Bickerton. Viscoelastic response of dry and wet fibrous materials during infusion processes. *Composites Part A: Applied Science and Manufacturing*, 37(6 SPEC. ISS.):868–873, 2006. ISSN 1359835X. doi: 10.1016/j.compositesa.2005.02.008.

[43] B. Yenilmez, B. Caglar, and E. M. Sozer. Viscoelastic modeling of fiber preform compaction in vacuum infusion process. *Journal of Composite Materials*, 51(30):4189–4203, 2017. ISSN 1530793X. doi: 10.1177/0021998317699983.

[44] B. Yenilmez and E. M. Sozer. Compaction of e-glass fabric preforms in the Vacuum Infusion Process, A: Characterization experiments. *Composites Part A: Applied Science and Manufacturing*, 40(4):499–510, 2009. ISSN 1359835X. doi: 10.1016/j.compositesa.2009.01.016. URL http://dx.doi.org/10.1016/j.compositesa.2009.01.016.

[45] N. C. Correia, F. Robitaille, A. C. Long, C. D. Rudd, P. Šimáček, and S. G. Advani. Analysis of the vacuum infusion moulding process: I. Analytical formulation. *Composites Part A: Applied Science and Manufacturing*, 36(12):1645–1656, 2005. ISSN 1359835X. doi: 10.1016/j.compositesa.2005.03.019.

[46] J. A. Acheson, P. Šimáček, and S. G. Advani. The implications of fiber compaction and saturation on fully coupled VARTM simulation. *Composites Part A: Applied Science and Manufacturing*, 35 (2):159–169, 2004. ISSN 1359835X. doi: 10.1016/j.compositesa.2003.02.001.

[47] A. Hammami and B. R. Gebart. Analysis of the vacuum infusion molding process. *Polymer Composites*, 21(1):28–40, 2000. ISSN 02728397. doi: 10.1002/pc.10162.

[48] N. C. Correia, F. Robitaille, A. C. Long, C. D. Rudd, P. Šimáček, and S. G. Advani. Use of resin transfer molding simulation to predict flow, saturation and compaction in the VARTM process. In *ASME International Mechanical Engineering Congress and Exposition, Proceedings*, pages 61–68, 2002. ISBN 0791836401. doi: 10.1115/IMECE2002-39696.

[49] D. Modi, M. Johnson, A. Long, and C. Rudd. Analysis of pressure profile and flow progression in the vacuum infusion process. *Special Issue on the 12th European Conference on Composite Materials, ECCM 2006*, 69(9):1458–1464, 2009. ISSN 02663538. doi: 10.1016/j.compscitech.2008.05.026. URL http://dx.doi.org/10.1016/j.compscitech.2008.05.026.

[50] H. M. Andersson, T. S. Lundström, and B. R. Gebart. Numerical model for vacuum infusion manufacturing of polymer composites. *International Journal of Numerical Methods for Heat and Fluid Flow*, 13(2-3):383–394, 2003. ISSN 09615539. doi: 10.1108/09615530310464553.

[51] P. Celle, S. Drapier, and J. M. Bergheau. Numerical modelling of liquid infusion into fibrous media undergoing compaction. *European Journal of Mechanics, A/Solids*, 27(4):647–661, 2008. ISSN 09977538. doi: 10.1016/j.euromechsol.2007.11.002.

[52] R. S. Pierce, B. G. Falzon, and M. C. Thompson. A multi-physics process model for simulating the manufacture of resin-infused composite aerostructures. *Composites Science and Technology*, 149: 269–279, 2017. ISSN 02663538. doi: 10.1016/j.compscitech.2017.07.003. URL `http://dx.doi.org/10.1016/j.compscitech.2017.07.003`.

[53] Q. Govignon, S. Bickerton, and P. A. Kelly. Simulation of the reinforcement compaction and resin flow during the complete resin infusion process. *Composites Part A: Applied Science and Manufacturing*, 41(1):45–57, 2010. ISSN 1359835X. doi: 10.1016/j.compositesa.2009.07.007. URL `http://dx.doi.org/10.1016/j.compositesa.2009.07.007`.

[54] T. Gajjar, D. B. Shah, S. J. Joshi, and K. M. Patel. Analysis of process parameters for composites manufacturing using vacuum infusion process. *Materials Today: Proceedings*, 21:1244–1249, 2020. ISSN 22147853. doi: 10.1016/j.matpr.2020.01.112. URL `https://doi.org/10.1016/j.matpr.2020.01.112`.

[55] J. Vilà, C. González, and J. Llorca. A level set approach for the analysis of flow and compaction during resin infusion in composite materials. *Composites Part A: Applied Science and Manufacturing*, 67:299–307, 2014. ISSN 1359835X. doi: 10.1016/j.compositesa.2014.09.002.

[56] D. Adhikari, S. Gururaja, and S. Hemchandra. Vacuum infusion in porous preform with different mould configurations: Flow simulation and experimental validation. *Journal of Reinforced Plastics and Composites*, 2020. ISSN 15307964. doi: 10.1177/0731684420960209.

[57] B. Chen, A. H. Cheng, and T. W. Chou. Nonlinear compaction model for fibrous preforms. *Composites Part A: Applied Science and Manufacturing*, 32(5):701–707, 2001. ISSN 1359835X. doi: 10.1016/S1359-835X(00)00148-2.

[58] F. Robitaille and R. Gauvin. Compaction of textile reinforcements for composites manufacturing. I: Review of experimental results. *Polymer Composites*, 19(2):198–216, 1998. ISSN 02728397. doi: 10.1002/pc.10091.

[59] R. Robitaille, F., Gauvin. Compaction of Textile Reinforcements for Composites Manufacturing. II: Compaction and Relaxation of Dry and H2O-Saturated Woven Reinforcements. *Journal of Chemical Information and Modeling*, 53(9):1689–1699, 1998. ISSN 1098-6596.

[60] X. L. Liu, P. J. Falzon, R. Sweeting, and R. Paton. Effective compressibility and permeability of multi-layer non-crimp fiberglass reinforcements. *Journal of Reinforced Plastics and Composites*, 23(8):861–879, 2004. ISSN 07316844. doi: 10.1177/0731684404033378.

[61] W. Wu and W. Li. A novel material for simulation on compaction behavior of glass fiber non-crimp fabric. *Composite Structures*, 219(2999):8–16, 2019. ISSN 02638223. doi: 10.1016/j.compstruct.2019.03.006. URL https://doi.org/10.1016/j.compstruct.2019.03.006.

[62] A. A. Somashekar, S. Bickerton, and D. Bhattacharyya. An experimental investigation of non-elastic deformation of fibrous reinforcements in composites manufacturing. *Composites Part A: Applied Science and Manufacturing*, 37(6 SPEC. ISS.):858–867, 2006. ISSN 1359835X. doi: 10.1016/j.compositesa.2005.06.012.

[63] Q. Govignon, S. Bickerton, J. Morris, and J. Lin. A stereo photography system for monitoring full field thickness variation during resin infusion. *Proceedings of FPCM8 Conference*, (July):231–239, 2006.

[64] A. George, P. Hannibal, M. Morgan, D. Hoagland, and S. E. Stapleton. Compressibility measurement of composite reinforcements for flow simulation of vacuum infusion. *Polymer Composites*, 40 (3):961–973, 2019. ISSN 15480569. doi: 10.1002/pc.24770.

[65] S. V. Lomov, I. Verpoest, M. Barburski, and J. Laperre. Carbon composites based on multiaxial multiply stitched preforms. Part 2. KES-F characterisation of the deformability of the preforms at low loads. *Composites Part A: Applied Science and Manufacturing*, 34(4):359–370, 2003. ISSN 1359835X. doi: 10.1016/S1359-835X(03)00025-3.

[66] S. V. Lomov, M. Barburski, T. Stoilova, I. Verpoest, R. Akkerman, R. Loendersloot, and R. H. Ten Thije. Carbon composites based on multiaxial multiply stitched preforms. Part 3: Biaxial tension, picture frame and compression tests of the preforms. *Composites Part A: Applied Science and Manufacturing*, 36(9):1188–1206, 2005. ISSN 1359835X. doi: 10.1016/j.compositesa.2005.01.015.

[67] N. Pearce and J. Summerscales. The compressibility of a reinforcement fabric. *Composites Manufacturing*, 6(1):15–21, 1995. ISSN 09567143. doi: 10.1016/0956-7143(95)93709-S.

[68] Y. Duan, Z. Tan, Y. Zhao, and J. Sun. Compression responses of preform in vacuum infusion process. *Chinese Journal of Aeronautics*, 21(4):370–377, 2008. ISSN 10009361. doi: 10.1016/S1000-9361(08)60048-5.

[69] J. Cao, R. Akkerman, P. Boisse, J. Chen, H. S. Cheng, E. F. de Graaf, J. L. Gorczyca, P. Harrison, G. Hivet, J. Launay, W. Lee, L. Liu, S. V. Lomov, A. Long, E. de Luycker, F. Morestin, J. Padvoiskis, X. Q. Peng, J. Sherwood, T. Stoilova, X. M. Tao, I. Verpoest, A. Willems, J. Wiggers, T. X. Yu, and B. Zhu. Characterization of mechanical behavior of woven fabrics: Experimental methods and benchmark results. *Composites Part A: Applied Science and Manufacturing*, 39(6):1037–1053, 2008. ISSN 1359835X. doi: 10.1016/j.compositesa.2008.02.016.

[70] A. X. Yong, A. Aktas, D. May, A. Endruweit, S. V. Lomov, S. Advani, P. Hubert, S. G. Abaimov, D. Abliz, I. Akhatov, M. A. Ali, S. Allaoui, T. Allen, D. C. Berg, S. Bickerton, B. Caglar, P. Causse,

A. Chiminelli, S. Comas-Cardona, M. Danzi, J. Dittmann, C. Dransfeld, P. Ermanni, E. Fauster, A. George, J. Gillibert, Q. Govignon, R. Graupner, V. Grishaev, A. Guilloux, M. A. Kabachi, A. Keller, K. Kind, D. Large, M. Laspalas, O. V. Lebedev, M. Lizaranzu, A. C. Long, C. López, K. Masania, V. Michaud, P. Middendorf, P. Mitschang, S. van Oosterom, R. Schubnel, N. Sharp, P. Sousa, F. Trochu, R. Umer, J. Valette, and J. H. Wang. Experimental characterisation of textile compaction response: A benchmark exercise. *Composites Part A: Applied Science and Manufacturing*, 142 (June 2020), 2021. ISSN 1359835X. doi: 10.1016/j.compositesa.2020.106243.

[71] M. Uy and J. K. Telford. Optimization by design of experiment techniques. *IEEE Aerospace Conference Proceedings*, 2009. ISSN 1095323X. doi: 10.1109/AERO.2009.4839625.

[72] B. Richardson. Limitations on the use of mathematical models in transportation policy analysis. *Motor Vehicle Manufacturers Association*, pages 1–13, 1979. URL `http://deepblue.lib.umich.edu/handle/2027.42/509`.

Appendix A

Symbolic Computation

A.1 Continuity equation

The continuity equation in its original form represents a three-dimensional volume and relates its rates of expansion or contraction according to its media porosity and fluid flow:

$$\frac{\partial}{\partial t}\int_V (\rho \cdot \phi)\, dV + \oint_S (\rho \cdot u \cdot \hat{n}\rho \cdot u \cdot \hat{n})\, dS = 0\,. \tag{A.1}$$

This section presents the simplifications of this formula to a unidirectional flow which reduce the complexity of the Control Volume (C.V.), figure A.1. These manipulations were presented in [45].

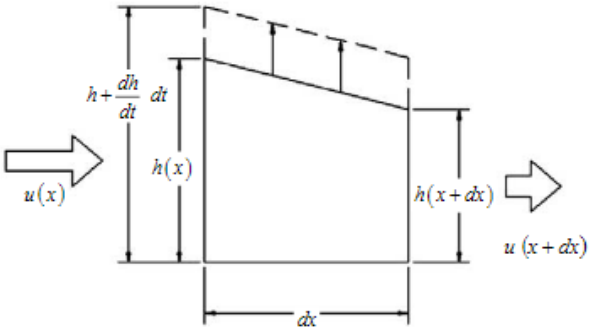

Figure A.1: Control Volume, [45].

The porosity ϕ of a fabric is calculated by its FVF, $\phi = 1 - V_f$. Assuming that porosity represents a negligible variation of the C.V.:

$$(u_0 h_0 - u_i h_i) = -\frac{\partial}{\partial t}\left[\phi \cdot \int_V dV\right]\,. \tag{A.2}$$

Integrating over the volume leads to a differential form:

$$(u_0 h_0 - u_i h_i) = -\frac{\partial}{\partial t}\left[\phi \cdot h \cdot \partial x\right]\,. \tag{A.3}$$

Changing porosity to the FVF variable:

$$\partial(uh) = -\partial x \cdot \frac{\partial}{\partial t}\left[(1 - V_f) \cdot h\right] . \tag{A.4}$$

Due to equation [2.5], the term $V_f \cdot h$ is constant:

$$\frac{\partial h}{\partial t} = -\frac{\partial}{\partial x}\left(\vec{u}h\right) . \tag{A.5}$$

A.2 Continuity equation & *Darcy's* law

To reach the ODE, it is necessary to combine both the continuity equation and Darcy's Law:

$$\frac{\partial h}{\partial t} = -\frac{\partial\left(-\dfrac{h \cdot K}{\mu} \cdot \dfrac{\partial P}{\partial x}\right)}{\partial x} , \tag{A.6}$$

Expanding the partial differentials,

$$\frac{\partial h}{\partial t} = \frac{1}{\mu} \cdot \left[\left(K \cdot \frac{\partial h}{\partial x} + h\frac{\partial K}{\partial x}\right) \cdot \frac{\partial P}{\partial x} + hK \cdot \left(\frac{\partial^2 P}{\partial x^2}\right)\right] . \tag{A.7}$$

Both pressure and permeability are functions of pressure, which is a function of the position, $h(P(x))$ and $K(P(x))$.

$$\frac{\partial h}{\partial t} = \frac{1}{\mu} \cdot \left[\left(K \cdot \frac{\partial h}{\partial P} + h\frac{\partial K}{\partial P}\right) \cdot \left(\frac{\partial P}{\partial x}\right)^2 + hK \cdot \left(\frac{\partial^2 P}{\partial x^2}\right)\right] . \tag{A.8}$$

Introducing a new dimensionless variable, α, that allows to scale the pressure distribution from inlet to the flow front. Thus, a new derivative emerges,

$$\alpha = \frac{x}{L} \quad \Rightarrow \quad \frac{\partial P}{\partial x} = \frac{\partial P}{\partial \alpha} \cdot \frac{\partial \alpha}{\partial x} \quad \Leftrightarrow \quad \frac{\partial P}{\partial x} = \frac{1}{L} \cdot \frac{\partial P}{\partial \alpha} , \tag{A.9}$$

where L is the instantaneous flow front position. Including this new derivative,

$$\frac{\partial h}{\partial t} = \frac{1}{\mu L^2} \cdot \left[\left(K \cdot \frac{\partial h}{\partial P} + h\frac{\partial K}{\partial P}\right) \cdot \left(\frac{\partial P}{\partial \alpha}\right)^2 + hK \cdot \left(\frac{\partial^2 P}{\partial \alpha^2}\right)\right] . \tag{A.10}$$

Looking at the LHS of the equation,

$$\frac{\partial h}{\partial t} = \frac{\partial h}{\partial \alpha} \cdot \frac{\partial \alpha}{\partial L} \cdot \frac{\partial L}{\partial t} \quad \Leftrightarrow \quad \frac{\partial h}{\partial t} = \frac{\partial h}{\partial \alpha} \cdot \left(-\frac{x}{L^2}\right) \cdot \frac{\partial L}{\partial t} . \tag{A.11}$$

Due to constant flow rate in unidirectional flow,

$$\frac{\partial L}{\partial t} \cdot [h]_{\alpha=1} = uh . \tag{A.12}$$

Being h^* the normalised thickness at the flow front,

$$h^* = \frac{h}{[h]_{\alpha=1}} \Rightarrow \frac{\partial L}{\partial t} = uh^* \,. \tag{A.13}$$

Using *Darcy's* Law for the averaged fluid velocity,

$$u = \frac{K}{\mu} \cdot \frac{\partial P}{\partial x} \Rightarrow \frac{\partial h}{\partial t} = \frac{K \cdot x \cdot h^*}{\mu \cdot L^2} \cdot \frac{\partial h}{\partial \alpha} \cdot \frac{\partial P}{\partial \alpha} \cdot \frac{\partial \alpha}{\partial x} \,. \tag{A.14}$$

Since

$$x \cdot \frac{\partial \alpha}{\partial x} = x \cdot \frac{1}{L} = \alpha \,, \tag{A.15}$$

it can be written

$$\frac{\partial h}{\partial t} = \frac{K \cdot \alpha \cdot h^*}{\mu \cdot L^2} \cdot \frac{\partial h}{\partial \alpha} \cdot \frac{\partial P}{\partial \alpha} \,, \tag{A.16}$$

which leads to

$$\frac{\partial h}{\partial t} = \frac{K \cdot \alpha \cdot h^*}{\mu \cdot L^2} \cdot \frac{\partial h}{\partial P} \cdot \left(\frac{\partial P}{\partial \alpha}\right)^2 \,. \tag{A.17}$$

Including this manipulation of the LHS,

$$\frac{K \cdot \alpha \cdot h^*}{\mu \cdot L^2} \cdot \frac{\partial h}{\partial P} \cdot \left(\frac{\partial P}{\partial \alpha}\right)^2 = \frac{1}{\mu L^2} \cdot \left[\left(K \cdot \frac{\partial h}{\partial P} + h\frac{\partial K}{\partial P}\right) \cdot \left(\frac{\partial P}{\partial \alpha}\right)^2 + hK \cdot \left(\frac{\partial^2 P}{\partial \alpha^2}\right)\right] \,, \tag{A.18a}$$

$$\Leftrightarrow \quad hK \cdot \frac{\partial^2 P}{\partial \alpha^2} = \left[(h^* \alpha K - K) \cdot \frac{\partial h}{\partial P} - h \cdot \frac{\partial K}{\partial P}\right] \cdot \left(\frac{\partial P}{\partial \alpha}\right)^2 \,, \tag{A.18b}$$

$$\Leftrightarrow \quad \frac{\partial^2 P}{\partial \alpha^2} = \left(\frac{h^* \cdot \alpha - 1}{h} \cdot \frac{\partial h}{\partial P} - \frac{1}{K} \cdot \frac{\partial K}{\partial P}\right) \cdot \left(\frac{\partial P}{\partial \alpha}\right)^2 \,, \tag{A.18c}$$

reaching the ODE in its final form.

A.3 Empirical formulas derivatives

The empirical formulas used for a first step are:

$$V_f = V_{f_0} \cdot P_c^B \,, \tag{A.19a}$$

$$K = k_o \cdot \frac{(1 - V_f)^3}{V_f^2} \,, \tag{A.19b}$$

which must be related with

$$P_c = P_{atm} - P_{vac} - P_r \,, \tag{A.20a}$$

$$h = \frac{\rho_{sup} \cdot nol}{\rho_{bulk} \cdot V_f} \,. \tag{A.20b}$$

The derivatives of thickness and permeability can be splitted in

$$\frac{dh}{dP} = \frac{dh}{dV_f} \cdot \frac{dV_f}{dP_c} \cdot \frac{dP_c}{dP} \,, \tag{A.21a}$$

$$\frac{dK}{dP} = \frac{dK}{dV_f} \cdot \frac{dV_f}{dP_c} \cdot \frac{dP_c}{dP} \,. \tag{A.21b}$$

For the compaction:

$$\begin{cases} \dfrac{dh}{dV_f} = -\dfrac{\rho_{sup} \cdot nol}{\rho_{bulk}} \cdot \dfrac{1}{V_f^2} \\ \dfrac{dV_f}{dP_c} = V_{f_0} B \cdot P_c^{B-1} \\ \dfrac{dP_c}{dP} = -1 \end{cases} \quad \Rightarrow \quad \frac{dh}{dP} = \frac{\rho_{sup} \cdot nol}{\rho_{bulk}} \cdot \frac{B}{P_c^{B+1} \cdot V_{f_0}} \,. \tag{A.22}$$

For the permeability:

$$\begin{cases} \dfrac{dK}{dV_f} = -\dfrac{k_0 \cdot (1 - V_f)^2 \, (V_f + 2)}{V_f^3} \\ \dfrac{dV_f}{dP_c} = V_{f_0} B \cdot P_c^{B-1} \\ \dfrac{dP_c}{dP} = -1 \end{cases} \Rightarrow \frac{dK}{dP} = \frac{k_0 B}{V_{f_0}^2} \cdot \left(-3 V_{f_0} P_c^{-B-1} + V_{f_0} P_c^{B-1} + 2 P_c^{-2B-1} \right) \,. \tag{A.23}$$

A.4 Numerical solutions

This section presents the manipulations, and FDM applied to calculate the numerical solutions for both models.

A.4.1 Correia et al. model

Starting from the ODE, a second-order central difference is applied to the LHS and a first-order central difference to the derivative of pressure per α in the Right Hand Side (RHS):

$$\frac{\partial^2 P}{\partial \alpha^2} = \frac{(P_{n-1} - 2P_n + P_{n+1})}{\alpha^2} \,, \tag{A.24a}$$

$$\left(\frac{\partial P}{\partial \alpha} \right)^2 = \left(\frac{P_{n+1} - P_{n-1}}{2\alpha} \right)^2 \,. \tag{A.24b}$$

When substituted in the ODE, the numerical solution is achieved

$$(P_{n-1} - 2P_n + P_{n+1})|_i = \left[\left(\frac{h_n^* \alpha_n - 1}{h_n} \cdot \left(\frac{\partial h}{\partial P} \right)_n - \frac{1}{K_n} \cdot \left(\frac{\partial K}{\partial P} \right)_n \right) \cdot \left(\frac{P_{n+1} - P_{n-1}}{2} \right)^2 \right] \Bigg|_{i-1} \,. \tag{A.25}$$

A.4.2 Akif Yalcinkaya and Sozer model

Applying a first-order central finite difference in this model ODE,

$$\frac{\left(Kh \cdot \dfrac{\partial P}{\partial x} \right)_{i+1} - \left(Kh \cdot \dfrac{\partial P}{\partial x} \right)_{i-1}}{2 \cdot \Delta x} = 0 \quad for \quad 2 \leq i \leq N - 1 \,, \tag{A.26}$$

and the pressure gradient term also suffers a first-order central finite difference,

$$\left.\frac{\partial P}{\partial x}\right|_i = \frac{P_{i+1} - P_{i-1}}{2\Delta x}\,. \tag{A.27}$$

The fluid pressure is calculated by

$$P_i = \frac{P_{i-2}K_{i-1}h_{i-1} + P_{i+2}K_{i+1}h_{i+1}}{K_{i-1}h_{i-1} + K_{i+1}h_{i+1}} \quad for \quad 3 \leq i \leq N-2\,, \tag{A.28a}$$

$$P_2 = \frac{1}{4}\left[\frac{K_3 h_3\left(-P_5 + 4P_4 - 3P_3\right)}{k_1 h_1} + P_3 + 3P_1\right]\,, \tag{A.28b}$$

$$P_{N-1} = \frac{1}{4}\left[\frac{K_{N-2} h_{N-2}\left(-P_{N-4} + 4P_{N-3} - 3P_{N-2}\right)}{k_N h_N} + P_{N-2} + 3P_N\right]\,. \tag{A.28c}$$

Appendix B

Material characterisation tests

B.1 Data analysis - 1

The individual plots and other information regarding the tests will be provided in this section.

B.1.1 Unloading & Relaxation

Only the revised tests of the first round are presented since the ones previous to these do not have major relevancy. They are divided according to the number of layers, figures B.1, B.2 and B.3.

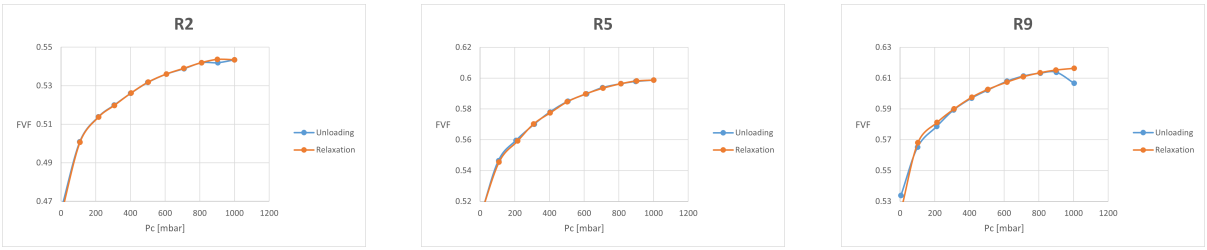

(a) Second run. (b) Fifth run. (c) Ninth run.

Figure B.1: Revised individual tests for $nol = 4$.

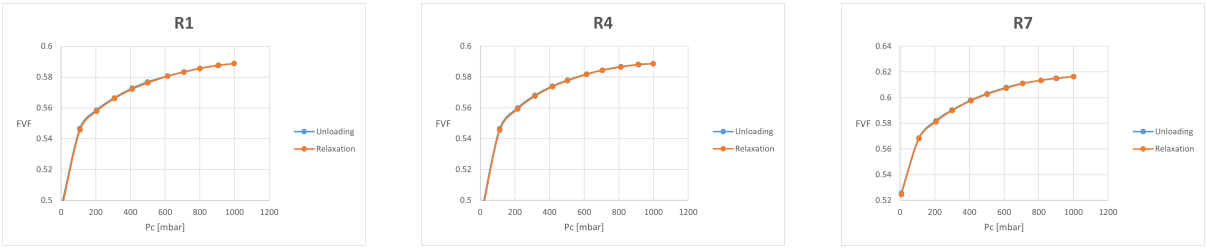

(a) First run. (b) Fourth run. (c) Seventh run.

Figure B.2: Revised individual tests for $nol = 8$.

It is possible to observe a discrepancy in the point with the highest compaction pressure in the ninth run, R9. A possible justification for that unusuality may be the influence of the vacuum pump tilting on the mould or any possible knock by accident on the table supporting the mould.

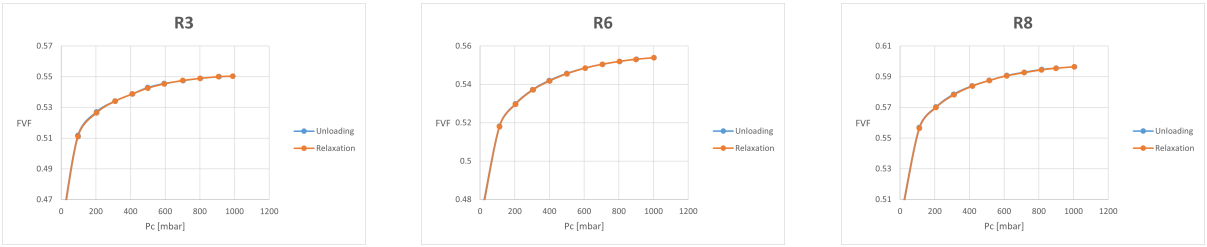

(a) Third run. (b) Sixth run. (c) Eighth run.

Figure B.3: Revised individual tests for $nol = 16$.

B.2 Data analysis - 2

B.2.1 Unloading

The individual plots for the tests conducted with the improved methodology are presented in figures B.4, B.5 and B.6.

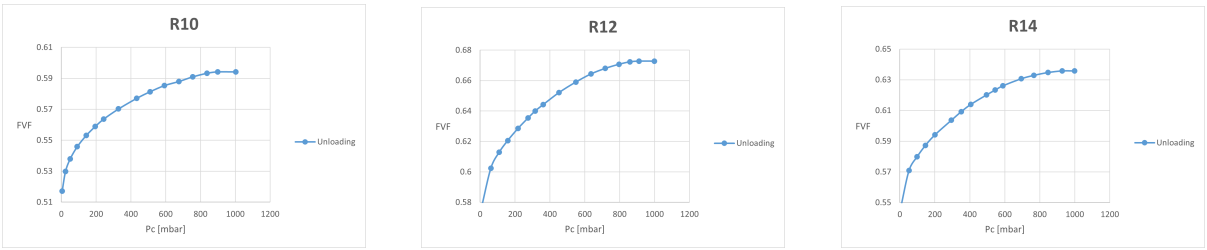

(a) Tenth run. (b) Tewlfth run. (c) Fourteenth run.

Figure B.4: Individual unloading tests for $nol = 4$ with new procedure.

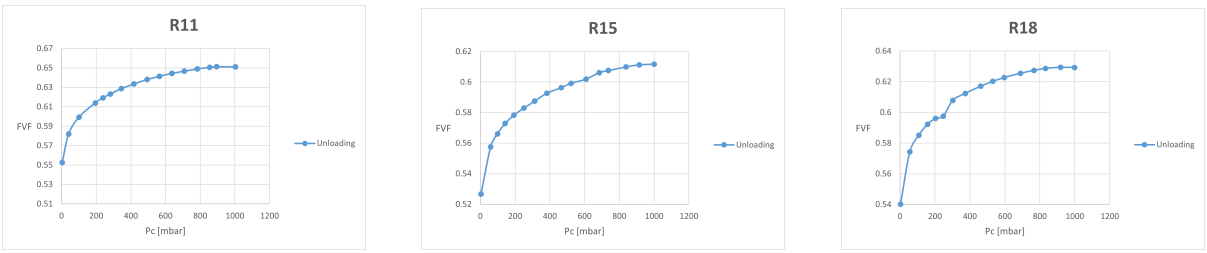

(a) Elevnth run. (b) Fifteenth run. (c) Eighteenth run.

Figure B.5: Individual unloading tests for $nol = 8$ with new procedure.

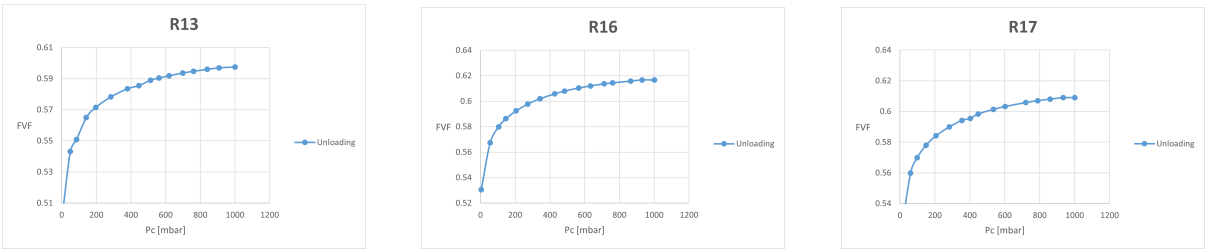

(a) Thirteenth run. (b) Sixteenth run. (c) Seventeenth run.

Figure B.6: Individual unloading tests for $nol = 16$ with new procedure.

The eighth run, R8, has one measurement slightly deviated from the curve. This deviation may result from a possible knock by accident on the table supporting the mould, as seen previously in R9.

For the number of layers of thirty-two, the individual plots are presented in figure B.7.

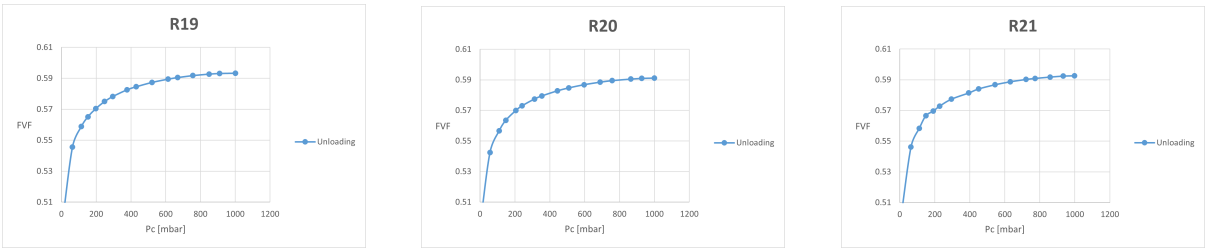

(a) Nineteenth run. (b) Twentieth run. (c) Twenty-first run.

Figure B.7: Individual unloading tests for $nol = 32$ with new procedure.

B.2.2 Settling

The individual plots per test of the thickness variation during this stage are plotted in figures B.8, B.9 and B.10.

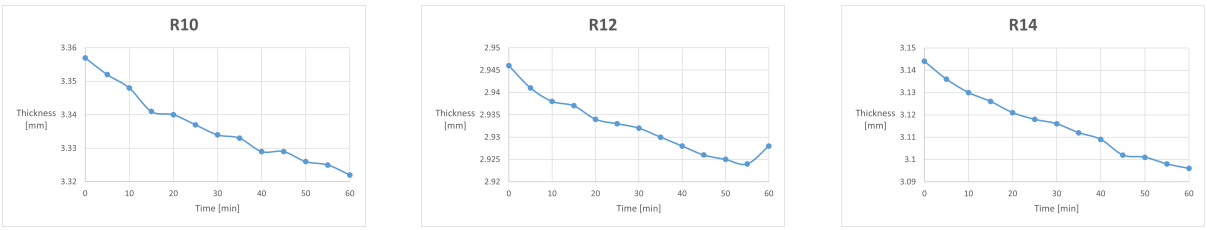

(a) Tenth run. (b) Tewlfth run. (c) Fourteenth run.

Figure B.8: Individual settling tests for $nol = 4$ with new procedure.

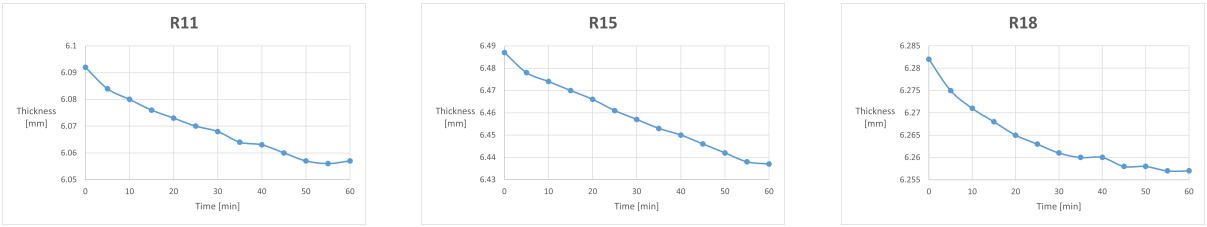

(a) Elevnth run. (b) Fifteenth run. (c) Eighteenth run.

Figure B.9: Individual settling tests for $nol = 8$ with new procedure.

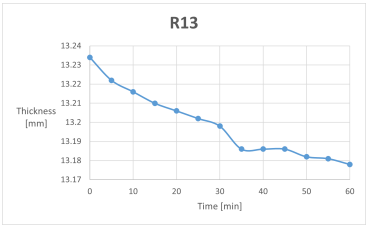

(a) Thirteenth run.

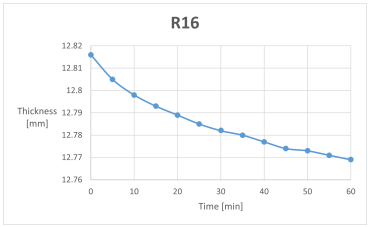

(b) Sixteenth run.

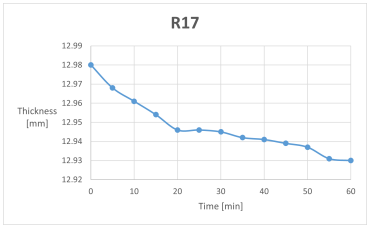

(c) Seventeenth run.

Figure B.10: Individual settling tests for $nol = 16$ with new procedure.

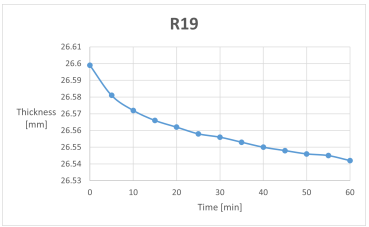

(a) Nineteenth run.

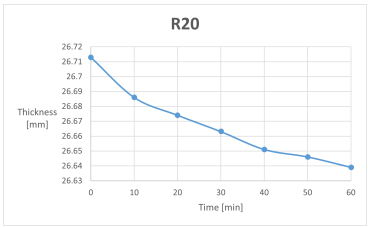

(b) Twentieth run.

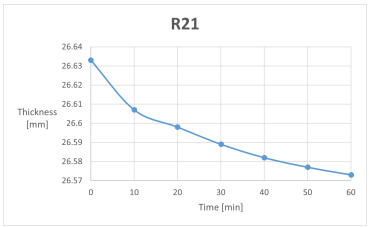

(c) Twenty-first run.

Figure B.11: Individual settling tests for $nol = 32$ with new procedure.